# Energy and Exergy Based Analysis of A Multi-Fuelled SI Engine

Adnan Morshed

Department of Mechanical Engineering

BANGLADESH UNIVERSITY OF ENGINEERING AND TECHNOLOGY

A thesis submitted for the degree of

*Master of Science*

November 9, 2013

# Certificate of Approval

The thesis titled, **"Energy and Exergy Based Analysis of A Multi-Fuelled SI Engine"**, submitted by **Adnan Morshed**, Roll No: **0411102065 P**, Session: **April, 2011**, has been accepted as satisfactory in partial fulfillment of the requirements for the degree of **MASTER OF SCIENCE IN MECHANICAL ENGINEERING** on **November 9, 2013**.

---

Dr. Md. Zahurul Haq — Chairman (Supervisor)
Professor
Department of Mechanical Engineering
BUET, Dhaka - 1000

---

Dr. Md. Ehsan — Member (Ex-officio)
Professor & Head
Department of Mechanical Engineering
BUET, Dhaka - 1000

---

Dr. Mohammad Arif Hasan Mamun — Member (Internal)
Professor
Department of Mechanical Engineering
BUET, Dhaka - 1000

---

Dr. Md. Abdur Razzak Akhanda — Member (External)
Professor & Head
Department of Mechanical and Chemical Engineering,
IUT, Board Bazaar, Gazipur - 1704

# Candidate's Declaration

It is hereby declared that this thesis or any part of it has not been submitted elsewhere for the award of any degree or diploma.

_____

Adnan Morshed

# Acknowledgements

All of the work on this thesis has been done at BUET, my beloved alma mater. I would like to thank everyone at BUET, who helped me one way or other in course of writing it. In particular I should like to thank Professor Dr. Md. Zahurul Haq for providing much needed guidance and supervision from the beginning to this point. I am grateful to him for the numerous discussions, which elucidated many obscure ideas.

I wish to acknowledge my indebtedness to the LaTeX community all over the world for their kind support. Thanks are also due to my family, colleagues and students for their support and encouragement.

Finally, I wish to thank almighty Allah for everything I have and everything I don't.

# Abstract

In the present work, energy and exergy based analyses of a single cylinder, four-stroke, spark ignition engine fuelled by six different fuels namely iso-octane, methane, hydrogen, methanol, ethanol and n-butanol have been carried out. Wiebe function is used to predict realistic burn rates. Since the Wiebe function parameters are generally optimized for conventional fuels, the current study modifies them for different alternative fuels using available burning velocity data. Heat losses throughout the cycle have been predicted by appropriate empirical correlations. Detailed equilibrium calculations provided the properties of the mixture inside the cylinder. Analyses are carried out to quantify energy and exegy of the premixed fuel-air mixture inside the engine cylinder at various phases of the cycle and some results obtained from the study are validated against data available in literature. Effect of variation in speed, equivalence ratio on energy and exergy based parameters were studied, and their variation with change in fuel were observed. Results show that about $34 - 42\,\%$ of energy contained in the fuel is converted into useful work and the work quantity is found to increase with engine speed. Exergy destruction associated with exhaust losses are found significantly lower than the corresponding energy values for all fuels. The present study highlights the necessity of both energy and exergy analyses for comprehensive analysis of engine performance with alternative fuels.

# List of Symbols

| | |
|---|---|
| $a_{ch}$ | Chemical exergy |
| $a_Q$ | Exergy transfer with heat |
| $a_{th}$ | Thermomechanical exergy |
| $a_{total}$ | Total exergy |
| $a_W$ | Exergy transfer with work |
| $f$ | Residual mass fraction |
| $g$ | Specific Gibbs free energy |
| $h$ | Specific enthalpy |
| $N$ | Engine speed |
| $P$ | Gas pressure inside cylinder |
| $R$ | Specific gas constant |
| $R_c$ | Compression ratio |
| $s$ | Specific entropy |
| $T$ | Gas temperature inside cylinder |
| $u$ | Specific internal energy |
| $u_l$ | Laminar burning velocity |
| $V$ | Volume |
| $x_i$ | Mole fraction of species $i$ |
| $\epsilon$ | Rational exergetic efficiency |
| $\gamma$ | Specific heat capacity ratio |
| $\mu$ | Specific chemical potential |
| $\phi$ | Fuel-air equivalence ratio |
| $\theta$ | Crank angle |
| **Subscripts** | |
| $ref$ | Reference state |
| $r$ | identifies a heat source |
| $i$ | identifies constituent of a mixture |
| 0 | Restricted equilibrium with the environment |
| 00 | Unrestricted equilibrium with the environment |

# Contents

# List of Figures

# List of Tables

# Chapter 1

# Introduction

Proliferation of the internal combustion engine as a transformer of chemical and thermal energy over the last fifty years, specially in the automotive sector has had profound impact on the human civilization, both positive and negative. On one hand, it has served as a liberator of the human race allowing mobility, speed and efficiency [1]. Services like mass- and cargo-transportation, expedition, sports, and power generation have been the major beneficiary of its development. This phenomenal development has also had worldwide financial, social and most importantly environmental impact. Widespread availability and small size meant, every country by the eighties have become so much dependent on them, that they took very little notice of how quickly the fuel reserves are declining, or how badly the environment is being affected by this reciprocating source of continuous pollution.

Eventually, rational voices descended over the fast degrading air quality and associated problems being caused by air pollution and governments started to implement engine exhaust and noise regulations [2]. This was a good thing though. Because, it had opened a brand new window of research into engine efficiency, combustion science, automotive electronics, aerodynamics, exhaust treatment, and a host of other technologies. This also raised another critical question. Though automotive technology has had significant advances over the last three decades, the efficiency of an internal combustion engine is worryingly small compared to other power generation alternatives, barring the aspect of mobility. Raising questions about efficiency, specially for comparison brought questions about

the definition of efficiency itself. The concept of efficiency in the traditional sense is based on the axiom of conservation of energy, or the first law of thermodynamics. The pitfall of this concept originates with the very law: it accounts for energy quantity only, but never for the quality. The quality of energy in the thermodynamic sense is synonymous to its ability to be transformed to useful work, as stipulated by the second law of thermodynamics, which bestows a much greater glory on ordered forms of energy (e.g. work) than disordered form of energy (e.g. heat) [3]. Thus if an internal combustion engine converts thirty percent of thermal energy to useful work, we get delighted; and if an electric motor is converting eighty percent of the electricity to mechanical work, we are certain that something is wrong with the motor. Clearly then, there is problem with this definition of efficiency, specially when comparing two different kinds of energy transformation. Thankfully, second law provides us another way to measure and compare performance of energy conversions. This is called the exergy method.

Unlike energy, exergy or availability is not a conserved entity. Every irreversible process causes a loss in availability which is irrecoverable as dictated by the second law of thermodynamics. Since no natural process is totally reversible, we always have to accept some form of loss in availability no matter how hard we try. But acceptance of loss in availability should always be compensated by some economic justification. Non-existence of such a justification indicates that the availability loss results only from an error in the art of engineering. Thus presence of an availability loss invariably indicates the opportunity of a thermodynamic improvement [4].

Exergy is defined as the maximum theoretical work that can be obtained from a combined system (combination of a system and its reference environment) when the system comes into equilibrium (as thermally, mechanically and chemically) with the environment without violating any laws of thermodynamics. The maximum available work from a system emerges as the sum of two contributions: thermomechanical exergy and chemical exergy. Thermomechanical exergy is defined as the maximum extractable work from the combined system as the system comes into thermal and mechanical equilibria with the environment, and its value is calculated with respect to restricted dead-state condition. At the restricted dead-state conditions, no work potential exists between the system and

the environment due to temperature and pressure differences. In this state, the control mass is in thermomechanical equilibrium with the environment, but not necessarily in chemical equilibrium with it[5]. In principle, the difference between the compositions of the system at the restricted dead-state and the environment, and the difference in species concentrations between the system and environment can be used to obtain additional work to reach chemical equilibrium through reaction and diffusion respectively. The maximum additional work obtained in this way is called the chemical exergy [3].

Increasing strain on world fossil fuel reserves and the capricious nature of the crude oil market have strongly influenced the growth of interest in the research on alternative fuels [6]. Promising biofuels like alcohols are already emerging in the market to appease the burden on fossil fuels [7, 8]. Different blends of fuel mixtures are also being tested copiously [9, 10]. Another virile field is being occupied by the research on natural gas and hydrogen as alternative fuels [11]. While natural gas has seen large success in some regions, concerns over pollution are still impeding its use [12, 13]. Hydrogen on the other hand is the most promising alternative to traditional fuels in terms of pollutant formation, but is limited by lack of technology and infrastructure [14, 15, 16].

Modeling and simulation of the internal combustion engine is an invaluable tool for engine performance evaluation and development. Aided by an unwonted growth of digital computers, modeling has allowed exploration of engine operational parameters, and effect of their variation on performance and emission at the lowest possible expenses [17]. Level of detail of the model varies significantly still, depending on the nature of study. For example, effect of charge motion like swirl and tumble on combustion characteristics requires detailed three-dimensional fluid dynamic modeling of the transient flow pattern, while effect of spark timing on pollutant formation can be satisfactorily studied without any flow simulation. In the realm of engine modeling, exergy has been established as a key indicator in identifying the effects of variations in operational parameters and provide guidance for future developments [18].

## 1.1 Objectives of the Thesis

The objectives of this thesis are,

- to develop a basic zero dimensional thermodynamic model of spark ignition engine processes,
- to employ schemes in the model to account for
  - finite heat release,
  - realistic heat transfer,
  - residual gas fraction, and
  - variation in laminar burning velocities according to intake mixture and engine speed.
- to calculate mixture properties using detailed equilibrium analysis, and
- to calculate and compare performance of different fuels in terms of indicated values at various operating conditions through energy and exergy analysis.

## 1.2 Scope of the Thesis

The present work takes a thermodynamic approach to analyse spark ignition engine operation and compare its performance with different alternative fuels in pure form. Since the exergy approach is ideally suited for this kind of analysis, majority of the post-processing and analyses are done using the exergy method. The most relevant literature on engine modeling, Wiebe function, and exergy analyses have been reviewed in chapter 2 in a chronological order.

Comprehensive exergy analysis of thermodynamic systems require calculation of both physical and chemical exergies. In chapter 3, all the required terminology and concepts for the development of exergy balance equations are first discussed. Then, balance equations are developed for both control mass and control volume systems. Special attention has been paid to integrate chemical exergies of the contents of the system by ensuring calculation of both reactive and diffusive components.

Chapter 4 sees the mathematical and phenomenological development of a zero-dimensional model of the spark ignition engine. Realistic residual fraction calculation, heat release and heat transfer model are also incorporated. Intake and exhaust processes have also received necessary treatment. Calculation of properties throughout the analysis cycle is probably the most important output of the model. The present work makes use of a popular open-source chemical kinetic and equilibrium package named Cantera [19] to calculate mixture properties. The equilibrium calculation procedure employed by Cantera is also briefly explained in chapter 4, while the solution algorithm has been presented in appendix B. The chapter also deals with the pre-processing of the model, where burn durations of all fuel at different speeds are calculated.

Chapter 5 starts with the calculation of relevant properties and validation of the model against published data. Next, results from the first-law based analysis is presented. During these analyses, maximum brake torque condition have been maintained by tuning the model according to fuel, engine speed etc. Detailed, components-wise exergy analysis is presented next. Here, effect of different operating parameters on different exergy components have been studied and their results were shown. Next, distribution of total energy and exergies are presented for all six fuels to compare their relative performances. Finally, effects of mixture richness on the second law efficiency were studied and general conclusions about the sources of work potential loss and alternative fuels were drawn.

# Chapter 2

# Literature Review

The enormity of the present state of engine research makes reviewing it quite a challenge. Arguably, the best possible review to date would be the one written in 1988 [17]. However, research in many other areas like combustion, emission control, performance of alternative fuels, novel cycles and exergy have grown to a myriad level since then. This chapter attempts to review the most relevant ones in a chronological approach.

## 2.1 Spark Ignition Engine Modeling

The base point of spark ignition engine model is the thermodynamic model known as Otto cycle. Different models have been proposed modifying the assumptions or eliminating them; increasing in complexity. At the core of the model is the combustion process. Combustion is an exothermic process which releases energy in the form of heat. In spark ignition engines generally combustion is initiated at the end of compression stroke before TDC. In the ideal models, burn rate assumptions are made to get a constant volume combustion. Actual combustion process, however, is complex in nature. The complexities arise from phenomena like, non-uniform mixing of the charge, unsteady turbulent growth and propagation of the flame front, complex combustion chemistry in blend of hundreds of compounds and variations in the combustion chamber geometry [17]. Moreover, ideal models ignore the omnipresent effects of heat transfer, which introduces

significant variation from actual case. The constant volume assumption requires instantaneous burning, which is impossible due to finite burning velocities of the mixtures. More accurate models take a finite heat release approach in modeling the combustion process. Heywood [20], has made three broad classification of engine models based on their combustion modeling approach. These are

1. Zero-dimensional (thermodynamic),
2. Quasi-dimensional (thermodynamic with combustion chamber geometry inclusions),
3. Multi-dimensional (combination of thermodynamic model with combustion chamber flow dynamics).

In zero-dimensional models, empirical relations are used to determine the rate of charge burning. The thermodynamic governing equations, in this model, does not contain any partial derivative terms and time is the only independent variable. For quasi-dimensional models, a physical sub-model of the turbulent combustion process determines the burn rate. In multi-dimensional models, mass-, momentum-, energy-, and species-conversion equations are solved numerically in multi-dimensions to estimate the flame propagation through the combustion chamber. Although zero-dimensional models oversimplify the combustion process, multi-dimensional ones are not necessarily totally accurate in burn rate estimation as complex fluid flow and turbulent combustion introduces uncertainties. Even today, all three classes hold their respective places in the field due to their success in pointing out specific types of problems and parameters.

One of the earliest engine models was developed by Benson et al. (1977) showing good agreement with the measurements, but due to cyclic dispersion and maldistribution of fuel between cylinders the predictions of the emissions in the exhaust manifold adjacent to the cylinder were not so good [21]. Throughout the seventies and eighties Keck and co-workers have developed a number of correlations regarding burning velocity measurements and turbulent combustion [22, 23, 24]. Much of the later work in burning velocity and other combustion characteristics can be attributed to Bradley and co-workers [25, 26].

Bonatesta et al. (2008) studied the charge burn characteristics of a spark ignition engine fitted with a dual independent variable-valve-timing system at medium load and found changes in dilution mass fraction had the greatest influence in burn parameters, and presented empirical expressions for the flame development and the rapid burn angles [27]. Giansetti et al. (2007) worked with two new models for correlating residual fraction quantity, one based on 3-D computational fluid dynamic calculations and another one dimensional. Comparing the results with two different measurement techniques, they validated their model [28].

Another important section of engine research is the cycle-to-cycle variation. Closed-loop control of the combustion process in the internal-combustion engine on a cycle-to-cycle basis is desirable to achieve better fuel economy and reduce pollutant emissions. Morey et al. (2010) explored the possibility of monitoring the in-cylinder combustion process of a spark-ignition engine by measuring exhaust-gas temperature, and showed that coefficient of variation of maximum temperature follows the same trend as the coefficient of variation of indicated mean effective pressure [29]. Nakata et al (2011) investigated the impact of high-research-octane-number (RON) fuels on engine thermal efficiency, and showed that the lean boosted engine has higher potential to increase engine thermal efficiency than naturally aspirated (NA) engines and the combination of lean boosted engine and high-RON fuels gives around 44% engine thermal efficiency [30].

Reitz et al. (2011) have developed a reduced chemical kinetic mechanisms for the oxidation of representative surrogate components of a typical multi-component automotive fuel [9]. They have also been working on reacting flow simulation, development of KIVA and computational optimization of internal combustion engine simulations over the last decade [31]. Another flourishing field of computation is the large eddy simulation (LES) of combustion. For the appropriate applications, LES can offer significant advantages over traditional CFD approaches. For example, in internal combustion engines, LES can be used to study cycle-to-cycle variability, provide more design sensitivity for investigating both geometrical and operational changes, and produce more detailed and accurate results [32].

### 2.1.1 Developments of Thermodynamic Model

Zero-dimensional thermodynamic models are still the most popular among engine researchers for its simplicity and ease of application over a very wide range of problems that are still being addressed. Rakopoulos and co-workers have been using the thermodynamic models for second law based analysis [33, 18]. They also used thermodynamic formulation to investigate combustion irreversibilities [34, 35]. In another recent study, Dincer et al. (2010) used thermodynamic model to campare the performance of hydrogen combustion with gasoline [15]. There are numerous recent studies with the zero-dimensional thermodynamic model to explore problems like realistic heat transfer [36, 37], engine friction [38], etc.

Fontana et al. (2010) investigated the exhaust gas recirculation technique by carrying out an experimental analysis of a naturally aspirated, spark-ignition engine. Their results indicate that due to lower temperature levels within the combustion chamber, there is a decreased octane requirement, thus an optimal choice of spark advance is possible [39]. Shehata (2010)investigated cylinder pressure, performance parameters, heat release, specific heat ratio and duration of combustion for multi cylinder spark ignition engine using gasoline, kerosene and liquefied petroleum gas (LPG) separately. Employing fast fourier transformations (FFT) to cylinder pressure data transform from time domain into frequency domain he developed develop empirical correlation for calculating cylinder pressures at different engine speeds and different fuels [40].

Overall, thermodynamic modeling of spark ignition engines is one of the most vibrant branches of engine research worldwide at present. Increase in computational power is widening the range of problems it can address day by day.

### 2.1.2 Engine Heat Transfer

Throughout the last century, a number of heat transfer models have been developed, each getting more powerful as the power of digital computation grew. Nevertheless, the heat transfer problem is still not well understood because of the complex nature involving rapid temperature and heat flux swings, changing geometry, transient three-dimensional reactive flow patterns, instability and turbulence, cycle to cycle and engine to engine variations etc. [41]. This resulted in

a primordial dependence on correlations fitted with actual measurements.

The earlier models were global (one-zone) thermodynamic models, later growing into zonal, one-dimensional analytical and numerical fluid dynamic and to multidimensional numerical fluid-dynamic models. The earliest global correlation was from Nusselt (1923), whose mean piston speed term was later modified by Brilling, and Van Tyen [41].

Though, Eichelberg made the first measurement of the instantaneous heat flux, it was Annand (1963), who reviewed the past models and proposed a correlation for instantaneous spatial average coefficients [42]. Annand included parameters to account for the intensity of charge motion and radiant heat flux assuming gray-body radiation, and suggested that gas properties must be taken as the bulk-mean-temperature instead of the average of surface and mixture temperature calculated from the ideal gas law. He later extended his formula in collaboration with Ma by examining experimental results obtained in a DI diesel engine [41].

Possibly the most successful heat transfer correlation was proposed by Woschni in 1967, which was also a correlation for instantaneous spatial average coefficients based on the similarity law of steady turbulent heat transfer [43]. He decided that the experimental method using surface temperature was not suitable because of the considerable scatter in such data, and used a global heat balance instead to determine the total heat transferred to the combustion chamber walls for each process of a complete engine cycle [41, 43]. It is to be noted that Woschni formulated this correlation originally for a diesel engine, however it works surprisingly well with spark ignition engines.

For thermal stress calculations, correlations for instantaneous local coefficients have been proposed by Lefeuvre et al., and Dent and Sulaiman [44]. An alternative way was proposed by Krieger and Borman through zonal modeling, where the combustion chamber is divided into a relatively small number of zones each with its own temperature, heat-transfer coefficient, and heat-transfer surface history [17].

Extensive investigations have also been carried out for intake and exhaust system heat transfer, which is driven by much higher velocities than in-cylinder heat transfer. Though intake system heat transfer is usually described by steady,

turbulent pipe-flow correlations, the presence of liquid fuel in the intake makes the heat-transfer phenomena complicated [41]. More recent works on exhaust system heat transfer suggest it to be the largest in the entire cycle due to high gas velocities and temperatures, and large scale fluid motions [37].

Due to cycle-to-cyle and engine-to-engine variability [29], new models have been proposed [36], however they also are facing similar problems in being accounted universal. In case of alternative fuels, traditional models are no more satisfactory and new models are replacing them [11]. On the other hand majority of the researchers working with traditional fuels still prefer Woschni's correlation as it still is the best choice without being computationally prohibitive [45, 14].

### 2.1.3 Study of Finite Heat Release using Wiebe Function

Comprehensive combustion modeling can involve three-dimensional turbulent flow formulation with chemical kinetics. On the other hand, in simplified, one-dimensional analysis, the turbulent flame propagation can be estimated on the information available on turbulence intensity, spark timing, and laminar and turbulent burning velocities. Although the three-dimensional models try to address all the relevant physical and chemical phenomena, they may not be more accurate than the simpler models at predicting pressure and temperature because of the many uncertainties in modeling these complex phenomena [46].

In the nineteen-fifties, Russian engineer and scientist Ivan Ivanovitch Wiebe proposed a combustion rate model based on the chain reaction theory [47] in the following form:

$$x_b(\theta) = \begin{cases} 1 - \exp\left[-a\left(\frac{\theta-\theta_s}{\Delta\theta_b}\right)^m\right], & \text{if } \theta_s \leq \theta \leq \theta_s + \theta_b \\ 0, & \text{if } \theta < \theta_s,\ \theta > \theta_s + \theta_b \end{cases}$$

where, $x_b(\theta)$, is the mass fraction burnt at a crank-angle $\theta$, $\theta_s$ is the crank angle at the start of combustion, $\Delta\theta_b$ is the total combustion duration, $m$ is the Wiebe form factor and $a$ is the Wiebe efficiency factor.

Although not numerous, but several works can be found in the literature on parametric studies with the Wiebe function. Sher et al. [48] worked with

hydrogen-enriched gasoline. In modeling the combustion process, they used the correlation of laminar burning velocity by Metghalchi et al. [23], and suggested that both ignition delay and combustion duration are strong functions of burning velocity and engine speed. Rousseau et al.[13] studied the combustion characteristics of natural gas in a lean burn SI engine. In a single zone thermodynamic model, they considered the ignition delay period as 1% mass fraction burned. Within their working range, they found the Wiebe parameters for natural gas combustion to be linear functions of spark timing and equivalence ratio.

Bayraktar and Durgun [49] proposed correlation for combustion duration with gasoline. However, they did not consider the ignition delay period, and took the combustion duration as the crank angle interval from the time of spark discharge to the instant at which the charge is fully burned. Showing that for a given fuel, the combustion duration varies with compression ratio ($r_c$), engine speed ($N$), equivalence ratio and spark timing ($\theta_{spark}$), they fitted their experimental data to propose correlation with respect to reference operating conditions.

Lindström et al. [50] did a comprehensive parametric study on the effects of various engine parameters on Wiebe parameters. They used the laminar burning velocity correlations provided by Heywood [17]. Bonatesta and Shayler [27] studied the combustion process with variable valve timing. They found ignition delay and combustion duration to decrease as load is increased keeping other parameters constant. Using a modified laminar burning velocity corellation, they argued that, charge dilution due to valve overlap significantly influences burn characteristics of a given fuel and proposed ignition delay and combustion duration correlations considering charge density. They also incorporated effect of spark timing on 90% mass fraction burn duration and Wiebe form factor for gasoline combustion in a later work [51].

## 2.2 Use of Alternative Fuels in SI Engines

With the depletion of available fuel reserves, and the restrictions on exhaust emissions, research in the alternatives to traditional hydrocarbons have become pivotal in engine design. Alternative fuels are of interest since they can be refined from renewable feedstocks, and their emission levels can be much lower than

those of gasoline and diesel fueled engines [52]. The smaller volumetric energy density of alternative fuels is one of the major technical obstacle in engine design. They also lack a wide scale distribution and fueling infrastructure compared to for example, gasoline. However, alternative fuels have higher octane levels than gasoline, and can be operated at higher compression levels, and thus at higher efficiency [52]. Similarly other relevant properties include vapour pressure, heat of reaction, latent enthalpy of vaporization, and the relative volumes of energy. Since the internal combustion engine is air breathing, for a given equivalence ratio the energy injected depends on the fuel [53]. This is why numerous research is still active in the study of the behavior of the alternative fuels.

Over the last twenty years, burning velocities of different fuels have been calculated and correlations were developed. In 1982, Metghalchi and Keck developed correlations for methanol–isooctane blends [23]. Two years later, Gülder did the same for ethanol–isooctane blends [54]. Correlation for hydrogen and hydrogen-hydrocarbon mixture burning velocities were given by Milton and Keck who made the measurements in the same year. More recently Broustail et al. reviewed the previous alcohol-gasoline correlations and gave one for butanol-gasoline blends [55]. Bardley and co-workers have made burning velocity measurements of iso-octane–, and n-heptane–air mixtures [25], while Gu et al.(2000) measured the burning velocities of methane–air mixtures and proposed correlations [26].

Effect of different fuels in pure form and as blends in the spark ignition engine has long been a popular topic of research. Yacoub et al. (1998) blended alcohols with carbon numbers ranging from $C_1$ to $C_5$ individually with unleaded test gasoline. While lower alcohols improved knock resistance, higher alcohols showed degraded knock resistance when compared with neat gasoline. They also found that all alcohol-gasoline blends have reduction in CO emissions but higher alcohol-gasoline blends showed a pronounced increase in NOx emission rates when operating at high compression ratios. All the alcohols showed increased aldehyde emission [10]. Szwaja et al. (2010) studied the applications of n-butanol as a blending agent additive to gasoline to reduce the fossil part in the fuel mixture and in this way to reduce life cycle $CO_2$ emissions [8]. Çelik et al. (2011) used pure methanol at high compression ratios, and found good knock resistance. They

also recorded some decreases in CO, $CO_2$ and NOx emissions without any noticeable power loss when using methanol at the compression ratio of 6. By increasing the compression ratio from 6 to 10 with methanol, the engine power and brake thermal efficiency increased by up to 14% and 36%, respectively. Moreover, CO, $CO_2$ and NOx emissions were reduced [56].

The use of hydrogen as an engine fuel has a great potential for reducing exhaust emissions. With the exception of a little amount of hydrocarbon emissions originating from the lubricating oil, NOx is the only pollutant emitted [57].Sher et al. (1987) developed a model of a four-stroke engine fueled with hydrogen enriched gasoline including an empirical expression for the combustion process to represent the effect of the hydrogen enrichment on the combustion rate [48]. Verhelst et al. (2010) presented a comprehensive overview of the fundamentals of hydrogen combustion, details on the different mixture formation strategies and their emissions characteristics, measures to convert existing vehicles etc. [11].

Bayraktar et al. (2005) compared the performance of LPG in a spark ignition engine and showed that if LPG fueled SI engines are operated at the same conditions with those of gasoline fueled engines, significant improvements in exhaust emissions can be achieved [12]. Daniel et al. (2012) have worked with a new gasoline-alternative biofuel candidate, 2,5-dimethylfuran (DMF)and compared it to gasoline, ethanol, butanol and methanol so that its sensitivity can be positioned relatively [7]. They found that the four biofuels had improved spark sensitivity due to improved anti-knock qualities and sometimes increased charge-cooling which allowed the increase of $CO_2$ to be better minimized than with gasoline. They further recomended DMF as a cold-start fuel since it was the only biofuel to produce high exhaust gas temperatures, similar to gasoline and helpful for fast catalyst light-off, whilst maintaining high combustion stabilities.

Ebrahimi (2011) showed that the influence of first derivative of the specific heat ratio on the combustion parameters for natural gas operation is higher than that for gasoline operation. He also argued that the first derivative of the specific heat ratio for determination of combustion parameters should not be ignored [58].

Over the last decade, research in alternative fuels has been undertaken to allow different fuels with as little modification to the engine as possible. This objective has been mostly met with success in case of alcohol blends and natural

gas. Hydrogen whoever has proved harder than others in this aspect.

## 2.3 Second Law based Analysis

Energy in our world is found manifested in many forms, each with its own characteristics and its quality. The historical acceptance of the quality of energy finds itself in performing mechanical work. Hence, quality of energy today is synonymous with its capacity to cause change or do useful work. Natural observation shows that particular forms of energy differ in their ability to be transformed into other forms. Moreover, this ability is found to be dependent on composition and state properties of both system and surrounding. It is then only rational to have the quality index of energy acknowledge the transformability of a certain form of energy with respect to the environment; a fact overlooked by the universal law of energy conservation. Exergy bridges this gap in the analysis of energy transformations by using the second law of thermodynamics, which imposes certain restrictions in the direction and amount of energy transformations. Exergy is a measure of the maximum derivable work output (or, the minimum required work input) from a given thermodynamic process with specified conditions for both system and surrounding [3].

Though the quest for qualitative energy index can be traced back to the work of Gibbs [59] as available energy, the term exergy was first coined by Zoran Rant in 1953 from greek root words [60]. Exergy means that fraction of the total energy that can be extracted as work. The concept of exergy has been greatly explored and brought up to the applied sciences over the past 50 years [18].

Much of the earlier works on the developments in the applied level can be attributed to Szargut and Kotas in the eighties [61, 62, 63]. Specially the works on standard chemical exergy of the elements and some compounds by Szargut et al. has to be mentioned as one of the seminal works in this field [64, 3]. On the other hand, there has been a parallel theoretical development of the exergy concept from pure thermodynamic point of view by Haywood [65] and Sussman [66, 67].

It was not long before the concepts of second law analysis and exergy destruction started appearing in combustion analyses. In 1983, Beretta and Keck [68]

produced an analytical solution of energy and entropy balance in a combustion chamber. One of the pioneering work with exergy in internal combustion engine application was presented by Van Gerpen et al. [69] in 1990. They used a two zone thermodynamic model for calculating irreversibility in diesel combustion. Rakopoulos [33] in 1993 presented a detailed exergetic analysis using a two-zone spark ignition model with experimental validations. He carried out a number of parametric analyses and compared the first- and second-law efficiencies. More recently, Teh et al. also did an elaborate second law analysis for efficiency maximization in spark ignition engines [70, 71].

The concept of exergy makes it ideal for comparing the relative superiority of different energy sources. This aspect has been used by a large number of researchers over the last decade for the comparison of alternative fuel performance. While Nieminen et al. [15] worked with hydrogen, Rakopoulos et al. analyzed hydrogen/natural gas blends and biogas/hydrogen blends from second-law perspective [35, 34]. Caton worked with eight different fuels including alcohols, hydrogen etc., and compared their performances from both first law and second law perspectives [14]. He showed, for the same operating conditions, the destruction of exergy during the combustion process ranged between about 8% (for carbon monoxide) and 21% (for isooctane) of the fuel exergy depending on the specific fuel, and commented that the differences of the exergy destruction during combustion were related to the complexity of the fuel molecule and the presence (or lack) of oxygen atoms in the fuel molecule.

Among other properties, combustion characteristics of a fuel is largely dependent on its burning velocity. However, it has been noted that the aforementioned modeling works involving comparison of different fuels took little notice of this fact. For example, the fastest combustion of hydrogen produces the least amount of combustion irreversibility, so the engine model should adjust according to its burning velocity. In the present work necessary adjustments have been made in the model for different fuels according to their respective burning velocities before detailed thermodynamic analyses [16].

# Chapter 3

# Exergy

## 3.1 Exergy and its Physical Meaning

The concept of availability or in a more preferable nomenclature [60], exergy comes purely from thermodynamics. At the core, it is an extension of the second law of thermodynamics, constrained by the bounds of first law, expressing the quality of energy in a useful form. Although the second law has had its root stretched for more than a century, the concept of exergy is relatively new and in the form of a tool for thermodynamic assessment, its widespread use is rather a recent phenomena. In this chapter, after establishing the necessary background, necessary relations will be developed for exergetic calculations in a control region. Modifications will be made from these relations, as necessary, when they are applied to a closed- or control mass system.

The formal definition of exergy of a system or resource can be given [72] as the maximum amount of work that can be obtained from the system or resource when it is brought to equilibrium with the surroundings through reversible processes in which the system is allowed to interact only with the environment.

Before introducing mathematical rigour, it is important to establish some important terminology unique to thermodynamic, or to be more specific, exergetic analyses.

**Environment:** The environment is defined as a very large body or medium in the state of perfect thermodynamic equilibrium implying there is no gradients

or differences involving pressure, temperature, chemical potential, kinetic or potential energy. The environment may interact with systems in three different ways:

1. Through thermal interaction as a reservoir of thermal energy at temperature $T_0$.
2. Through mechanical interaction as a reservoir of unusable $P_0 \mathrm{d}V$ work.
3. Through chemical interaction as a reservoir of a substance of low chemical potential in stable equilibrium.

For the present work the environment has been defined at a temperature $T_0 = 298.15\,\mathrm{K}$, and pressure $P_0 = 1.01325\,\mathrm{bar}$. The chemical composition of the reference environment is taken as defined in [3]:

Table 3.1: Reference Substances

| Chemical element | Chemical symbol | Mole fraction in dry air | Standard partial pressure in the environment $P_{i,00}$, bar |
|---|---|---|---|
| Ar | Ar | 0.00933 | 0.00907 |
| C | $CO_2$ | 0.0003 | 0.000294 |
| D | $D_2O(g)$ | – | 0.00000137 |
| H | $H_2O(g)$ | – | 0.0088 |
| He | He | 0.000005 | 0.0000049 |
| Kr | Kr | 0.000001 | 0.00000098 |
| N | $N_2$ | 0.7803 | 0.7583 |
| Ne | Ne | 0.000018 | 0.0000177 |
| O | $O_2$ | 0.2099 | 0.2040 |
| Xe | Xe | 0.00000009 | 0.000000088 |

**Equilibrium:** Definition of two types of equilibria are necessary,

**Restricted Equilibrium ($P_0, T_0$):** At restricted equilibrium, mechanical and thermal equilibrium between the system and the environment is established, i.e., $P = P_0$ and $T = T_0$. The term *restricted* implies there is a physical restriction between the system and environment

preventing exchange of matter. The state of restricted equilibrium will be referred to as the environmental state.

**Unrestricted Equilibrium ($P_{00}, T_{00}, x_{00}$):** In addition to mechanical and thermal equilibrium ($P = P_0 = P_{00}$ and $T = T_0 = T_{00}$), when conditions for chemical equilibrium, i.e., equalization of chemical potentials is satisfied between the system and the surrounding, the unrestricted equilibrium or the dead state is achieved.

**Reference Substances:** Suitable substances that are present in the defined environment with known concentration, for calculation of chemical exergy of any given element or species. Among different environmental substances containing a particular chemical element the one with the lowest chemical potential is most suitable as a reference substance. For example, the reference substances for $C_8H_{18}$ are $CO_2$ (for carbon) and $H_2O$ (for hydrogen) in their dead states.

## 3.2 Classification of Exergy of a Thermodynamic System

A brief component-wise summary will be given in this section. First exergy transfer with work and heat interaction, which are common to both control-region and control-mass formulation will be presented. The exergy transfer with a given mass of matter will be detailed. From there, exergy of a closed system shall be presented.

### 3.2.1 Exergy associated with work transfer, $(a_W)$

Exergy associated with work transfer is equal in magnitude and expressed with the same sign as the amount work it corresponds to. Hence,

$$a_W = w = w_x + w_{cs} \tag{3.1}$$

where $w_x$ is the shaft work, and $w_{cs}$ is the work due to change in volume of the

control region. It should be noted that, work transfer denoted by $w$ is the useful work, which considers the losses incurred to the environment or gains achieved from it, defined as

$$w = \int (P - P_0) d\nu \tag{3.2}$$

Since, exergy is defined to be the maximum possible work output considering all practical losses, this definition of useful work is synonymous to the definition of exergy of a system.

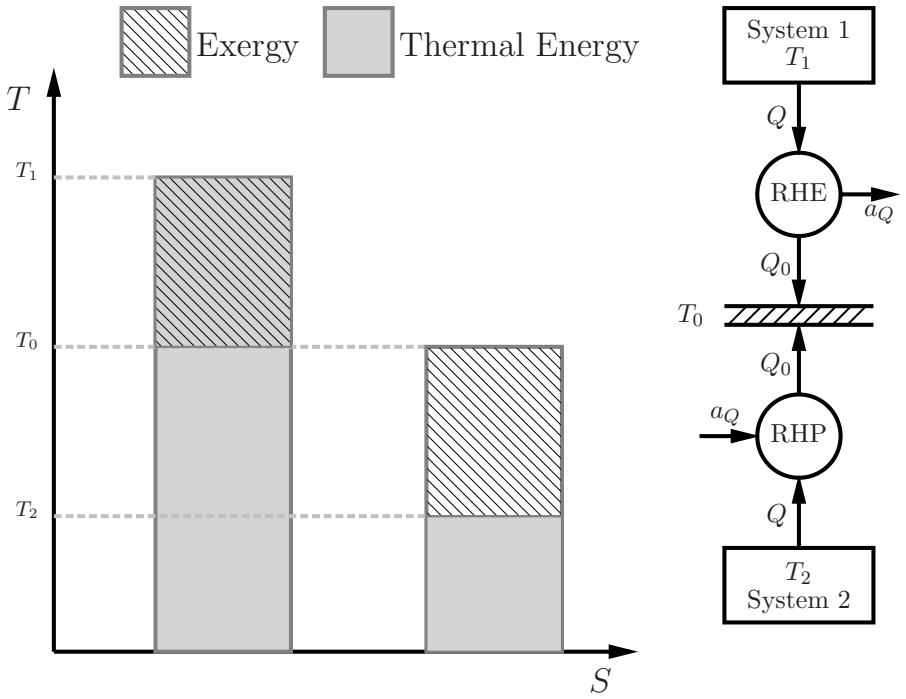


Figure 3.1: Exergy Transfer with Heat

### 3.2.2 Exergy associated with heat transfer, $(a_Q)$

The exergy of heat transfer at the control surface is determined from the maximum obtainable work from it using the environment as a reservoir of zero-grade thermal energy. For a heat transfer of $q$ and a temperature at the control surface where heat transfer is taking place $T$, the maximum possible conversion from

thermal efficiency to work is

$$a_Q = \left[1 - \frac{T_0}{T}\right] \cdot q \tag{3.3}$$

When the source temperature is lower than that of the environment, the exergy can be viewed as the minimum work input required in a reversible heat pump (RHP) to maintain that low temperature, as shown in Fig. 3.1.

### 3.2.3 Themomechanical exergy, $(a_{th})$

The thermomechanical exergy is equal to the maximum amount of work available when a stream of substance is brought from its initial state to the environmental state defined by $P_0$ and $T_0$, by physical processes involving only thermal interaction with the environment. For any given state it is given by

$$a_{th} = (h - T_0 s) - (h_0 - T_0 s_0) \tag{3.4}$$

where,

| | |
|---|---|
| $h$ | is the specific enthalpy of the stream at the given state |
| $s$ | is the specific entropy of the stream at the given state |
| $h_0$ | is the specific enthalpy of the stream at environmental state |
| $s_0$ | is the specific entropy of the stream at environmental state |

For a closed-mass system the expression is changed to

$$a_{th} = (u + P_0 \upsilon - T_0 s) - (u_0 + P_0 \upsilon_0 - T_0 s_0) \tag{3.5}$$

where,

| | |
|---|---|
| $u$ | is the specific internal energy at the given state |
| $\upsilon$ | is the specific volume at the given state |
| $u_0$ | is the specific internal energy at environmental state |
| $\upsilon_0$ | is the specific volume at environmental state |

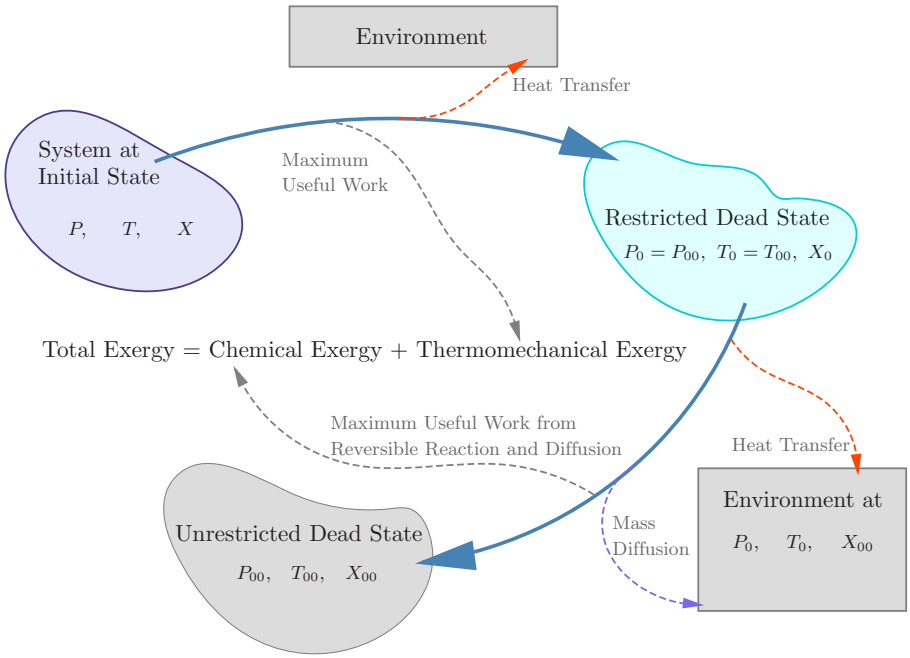


Figure 3.2: Components of Exergy

### 3.2.4 Chemical exergy, $(a_{ch})$

Thermodynamically, the maximum work of a chemical reaction can be put as,

$$[w_x]_{MAX} = -\Delta g^0 \tag{3.6}$$

where $\Delta g^0$ is the standard value of Gibbs function of the reaction. The relevance if equation (3.6) is not limited to chemical processes. Work in any reversible isothermal steady flow process (e.g., diffusion) is equal to the decrease of the Gibbs function of the stream [3].

#### 3.2.4.1 Chemical exergy of reference substances

When the system contains any of the reference substances, its difference in concentration from that of the environment is the source of work potential which could be equilibrated through diffusion. Hence, molar chemical exergy for a ref-

erence substance is given by,

$$\tilde{a}_{ch,rs} = (\mu_0 - \mu_{00})_{rs} \tag{3.7}$$

which under ideal gas assumptions, can be shown as

$$\tilde{a}_{ch,rs} = RT_0 \ln \frac{P_0}{P_{00,rs}} \tag{3.8}$$

where, the subscript $rs$ denotes reference substance, and

| | |
|---|---|
| $\mu_0$ | is the chemical potential of the substance at environmental state |
| $\mu_{00}$ | is the chemical potential of the substance at dead state |
| $R$ | is the gas constant |
| $P_{00,rs}$ | is the partial pressure of the substance in the reference environment |

#### 3.2.4.2 Chemical exergy of non-reference substances

These substances are first converted to reference substances using fictitious reversible reactions involving only one mole of the reference substance while only heat transfer with the atmosphere is allowed. Thus chemical exergy for these substances comprises of the the maximum work from these reactions, minus chemical exergies of the reactant reference substances taken from the environment, plus chemical exergies of the product reference substances. If the reference reaction takes $j$ reference reactant species from the environment and one mole of the non-reference substance, and produces $k$ reference products, the maximum work of this reaction is

$$-\Delta g^0 = -\left( \sum_{prod,rs} n_k g_k^0 - \sum_{reac,rs} n_j g_j^0 - g_{nrs}^0 \right) \tag{3.9}$$

Hence the expression for molar chemical exergy becomes

$$\tilde{a}_{ch,nrs} = -\Delta g^0 - \sum_{reac} n_j \ (\tilde{a}_{ch,rs})_j + \sum_{prod} n_k \ (\tilde{a}_{ch,rs})_k \tag{3.10}$$

where, the subscript $nrs$ denotes non-reference substance, and

$n_j$ is the number of moles of $j$-th reactant reference substance
$n_k$ is the number of moles of $k$-th product reference substance

#### 3.2.4.3 Chemical exergy of a mixture

If the substances form an ideal gas mixture, for example gaseous fuels, combustion products, etc., the constituents of the mixture are separated by an ideal device through an reversible and isothermal separation and compression process. The work required for these precesses per mole of the gas mixture is

$$\sum_i [\tilde{w}_{mix}]_{rev} = \tilde{R}T_0 \sum_i x_i \ln x_i \tag{3.11}$$

where $x_i$ is the mole fraction of the $i$-th component in the mixture. Thus exergy of the mixture is equal to the sum of molar chemical exergies of the constituents plus the reversible work that goes into separating them.

$$\tilde{a}_{ch,mix} = \sum_i \tilde{a}_{ch,i} + \tilde{R}T_0 \sum_i x_i \ln x_i \tag{3.12}$$

Investigation of equation (3.12) reveals the last summation term on the right to be negative. Physically, it signifies the reduction in work potential of the constituents as they form a mixture.

## 3.3 Exergy Balance of a Thermodynamic System

With the components defined, total exergy of a system or stream is defined as the sum of thermomechanical and chemical components.

$$a_{total} = a_{th} + a_{ch} \tag{3.13}$$

where for open systems, $a_{th}$ is calculated using equation (3.4), and for a closed system equation (3.5) is used instead.

Hence, the general exergy balance can now be expressed in extensive form using the component definitions stated in the previous subsections as

$$A_i + A_Q = A_e + A_W + I \tag{3.14}$$

where

| | |
|---|---|
| $A_i$ | is the initial exergy of the system or stream, |
| $A_e$ | is the final exergy of the system or stream, |
| $A_Q$ | is the exergy transfer with heat, |
| $A_W$ | is the exergy transfer with work, and |
| $I$ | is the generated irreversibility defined as follows. |

### 3.3.1 Irreversibility

Exergy is not a conserved property. It is destroyed by the generation of entropy. The second law provides useful relations concerning entropy generation through dissipative (e.g., fluid friction, ohmic resistance) and spontaneous non-equilibrium processes (e.g., spontaneous chemical reactions, free diffusion, unrestrained expansion, equalisation of temperature, etc.), called in general exergetic terms, irreversibilities of a process. The Gouy-Stodola relation [3] provides a convenient measure of irreversibility of a process in an open system with multiple inlets and outlets, and a number of thermal interactions at different temperatures as

$$I = T_0 \left[ \sum_{OUT} m_e s_e - \sum_{IN} m_i s_i - \sum_r \frac{Q_r}{T_r} \right] \tag{3.15}$$

For a closed mass, which can be modified as

$$I = T_0 \left[ \Delta S - \sum_r \frac{Q_r}{T_r} \right] \tag{3.16}$$

where $T_r$ is the temperature at the system boundary with a heat interaction $Q_r$.

### 3.3.2 Rational Exergetic Efficiency

Rational exergetic efficiency or, *effectiveness* is defined as the ratio of the sum of all output exergy, $A_{Output}$ over the sum of all input exergy, $A_{Output}$

$$\epsilon = \frac{A_{Outout}}{A_{Input}} \tag{3.17}$$

This definition of efficiency is superior to the conventional definition as it considers the quality of energy using the exergy concept. Thus, it allows more sensible direction in energy auditing, decision making and thermodynamic design of power systems.

# Chapter 4

# Thermodynamic Modeling of SI Engine Processes

In the realm of engine research, many show a penchant for experimental works, since they are without doubt, the true results under practical circumstances. However, experimentation must also face problems like reliability of measurement, economic and time constraints, and most importantly, most of the key variables must be kept constant in order to study a particular characteristics. Modeling of engine processes allows to overcome these problems with ease. Specially, effects parametric variations on one or a group of operating characteristics can be easily studied through an engine model. With adequate experimental validation, the analysis can be extended into much depth with significant reduction in expenses in time and money. Increase in computational power and employment of strict regulations has been working as the driving force in the phenomenal evolution of analyses of engine processes. As our understanding of the physics that governs these processes gets better, the models give a closer approximation of the actual processes and so do the results [16]. Modeling of internal combustion engine processes and subsequent simulation provides the baseline of modern engine analysis.

The basic spark ignition cycle, consisting of induction, compression, combustion, expansion and exhaust strokes are the starting point for thermodynamic analysis of an internal combustion engine. In order to get beyond the ideal cy-

cle, its assumptions must be replaced with actual phenomena. For example, the isentropic compression and expansion processes must accommodate heat transfer effects, while intake and exhaust processes must be defined in such a way that residual fractions can be reliably calculated. Compared to other processes, the combustion and expansion of burning gases, is ruefully inaccurate in its assumptions. This is why, combustion modeling becomes the prime concern when an engine model is to be developed. Wiebe function has been successfully used for a long time in thermodynamic models to estimate the actual phased burn characteristics. The properties however must be calculated through detailed equilibrium analysis, which is why many detailed chemical equilibrium and kinetics algorithms are used today to reliably estimate in-cylinder properties.

## 4.1 Geometric Parameters

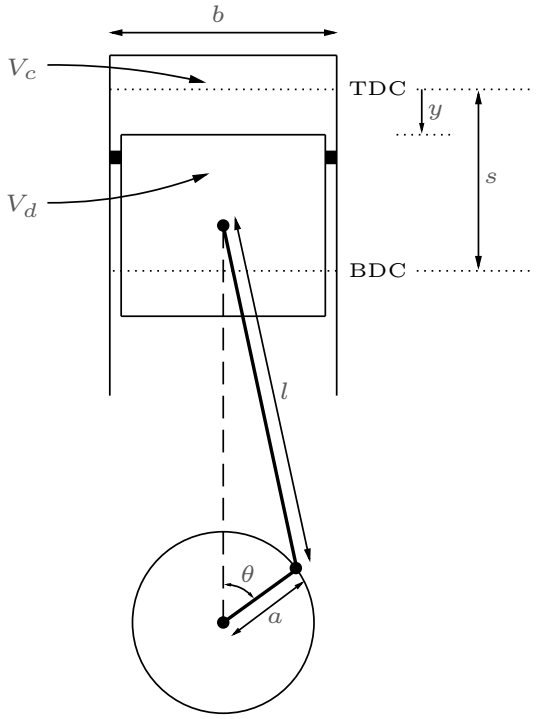


Figure 4.1: Geometry of cylinder, piston, connecting rod and crankshaft

A number of geometric parameters are used in the mathematical description of the engine. Figure 4.1 represents a cylinder, crankshaft, connecting rod and head assembly of an engine. Geometric parameters such as, bore, $b$; connecting rod length, $l$; crank radius, $a$; stroke, $s = 2a$; and crank angle, $\theta$ are of particular interest. At a crank angle of $\theta = 0°$, the charge volume is minimum. At this position, piston is said to be at the top dead center (TDC) and the volume ($V_{TDC}$) is commonly referred to as the clearance volume, $V_c$. On the other hand, at a crank angle of $\theta = 180°$, the charge volume is maximum. At this position, piston is said to be at the bottom dead center (BDC) and the volume is $V_{BDC}$. The ratio of the maximum volume to the minimum volume is defined as the compression ratio, $R_c$,

$$R_c = \frac{V_{BDC}}{V_{TDC}} = \frac{V_{BDC}}{V_c} \tag{4.1}$$

The displacement volume, $V_d$, is the difference between the maximum and minimum volume. For a single cylinder,

$$V_d = V_{BDC} - V_{TDC} = V_{BDC} - V_c = \frac{\pi}{4} b^2 s \tag{4.2}$$

The instantaneous stroke, $y(\theta)$, is given as [17],

$$y(\theta) = l + a - \left[ \left( l^2 - a^2 \sin^2 \theta \right)^{1/2} + a \cos \theta \right] \tag{4.3}$$

And the instantaneous volume, $V(\theta)$, at any crank angle is [17]

$$\begin{aligned} V(\theta) &= V_c + \frac{\pi}{4} b^2 y \\ &= \frac{V_d}{R_c - 1} + \frac{V_d}{2} \left[ \frac{2l}{s} + 1 - \cos \theta - \left\{ \left( \frac{2l}{s} \right)^2 - \sin^2 \theta \right\}^{1/2} \right] \end{aligned} \tag{4.4}$$

The combustion chamber surface area, $A(\theta)$, at a crank angle $\theta$ is given by [17],

$$
\begin{aligned}
A(\theta) &= A_{piston} + A_{head} + A_{wall} \\
&= \frac{\pi}{4} b^2 + \frac{\pi}{4} b^2 + \pi b y \\
&= 2V_d \left[ \frac{1}{s} + \frac{1}{b} \left\{ \frac{2l}{s} + 1 - \cos\theta - \left( \left( \frac{2l}{s} \right)^2 - \sin^2\theta \right)^{1/2} \right\} \right]
\end{aligned} \tag{4.5}
$$

The mean piston, $\bar{U}_p$, speed for a rotational speed of $N$ revolutions per second is,

$$
\bar{U}_p = 2Ns \tag{4.6}
$$

While the instantaneous piston speed, $U_p$, can be found by differentiating the instantaneous stroke, $y$, with respect to time [17].

$$
\begin{aligned}
U_p(\theta) &= \frac{\mathrm{d}}{\mathrm{d}t} y(\theta) \\
&= 2\pi N \frac{\mathrm{d}}{\mathrm{d}\theta} y(\theta) \\
&= 2\pi N\, a \sin\theta \left[ 1 + \frac{\cos\theta}{\left\{ \left( \frac{l}{a} \right)^2 - \sin^2\theta \right\}^{1/2}} \right] \\
&= \frac{\pi}{2} \bar{U}_p \sin\theta \left[ 1 + \frac{\cos\theta}{\left\{ \left( \frac{l}{a} \right)^2 - \sin^2\theta \right\}^{1/2}} \right]
\end{aligned} \tag{4.7}
$$

## 4.2 The Spark Ignition Cycle

### 4.2.1 Ideal Cycle Model

The ideal thermodynamic cycle for spark ignition engines, the Otto cycle, breaks the engine operation into a sequence of separate processes as shown in figure 4.2. These are intake $(6-1)$, compression $(1-2)$, combustion $(2-3)$, expansion

$(3-4)$, and exhaust $(4-5-6)$. The assumptions required for such simplification changes the model in varying degrees from the actual case. For example, the isentropic assumption during the compression process produces very little variation from the actual, while the constant volume and adiabatic assumptions during the expansion stroke induces large deviation from the real cycle. Applying the first and second laws of thermodynamics, during compression stroke

$$\frac{\upsilon_1}{\upsilon_2} = R_c, \tag{4.8}$$

where $\upsilon_i$ is the specific volume of the mixture at state $i$. The process being adiabatic and reversible

$$s_1 = s_2 \tag{4.9}$$

And the compression work is

$$W_C = U_1 - U_2 = m(u_1 - u_2) \tag{4.10}$$

where $u_i$ is the specific internal energy of the mixture of mass $m$ at state $i$. During combustion, considering the ideal assumptions,

$$\upsilon_2 = \upsilon_3 \tag{4.11}$$

and

$$u_3 - u_2 = 0 \tag{4.12}$$

Finally, during expansion

$$\frac{\upsilon_4}{\upsilon_3} = R_c, \tag{4.13}$$

and

$$s_4 = s_3 \tag{4.14}$$

The expansion work is

$$W_E = U_3 - U_4 = m(u_3 - u_4) \tag{4.15}$$

The state of the mixture at point 1 in the cycle depends on the intake mixture

properties and the residual gas properties at the end of the exhaust stroke [17].

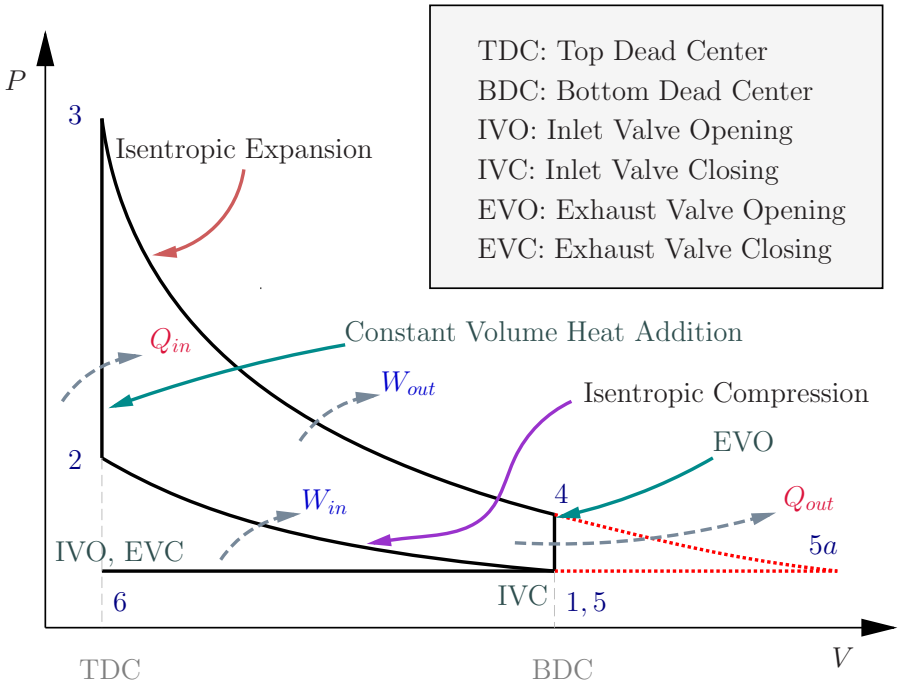


Figure 4.2: Ideal Spark Ignition Cycle

### 4.2.2 Intake and Exhaust Processes

At exhaust valve opening (point 4), at the bottom dead center, an expansion of the gases take place due to large pressure gradients. This is known as blowdown. One school of authors like Ferguson et al. [52] models this phenomena as isentropic with the gas expanding in a fictitious closed system from state 4 to state $5a$. However, unlike the closed expansion process from state 3 to state 4, the portion of gas coming out through the exhaust port goes through unrestrained expansion. Hence the isentropic assumption is inappropriate. From figure 4.3, volume before blowdown was $V_4$ and volume after blowdown is $V_{5a} = V_5 + V_{e5}$. As suggested by Ferguson et al. [52], if we ignore heat transfer for the process, the energy equation

for a gas expanding into an evacuated space yields

$$Q_{4-5a} - W_{4-5a} = U_{5a} - U_4$$

or

$$U_{5a} = U_4$$

which for an ideal gas becomes

$$T_{5a} = T_4$$

The change in entropy due to this process,

$$(S_{5a} - S_4)_{isol} = \frac{P_4 V_4}{T_4} \ln \frac{V_{5a}}{V_4} > 0$$

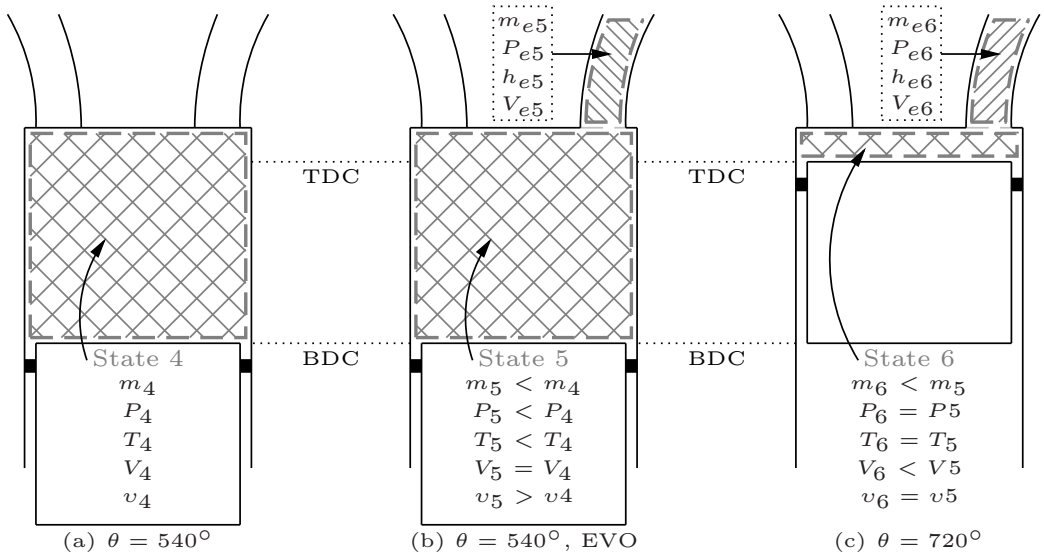


Figure 4.3: Blowdown and Exhaust Stroke

Hence, the present work starts the exhaust modeling by taking the blowdown process in an open system in two stages. As detailed in figure 4.3 (a) and (b), an open system is defined where mixture of mass $m_{e5}$ has throttled out, while mixture of mass $m_5$ is left inside during blowdown which expands isentropically. It is assumed that the kinetic energy acquired by each gas element as it is accelerated through the exhaust valve is dissipated in a turbulent mixing process in the

exhaust port into internal energy and flow work [17]. Using the unsteady state energy equation

$$\left(\frac{dE}{dt}\right)_{CV} = \dot{Q} - \dot{W} + \dot{m}_{in}h_{in} - \dot{m}_{out}h_{out}$$

Considering the adiabatic assumption, noting that $V_4 = V_5$, and integrating over time

$$U_5 - U_4 = -m_{e5}h_{e5} \tag{4.16}$$

Similarly, for the exhaust phase (figure 4.3 (b)-(c))

$$U_6 - U_5 = -P_e(V_6 - V_5) - m_{e6}h_{e6} \tag{4.17}$$

where $P_e = P_5 = P_6$ is the exhaust manifold pressure. Now adding equations (4.16) and (4.17)

$$U_6 - U_4 = P_e(V_5 - V_6) - (m_{e6}h_{e6} + m_{e5}h_{e5}) \tag{4.18}$$

Defining the mean specific enthalpy of the total exhausted mass $(m_{e5} + m_{e6}) = (m_4 - m_6)$ as $h_{ex}$

$$\begin{aligned} m_6u_6 - m_4u_4 &= P_eV_d - (m_4 - m_6)\,h_{ex} \\ \text{or} \qquad h_{ex} &= \frac{m_4u_4 - m_6u_6 + P_eV_d}{m_4 - m_6} \end{aligned} \tag{4.19}$$

## 4.3 Actual SI Cycle Modeling

### 4.3.1 Estimation of Residual Fraction

At this point, the residual mass fraction is defined as

$$f = \frac{m_6}{m_4} = \frac{V_6\upsilon_4}{V_4\upsilon_6} = \frac{\upsilon_4/\upsilon_6}{R_c} = \frac{\upsilon_4/\upsilon_5}{R_c} = \frac{1}{R_c}\left(\frac{P_5}{P_4}\right)^{1/\gamma} = \frac{1}{R_c}\left(\frac{P_e}{P_4}\right)^{1/\gamma} \tag{4.20}$$

For the intake process $(6-1)$, we note that, $P_6 = P_e$ and $P_1 = P_i$, where $P_i$

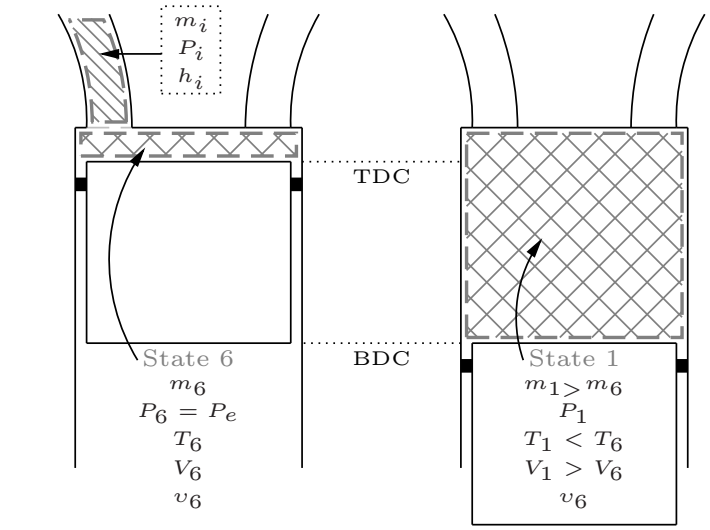


Figure 4.4: Intake Stroke

is the intake manifold pressure. Defining the intake mass as $m_i$

$$m_1 = m_6 + m_i \tag{4.21}$$

From transient energy analysis

$$U_1 - U_6 = -P_i(V_1 - V_6) + (m_1 - m_6)h_i \tag{4.22}$$

Considering $U_1 = m_1(h_1 - P_i\upsilon_1)$ and $U_6 = m_6(h_6 - P_e\upsilon_6)$, and simplifying equation (4.22)

$$m_1h_1 = m_6h_6 + (m_1 - m_6)h_i + V_6(P_i - P_e) \tag{4.23}$$

Also noting $f = {}^{m_6}/_{m_4} = {}^{m_6}/_{m_1}$, and $m_1 - m_6 = m_1(1 - f)$

$$h_1 = f\left[h_6 + \left(\frac{1}{f} - 1\right)h_i + (P_i - P_e)\upsilon_6\right] \tag{4.24}$$

Therefore, enthalpy at the end of intake stroke is not only just the average of the residual and intake enthalpies, but also includes the flow work term.

For the ease of mathematical formulation, the working fluid in the preceding ideal model will be assumed to be an ideal gas, with $c_v$ and $c_p$ constant throughout the engine operating cycle. We start by defining fuel-air equivalence ratio, $\phi$, as the stoichiometric air-fuel ratio, $A_s = (m_a/m_f)_{stoic}$, divided by the actual air-fuel ratio, $A = (m_a/m_f)$,

$$\phi = \frac{A_s}{A}, \tag{4.25}$$

where $m_a$ and $m_f$ are the inducted masses of air and fuel respectively. Since mass of the inducted intake mixture, $m_i = m_a + m_f$, we can write

$$\frac{m_f}{m_i} = \frac{\phi}{\phi + A_s} \tag{4.26}$$

Considering a complete constant volume adiabatic combustion,

$$m_1 c_v (T_3 - T_2) = m_f Q_{LHV}$$

Defining the specific internal energy decrease from equation (4.3.1) as $Q^*$,

$$Q^* = \frac{m_f}{m_1} Q_{LHV} = \frac{m_f}{m_i} \times \frac{m_i}{m_1} Q_{LHV} = \frac{\phi}{\phi + A_s}(1 - f) Q_{LHV} \tag{4.27}$$

Since

$$\frac{T_3}{T_2} = 1 + \frac{Q^*}{c_v T_1 R_c^{\gamma - 1}}$$

and

$$\frac{P_1}{P_4} = \frac{P_1}{P_2}\frac{P_2}{P_3}\frac{P_3}{P_4} = \frac{T_2}{T_3},$$

from equation (4.20)

$$f = \frac{1}{R_c}\left(\frac{P_e}{P_i}\right)^{1/\gamma}\left(\frac{P_i}{P_4}\right)^{1/\gamma} = \frac{1}{R_c}\frac{(P_e/P_i)^{1/\gamma}}{\left[1 + Q^*/(c_v T_1 R_c^{\gamma-1})\right]^{1/\gamma}} \tag{4.28}$$

Thus, the residual fraction increases as $P_i$ decreases below $P_e$, decreases as $R_c$ increases, and decreases as $Q^*/(c_v T_1)$ increases [17]. Through a similar analysis, the

temperature of the residual gas can be determined as

$$T_6 = T_1 \left(\frac{P_e}{P_i}\right)^{(\gamma-1)/\gamma} \left(1 + \frac{Q^*}{c_v T_1 R_c^{\gamma-1}}\right)^{1/\gamma} \tag{4.29}$$

Rewriting equation (4.24) as

$$c_p T_1 = f c_p T_6 + (1-f) c_p T_i - \frac{R T_1}{R_c}\left(\frac{P_e}{P_i} - 1\right), \tag{4.30}$$

and using equation (4.29) we get the temperature of the intake mixture at state point 1 as

$$T_1 = T_i \left(\frac{1-f}{1 - \left[1/(\gamma R_c)\right]\left[P_e/P_i + (\gamma - 1)\right]}\right) \tag{4.31}$$

With intake manifold pressure $P_i$, intake manifold temperature $T_i$, and exhaust manifold pressure $P_e$ as input parameters and an initial guess value of the residual fraction $f$, intake mixture temperature is calculated using equation (4.31). Then using equation (4.27) $Q^*/c_v T_1$ is calculated, whose value is used in equation (4.28) to check the value of $f$ and the process is reiterated from there until satisfactory precision is achieved.

### 4.3.2 Finite Heat Release Model

The finite heat release model is used to get a heat release profile from the start of combustion to exhaust valve opening that matches actual engine pressure data. This model is superior than the ideal as it can successfully show the affect of spark timing and phased burn characteristics of fuel-air mixtures. It has been previously observed that the pressure rise due to combustion is proportional to the corresponding increments of the burned mass fraction of the fuel-air mixture [73]. Hence, a reliable model of the mass burning rate can be used to calculate the thermodynamic state of the mixture during combustion and for parametric studies. The burn rate increases from a low value at spark discharge to a maximum when about half of the charge has been burnt. It then decreases down to zero as combustion nears completion. The initial flame development period is primarily influenced by fluid motion near the spark plug, mixture state and composition.

The bulk burning stage on the other hand is affected by chamber geometry, turbulence and overall mixture characteristics. Heywood [17] characterizes the energy-release aspects of combustion as,

**Flame-development angel,** $\theta_d$ The crank angle interval between the spark discharge and the time when a small but significant fraction of the cylinder mass has burned or fuel chemical energy has been released. This angle is sometimes called the ignition delay.

**Rapid-burning angle,** $\theta_r$ The crank angle interval required to burn the bulk of the charge. It is defined as the interval between the end of the flame-development stage (usually mass fraction burned or energy-release fraction of 10 percent) and the end of the flame propagation process (usually mass fraction burned or energy-release fraction of 90 percent).

**Overall burning angle,** $\Delta\theta_b$ The duration of overall burning process. It is the sum of $\theta_d$ and $\theta_r$.

The Wiebe function is popular as a flexible fitting tool for mass fraction burnt versus crank angle data. Among several versions found in the literature, the following form has been used in the present study:

$$x_b(\theta) = \begin{cases} 1 - \exp\left[-a\left(\frac{\theta-\theta_s}{\Delta\theta_b}\right)^m\right], & \text{if } \theta_s \leq \theta \leq \theta_s + \theta_b \\ 0, & \text{if } \theta < \theta_s,\ \theta > \theta_s + \theta_b \end{cases} \tag{4.32}$$

where,

$x_b(\theta)$, is the mass fraction burnt at a crank-angle, $\theta$
$\theta_s$, is the crank angle at the start of combustion
$\Delta\theta_b$, is the total combustion duration
$m$, is the Wiebe form and
$a$, is the Wiebe efficiency factor

Since it is difficult to point out the actual end of combustion, it is generally taken as an arbitrary limit such as 90% or 99% complete combustion [52]. The

Wiebe efficiency factor changes accordingly as given by, $a = \ln(1 - x_b)$. The Wiebe form factor $m$, dictates how early the mass fraction burnt curve rises [47].

Total heat input from fuel, considering residuals is

$$Q_{in} = m_f \cdot (1 - f) \cdot Q_{LHV} \tag{4.33}$$

The rate of heat release with respect to crank angle (or time) is obtained by differentiating the cumulative heat release Wiebe function.

$$\begin{aligned} \frac{\delta Q_{fuel}}{d\theta} &= Q_{in} \frac{dx_b}{d\theta} \\ &= \frac{ma}{\theta_b} Q_{in}(1 - x_b) \left( \frac{\theta - \theta_s}{\theta_b} \right)^{m-1} \end{aligned} \tag{4.34}$$

#### 4.3.2.1 Adjustment of Burning Velocities

Simulation in the present study is carried out maintaining MBT conditions for each fuel. This requires that half of the fuel mass is burnt at 10° ATDC [17]. To ensure this criterion, the start of combustion must be adjusted according to fuel. For example, hydrogen has a very high laminar burning velocity (Table 4.2) with consequent short burn duration, and therefore demands less spark-advance. This kind of adjustment allows to make a much profound comparison between different alternative fuels [16].

It has become widely accepted that turbulent flames in SI engines can be treated as an array of laminar flamelets with no turbulence structure residing within them and the actual burning parameters are usually normalized by laminar burning velocities [74, 75]. Additionally, burn duration also depends on engine speed, as at higher speed, the turbulence tends to make the burn duration shorter. Hence, following correlation [76] to adjust burn duration in response to change in engine speed and laminar burning velocity is used:

$$\frac{\Delta\theta_b}{\Delta\theta_{b,ref}} = \left[ \frac{N}{N_{ref}} \right]^{1/3} \left[ \frac{u_{l,ref}}{u_l} \right]^{2/3} \tag{4.35}$$

The subscript *ref* indicates a reference condition and $u_l$ is the laminar burning velocity. In the present study, experimental data of [33] are used as the reference,

and engine specification is reported in Table 4.1.

Table 4.1: Reference Engine Parameters

| $b$ | $s$ | $l$ | $R_c$ | $\theta_s$ | $\Delta\theta_b$ |
|---|---|---|---|---|---|
| 0.0763 m | 0.1111 m | 0.160 m | 7 | 330° | 60° |

The required angle for start of combustion is calculated using equation (4.32), where numerical value of $\theta$ is taken at 10° ATDC and 50% mass fraction burnt. Laminar burning velocities at 400 K temperature are used as some of liquid fuels may not form proper pre-mixture at 300 K. Calculated values of $\Delta\theta_b$ and $\theta_s$ for the fuels at three engine speeds are reported in Table 4.2.

Table 4.2: Spark Advance and Burn Duration

| Fuel | $u_l$ [m/s] | Speed [rpm] | $\Delta\theta_b$ [deg] | $\theta_s$ [deg,BTDC] | $P_{max}$ [MPa] | $T_{max}$ [K] |
|---|---|---|---|---|---|---|
| Iso-Octane | 0.537 [25] | 1000 | 44.2 | 15.1 | 4.54 | 2581 |
| | | 3000 | 63.8 | 26.3 | 4.24 | 2539 |
| | | 5000 | 75.6 | 33.0 | 4.10 | 2506 |
| Methane | 0.572 [26] | 1000 | 42.4 | 14.1 | 4.48 | 2640 |
| | | 3000 | 61.1 | 24.8 | 4.20 | 2599 |
| | | 5000 | 72.5 | 31.2 | 4.07 | 2565 |
| Hydrogen | 4.25 [24] | 1000 | 11.1 | -3.7 | 5.59 | 3308 |
| | | 3000 | 16.1 | -0.9 | 5.43 | 3297 |
| | | 5000 | 19.0 | 0.80 | 5.33 | 3284 |
| Methanol | 0.675 [77] | 1000 | 38.0 | 11.6 | 4.60 | 2556 |
| | | 3000 | 54.7 | 21.1 | 4.30 | 2520 |
| | | 5000 | 64.9 | 26.9 | 4.16 | 2490 |
| Ethanol | 0.640 [55] | 1000 | 39.3 | 12.4 | 4.60 | 2558 |
| | | 3000 | 56.7 | 22.3 | 4.29 | 2520 |
| | | 5000 | 67.2 | 28.2 | 4.15 | 2489 |
| Butanol | 0.585 [55] | 1000 | 41.8 | 13.7 | 4.58 | 2565 |
| | | 3000 | 60.2 | 24.2 | 4.27 | 2525 |
| | | 5000 | 71.4 | 30.6 | 4.13 | 2493 |

Several interesting features can be noted from the table. First, all fuels except hydrogen have laminar burning velocities ranging in between 0.53 $ms^{-1}$ to

0.68 $ms^{-1}$. Hydrogen on the other hand has the fastest burning velocity and corresponding highest values of peak cylinder pressure and temperature. Secondly, all three alcohols show very similar burning characteristics at corresponding engine speeds, which as shall be found later, yields very similar exergetic performance. It should be kept in mind that these kind of similarities for chemically similar fuels are mostly influenced by the choice of spark timing.

### 4.3.3 Calculation of Heat Losses

Any practical model of internal combustion engine must account for heat transfer since heat transfer affects engine performance, efficiency and emissions [17]. Heat transferred to the chamber walls result in lower average gas pressure and temperature, and lower work output. During the engine operation, the conditions are constantly varying depending on a host of factors such as intake port and combustion chamber configuration. Moreover, the combustion chamber surface area varies throughout the cycle. The heat flux to the surface of combustion chamber thus varies from zero to as high as 10 $MW/m^2$ and back to zero again in less than 10 millisecond [41]. As the intake mixture enters the cylinder, heat is transferred from the port walls and back of valve to the gas. Although for the short contact time, the heating effect is small, this intake heating contributes to reduction in volumetric efficiency. The compression process is nearly adiabatic but during combustion and expansion phases, the largest amount of heat transfer take place. The generalized formulation for the rate of heat transfer at an engine speed of $N$ revolutions per second can be expressed as

$$\frac{\delta Q_{ht}}{d\theta} = \frac{h_c(\theta)A(\theta)}{2\pi N} \times (T - T_{wall}) \tag{4.36}$$

To calculate the convective heat transfer coefficient $h_c$, the present work uses Woschni's equation, which is a widely-used correlation based on the similarity law of steady turbulent heat transfer [43]. This correlation represents spatially averaged combustion chamber heat fluxes since it uses the mean cylinder gas temperature.

$$h_c(\theta) = 3.26b^{-0.2}[P(\theta)]^{0.8}[T(\theta)]^{-0.55}[U_g(\theta)]^{0.8} \tag{4.37}$$

where the units of $h_c, b, P, T$, and $U_g$ are W/m$^2\cdot$ K, m, kPa, K, and m/s respectively. $U_g$ is the mean cylinder gas velocity given as [78]

$$U_g(\theta) = \left[C_1\bar{U}_p + C_2\frac{V_d T_r}{P_r V_r}\left\{P(\theta) - P_m(\theta)\right\}\right] \tag{4.38}$$

$P_m(\theta)$ is the motoring pressure also given in [78] as

$$P_m(\theta) = P_r\left(\frac{V_r}{V(\theta)}\right)^{1.3} \tag{4.39}$$

In equations (4.38) and (4.39), the terms $P_r, T_r,$ and$V_r$ represents respectively pressure, temperature and volume at some reference state such as inlet valve closing or start of combustion [17, 78].In the current study, inlet valve closing (state 1) was chosen as the reference state. In equation (4.38), $C_1$ and $C_2$ are constants given as [17]

| | | |
|---|---|---|
| For the gas exchange period: | $C_1 = 6.18$ | $C_2 = 0$ |
| For the gas compression period: | $C_1 = 2.28$ | $C_2 = 0$ |
| For the gas combustion and expansion period: | $C_1 = 2.28$ | $C_2 = 3.24 \times 10^{-3}$ |

## 4.4 Governing Equations of SI Engine Model

At this point, all the sub-models developed upto now is combined to produce the general governing equations. The internal combustion engine from intake valve closing upto exhaust valve opening can be considered as a closed system. Thus the differential closed system energy balance yields

$$\frac{\delta Q_{fuel}(\theta)}{d\theta} + \frac{\delta Q_{ht}(\theta)}{d\theta} - \frac{\delta W(\theta)}{d\theta} = \frac{\delta Q_{net}(\theta)}{d\theta} - \frac{\delta W(\theta)}{d\theta} = \frac{dU(\theta)}{d\theta} \tag{4.40}$$

where $\delta Q_{net}(\theta) = \delta Q_{fuel}(\theta) + \delta Q_{ht}(\theta)$. Taking $\delta W(\theta) = P(\theta)dV(\theta)$, $dU(\theta) = m_1 c_v dT$, and assuming ideal gas behavior

$$\frac{\delta Q_{net}(\theta)}{d\theta} - P(\theta)\frac{dV(\theta)}{d\theta} = \frac{c_v}{R}\left(P(\theta)\frac{dV(\theta)}{d\theta} + V(\theta)\frac{dP(\theta)}{d\theta}\right) \tag{4.41}$$

where $R$ is the gas constant. Now, solving for the pressure, $P$

$$\frac{dP(\theta)}{d\theta} = -\gamma \frac{P(\theta)}{V(\theta)} \frac{dV(\theta)}{d\theta} + \frac{\gamma - 1}{V(\theta)} \left( \frac{\delta Q_{net}(\theta)}{d\theta} \right) \tag{4.42}$$

where, $V(\theta)$ is calculated using equation (4.4) and ${}^{dV(\theta)}/_{d\theta}$ is calculated by differentiating the same with respect to the crank angle giving

$$\frac{dV(\theta)}{d\theta} = \frac{V_d}{2} \sin\theta \left[ 1 + \cos\theta \left\{ \left( \frac{2l}{s} \right)^2 - \sin^2\theta \right\}^{-1/2} \right] \tag{4.43}$$

which completes the thermodynamic model. Estimation of in-cylinder gas phase properties during the fast exothermic reaction phase known as combustion requires detailed thermo-chemical analysis of the processes involved. Before evaluating properties, each phase must be defined with appropriate constraints emerging from conservation laws and thermo-kinetic considerations [79]. Then using the thermodynamic description of the chemical system, conditions for equilibrium are to be satisfied. The resulting set of equations provide complete system description upon solution.

## 4.5 Equilibrium Calculation

The present work makes use of the open source package Cantera [19]. Cantera is a suite of object-oriented software tools for problems involving chemical kinetics, thermodynamics, and/or transport processes. Cantera provides types (or classes) of objects representing phases of matter, interfaces between these phases, reaction managers, time-dependent reactor networks, and steady one-dimensional reacting flows. It employs a stoichiometric description of chemical systems bounded by closed-system constraint (element-abundance equations) and uses Gibbs function minimization to calculate equilibrium by the Villars-Cruise-Smith (VCS) algorithm [19]. The basic description, governing equations and solution algorithm will be discussed in this chapter.

### 4.5.1 Chemical Stoichiometry

#### 4.5.1.1 Element-Abundance Equations

Any description of a closed system is operationally an expression of the law of conservation of mass. A closed system can be defined by a set of element-abundance equations expressing the conservation of the chemical elements making up the species of the system. There is one equation for each element, as follows:

$$\sum_{i=1}^{N} a_{ki}\, n_i = b_k; \qquad k = 1, 2, \ldots, M, \tag{4.44}$$

where $a_{ki}$ is the subscript to the $k$th element in the molecular formula of species $i$; $n_i$ is the number of moles of $i$ (in some basis amount of system); $b_k$ is the fixed number of moles of the $k$th element in the system; $M$ is the number of elements; and $N$ is the number of species. In vector-matrix form the element-abundance equations (4.44) are,

$$\mathbf{An} = \mathbf{b} \tag{4.45}$$

#### 4.5.1.2 Terminology

For clarity, some definitions [80] related to chemical system formulation are needed. These are as follows:

**chemical species:** a chemical entity distinguishable from other such entities by

1. Its molecular formula; or, failing that, by
2. Its molecular structure; or failing that, by
3. The phase in which it occurs.

**formula vector $\mathbf{a_i}$:** the vector of subscripts (usually integers) to the elements in the molecular formula of species.

**formula matrix A:** the $M \times N$ matrix in which column $i$ is $\mathbf{a_i}$; $\mathbf{A} = (\mathbf{a_1}, \mathbf{a_2}, \ldots, \mathbf{a_i}, \ldots, \mathbf{a_N})$; $\mathbf{A}$ is the coefficient matrix in the element-abundance equations (4.44).

**species-abundance vector n:** the vector of nonnegative real numbers representing the numbers of moles of the species in a basis amount of the chemical system; $\mathbf{n} = (n_1, n_2, \ldots, n_i, \ldots, n_N)^T; n_i \geqslant 0; \mathbf{n}$ also denotes the composition or compositional state of a system.

**element-abundance vector b:** the vector of (usually nonnegative) real numbers the number of moles of elements in a basis amount of the chemical system; $\mathbf{b} = (b_1, b_2, \ldots, b_i, \ldots, b_M)^T; \mathbf{b}$ is often specified by the relative amounts of reactants for the system.

**stoichiometric vector $\nu$:** any nonzero vector of $N$ real numbers satisfying the equation $\mathbf{A}\boldsymbol{\nu} = \mathbf{0}$. Hence

$$\mathbf{A}\boldsymbol{\nu}_j = \mathbf{0}; \quad (\boldsymbol{\nu}_j \neq \mathbf{0}); \quad j = 1, 2, \ldots, R, \tag{4.46}$$

which may also be written as

$$\sum_{i=1}^{N} a_{ki}\, \nu_{ij} = 0; \quad k = 1, 2, \ldots, M; \quad j = 1, 2, \ldots, R, \tag{4.47}$$

and $\nu_{ij} \neq 0$ for at least one $i$ for every $j$. The quantity $R$ is the maximum number of linearly independent solutions of equations (4.46) and is given by

$$R = N - C \tag{4.48}$$

where

$$C = \text{rank}(\mathbf{A}) \tag{4.49}$$

**complete stoichiometric matrix N:** an $N \times R$ matrix in which column $i$ is $\boldsymbol{\nu}_i$, and whose R columns are linearly independent stoichiometric vectors, with additional specification that $R = N - \text{rank}(\mathbf{A})$.

#### 4.5.1.3 General Solution

The general solution of equations (4.44) or (4.45), a set of $M$ linear equations in $N$ unknowns, is

$$\mathbf{n} = \mathbf{n}^{\circ} + \sum_{j=1}^{R} \boldsymbol{\nu}_j \xi_j \tag{4.50}$$

where $\mathbf{n}^{\circ}$ is any particular solution (e.g., an initial composition), the vector $(\boldsymbol{\nu}_1, \boldsymbol{\nu}_2, \ldots, \boldsymbol{\nu}_R)$ is the stoichiometric vector, and the quantities $\xi_j$ are a set of real parameters known as the extent-of-reaction parameter. Equation (4.50) can also be written as

$$n_i = n_i^{\circ} + \sum_{j=1}^{R} \nu_{ij} \xi_j; \quad i = 1, 2, \ldots, N \tag{4.51}$$

For fixed $\mathbf{n}^{\circ}$,

$$\left( \frac{\partial n_i}{\partial \xi_j} \right)_{\xi_{k \neq j}} = \nu_{ij}; \quad i = 1, 2, \ldots, N; \quad j = 1, 2, \ldots, R, \tag{4.52}$$

where the notation $\xi_{k \neq j}$ means all $\xi$'s other than the $j$th, and $\nu_{ij}$ is called the stoichiometric coefficient of the $i$th species in the $j$th vector. Thus $\nu_{ij}$ is the rate of change of the mole number of the $i$the species $n_i$ with respect to the reaction parameter $\xi_j$.

The conservation equation usually do not provide all the information required to determine the composition $\mathbf{n}$. The difference between the number of variables $N$ used to describe the composition and the maximum number of linearly independent equations relating $\{n_i\}$ is called the number of stoichiometric degrees of freedom $F_s$, and is the required number of additional relations among the variables required to determine any compositional state. If the state is an equilibrium state, these additional relations arise from the thermodynamic description of the system.

### 4.5.2 Chemical Thermodynamics and Equilibrium

Several potential functions are offered by the second law of thermodynamics which control the direction of natural or spontaneous processes. The particular potential function most appropriate for a given system is governed by the choice of thermodynamic variables. These are the independent variables whose specification defines the state of the system. For each potential function, there is a statement of the second law of thermodynamics that includes both the criterion for a natural process to occur and for its ultimate equilibrium state. Thus, for the entropy function $S$, the statement is

$$dS_{ad} \geqslant 0, \tag{4.53}$$

where subscript $ad$ refers to an adiabatic system; for the Gibbs function $G$,

$$dG_{T,P} \leqslant 0 \tag{4.54}$$

In each case the symbol $d$ refers to an infinitesimal change, the inequality refers to a spontaneous process and the equality to equilibrium. For relation (4.54), there is no work interaction involved other than that related to volume change ($PV$ work). Thus at equilibrium, depending on the constraints, entropy is at a (local) maximum, and the Gibbs function is at a minimum.

Using the Gibbs function, a homogeneous chemical system, open or closed, can be defined thermodynamically as

$$G = G(T, P, \mathbf{n}) \tag{4.55}$$

Also the complete differential as

$$dG = -S\,dT + V\,dP + \sum_{i=1}^{N} \mu_i\,dn_i \tag{4.56}$$

where the chemical potential for the species $i$, $\mu_i$, is defined by

$$\mu_i = \left(\frac{\partial G}{\partial n_i}\right) \tag{4.57}$$

The additivity equation for the total Gibbs function of the system is obtained by integration of equation (4.56) at fixed $T$, $P$ and composition:

$$G(T, P, \mathbf{n}) = \sum_{i=1}^{N} n_i \mu_i \tag{4.58}$$

Differentiation of this equation and comparison of the result with equation (4.56) leads to the Gibbs-Duhem equation for the system:

$$S\, dT - V\, dP + \sum_{i=1}^{N} n_i\, d\mu_i = 0 \tag{4.59}$$

which is the mathematical representation of thermodynamic criteria for chemical equilibrium. The details of the stoichiometric formulation, discretization, pre-processing and solution algorithm employed by Cantera has been presented in appendix B.

# Chapter 5

# Simulation and Results

## 5.1 Simulation of SI Engine Model

Governing equations of the SI engine are numerically solved for each time step. The time step used in the present study is 0.1° crank-angle. All liquid fuels are considered vapour at IVC. Since fuel vaporization process is a complex combination of fluid flow, heat transfer and fuel properties, it is difficult to establish a consistent and fair technique to accommodate the effects of fuel vaporization. Reported in Table 5.1 are some of the heat release parameters estimated for the fuels. Lower heating values (LHV) of fuels are found to vary significantly for different fuels. However, different fuel requires different amount of air to complete its combustion which results in variation in the values fuel mass-fraction, $y_s$. When the values of specific energy contained per unit mass of mixture, $(-\Delta h)T_0P_0$ for different fuels are observed, it is seen that their values converge to a narrow band around 2700 – 2900 kJ/kg-mix, except hydrogen which has the highest energy content per unit mass of mixture (3422 kJ/kg-mix). However, as the column of volumetric energy density suggests, stoichiometric mixture of hydrogen and methane has far less energy contained per unit volume than all other fuels, indicating, to have similar power output these mixtures must be compressed to allow induction of more energy per unit volume in the intake stroke. $(-\Delta g)T_0P_0$, denotes the specific exergy of the incoming charge which can be interpreted as the maximum work potential of the incoming stream. This should not be confused as

the only source of work potential since compression work done on this stream also increases its exergy. In SI engines, fixed volume of pre -mixture is inducted into engine cylinder and therefore the both the values of energy and exergy densities are important and their values have also been presented in Table 5.1 .

Although hydrogen has a very low fuel-air mass ratio, its much larger heating value compensates that deficiency resulting in the highest energy density per unit mass of mixture. However naturally aspirated internal combustion engines can only take a given volume of air-fuel mixture per cycle. From a volumetric point of view, very low density of hydrogen causes the mixture density to be lower than other fuel-air mixtures and consequently volumetric energy density is lowest for stoichiometric hydrogen-air mixture. This is why, in actual engines hydrogen is either port injected or directly injected towards the end of compression stroke in the cylinder at a much higher pressure to achieve necessary power output [11]. Tuning the perfect injection strategy is a complicated process varying with engine types and operating conditions, and consequently the complex process of modeling high pressure injection remained out of scope of the present study.

Table 5.1: Estimated Thermodynamic Properties of the Fuels

| Fuel | $y_s$ (-) | LHV (MJ/kg-fuel) | $T_{ad}$ (K) | $(-\Delta h)_{P_0T_0}$ (kJ/kg-mix) | $(-\Delta g)_{P_0T_0}$ (kJ/kg-mix) | $\rho(-\Delta h)_{P_0T_0}$ (kJ/m$^3$-mix) | $(\Delta g/\Delta h)_{P_0T_0}$ (-) |
|---|---|---|---|---|---|---|---|
| Iso-Octane | 0.0624 | 44.7 | 2270 | 2786 | 2873 | 3507 | 1.031 |
| Methane | 0.0552 | 50.0 | 2224 | 2760 | 2755 | 3052 | 0.998 |
| Hydrogen | 0.0285 | 120.0 | 2379 | 3422 | 3183 | 2668 | 0.930 |
| Methanol | 0.1346 | 21.1 | 2219 | 2841 | 2930 | 3424 | 1.022 |
| Ethanol | 0.1006 | 27.7 | 2235 | 2789 | 2866 | 3466 | 1.028 |
| Butanol | 0.0825 | 33.8 | 2257 | 2793 | 2878 | 3528 | 1.031 |

where,

$$
\begin{aligned}
y_s &\equiv \text{Stoichiometric fuel-air mass ratio} \\
(-\Delta h)_{P_0T_0} &\equiv \text{Specific energy (energy per unit mass of mixture)} \\
(-\Delta g)_{P_0T_0} &\equiv \text{Specific exergy (exergy per unit mass of mixture)} \\
\rho(-\Delta h)_{P_0T_0} &\equiv \text{Energy density (energy per unit volume of mixture)}
\end{aligned}
$$

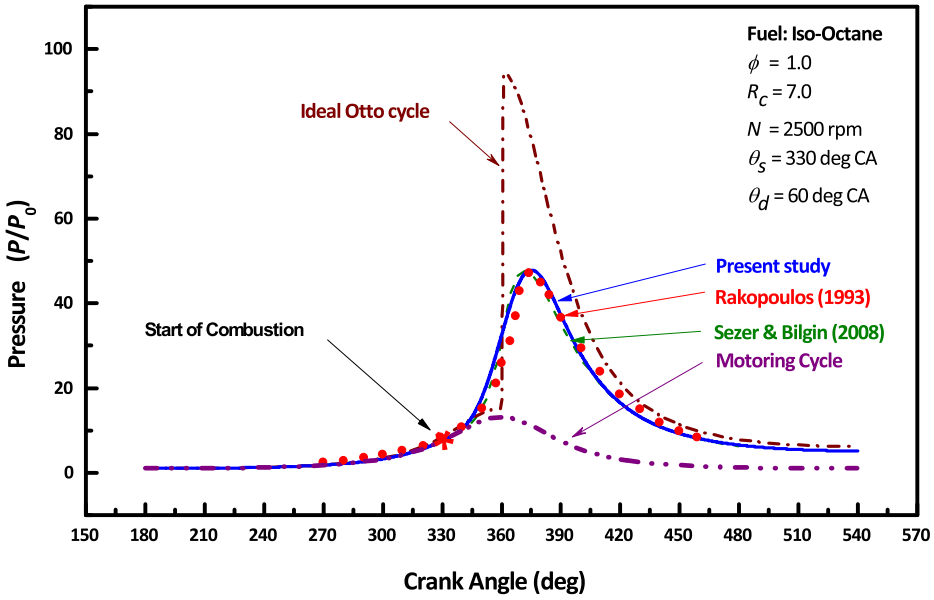


Figure 5.1: Validation of Model with Experimental Data

## 5.2 Results and Discussion

The variations of calculated gas pressure inside engine cylinder is plotted in Fig. 5.1 as a function of crank-angle for ideal Otto cycle and a modelled result for a compression ratio of 7.0 at both motoring and firing conditions. Experimental results of [33] and modeled results of [81] have also been reported for the purpose of validation. Since the compression process is almost isentropic, the curves show matching variations between ideal and actual cycle upto ignition. However, after the start of combustion, actual pressure change is much less than that of the ideal cycle since the actual combustion process is not instantaneous resulting in slower rate of heat release. As can be seen, the agreement between the predicted values and the experimental [33] and modelled [81] results are good. Comparison between the firing and motoring pressure curves shows the build-up in pressure due to combustion.

Shown in Fig. 5.2 are the indicator diagrams for iso-octane at ideal with constant $k$, ideal with actual $k$, and actual iso-octane, hydrogen and butanol combustion at identical operating conditions. Comparing the three cases for iso-octane, the ideal cases overestimate in-cylinder pressure for the most of the combustion

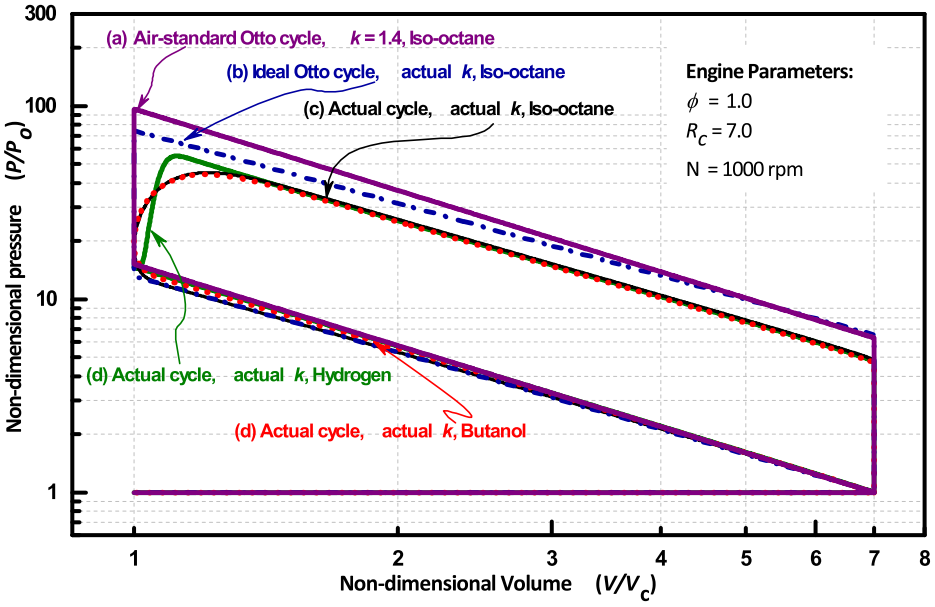


Figure 5.2: Indicator diagrams for different fuels

and expansion processes. This is because in the actual case, heat transfer during combustion and expansion stroke reduces the pressure and temperature significantly. It is also interesting to notice variations induced by calculating $k$ at each time-step, rather than holding it constant. Hydrogen shows the most semblance to the ideal case due to the fastest laminar burning velocity (Table 4.2) which results in almost constant volume combustion. Other fuels however vary from the ideal case in this respect but show little variations among themselves.

The cylinder pressure and temperature variation at 1000 rpm for all the six fuels is shown in Fig. 5.3 and Fig. 5.4 from intake valve closing to exhaust valve opening. The peak pressure and temperatures for different speeds have been reported in Table 4.2. Although burning velocity and fuel properties are varied, the spark timing adjustment yielded peak pressure for all fuels except hydrogen at the same crank angle as expected for MBT conditions. This is a good indication that, little modification is needed in SI engines in terms of comparable performance in alternative fuels if combustion parameters are correctly adjusted. It is to be noted that the slight rise in temperature of the intake charge in Fig. 5.4 is due to the mixing of the intake charge with the high temperature residuals.

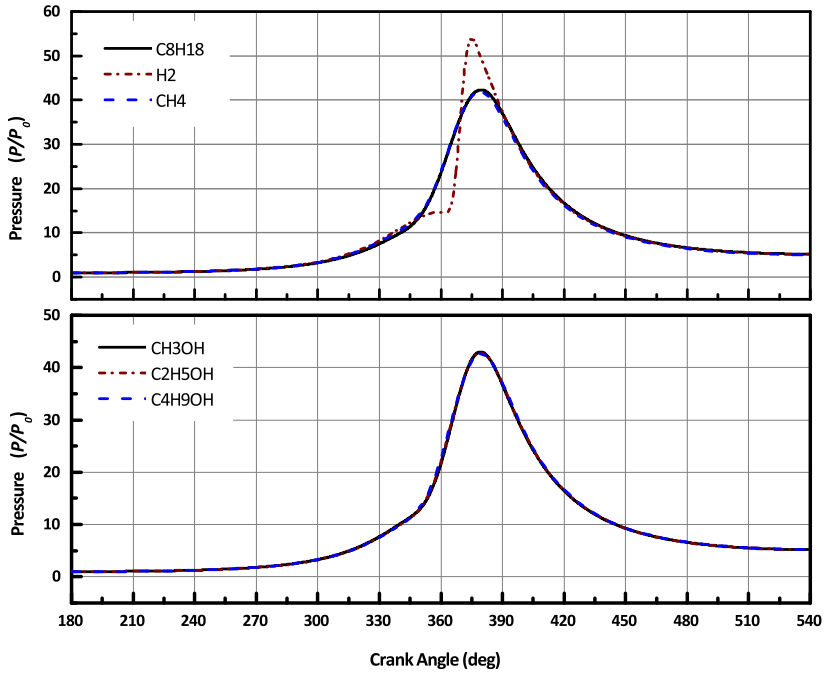


Figure 5.3: Variation of Pressure with Crank Angle

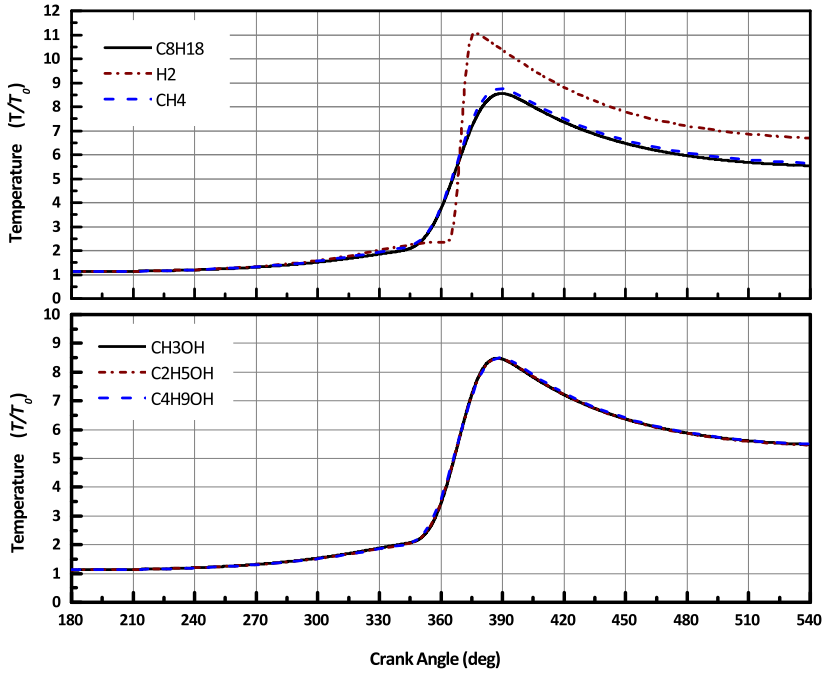


Figure 5.4: Variation of Temperature with Crank Angle

Variation of calculated mass fractions of fuel, oxygen, carbon dioxide, carbon monoxide and nitric oxide at 1000 rpm has been plotted from Fig. 5.5 to Fig. 5.10 with Iso-Octane and Hydrogen for lean, stoichiometric and rich conditions. In case of rich combustion, excess carbon monoxide is present in the burnt gas mixtures. Hydrogen combustion however is free from this kind of emissions. It is evident from the graphs that the model has good sensitivity to the change in operational parameters and can predict the composition of the reacting gas mixture quite successfully since, lean combustion shows no carbon monoxide or fuel species after completion of combustion, while rich burning yields carbon monoxide in the exhaust. Similarly, lean burning leaves excess oxygen at the exhaust, while stoichiometric and rich burning does not leave any oxygen molecules.

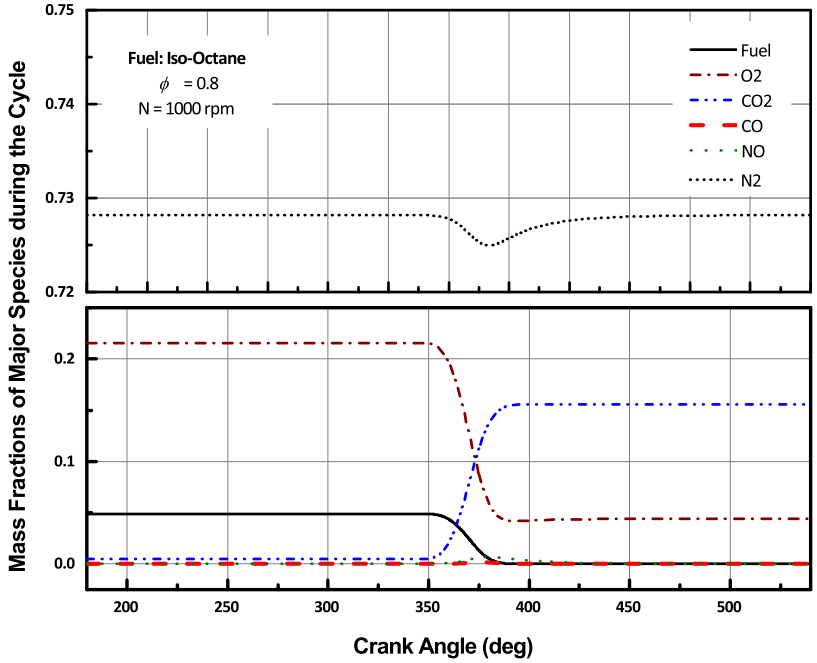


Figure 5.5: Variation of Mass Fraction in Iso-Octane Combustion at $\phi = 0.8$ with Crank Angle

Variation of heat transfer for all six fuels with crank angle are plotted in Fig. 5.11, and the effect of change in speed and equivalence ratio is presented in Fig. 5.12. All the fuels considered, except hydrogen, exhibit very close values at all crank-angles. Compared to the combustion process, the rate of heat transfers

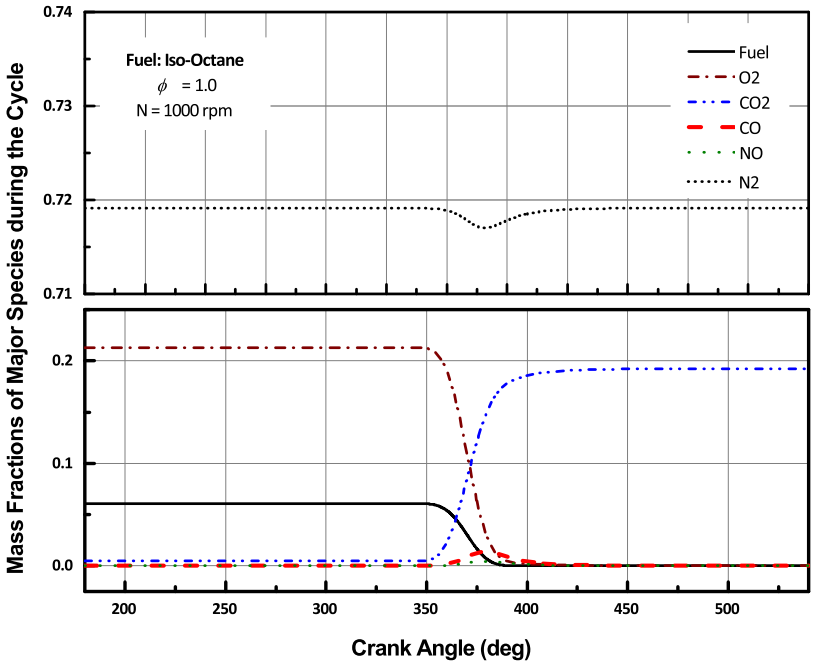


Figure 5.6: Variation of Mass Fraction in Iso-Octane Combustion at $\phi = 1.0$ with Crank Angle

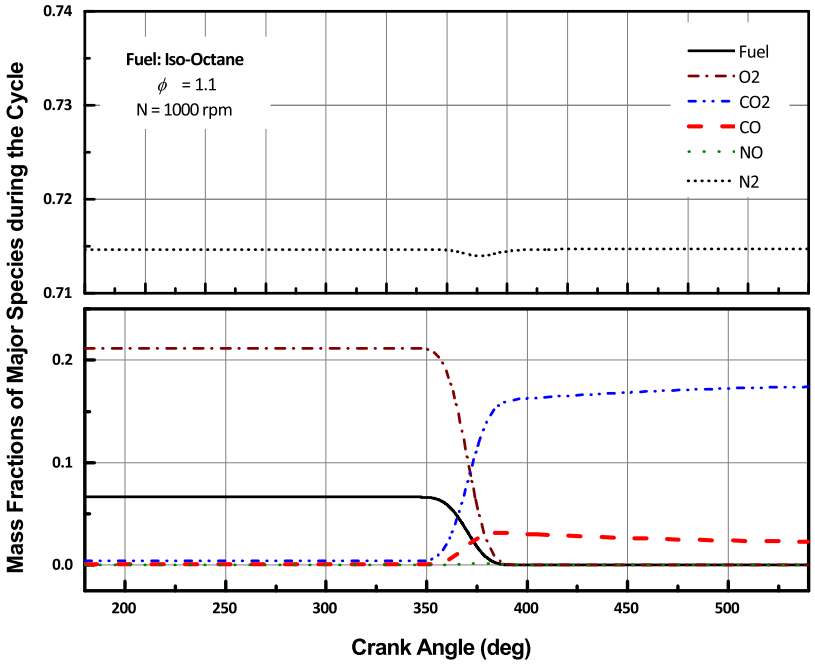


Figure 5.7: Variation of Mass Fraction in Iso-Octane Combustion at $\phi = 1.1$ with Crank Angle

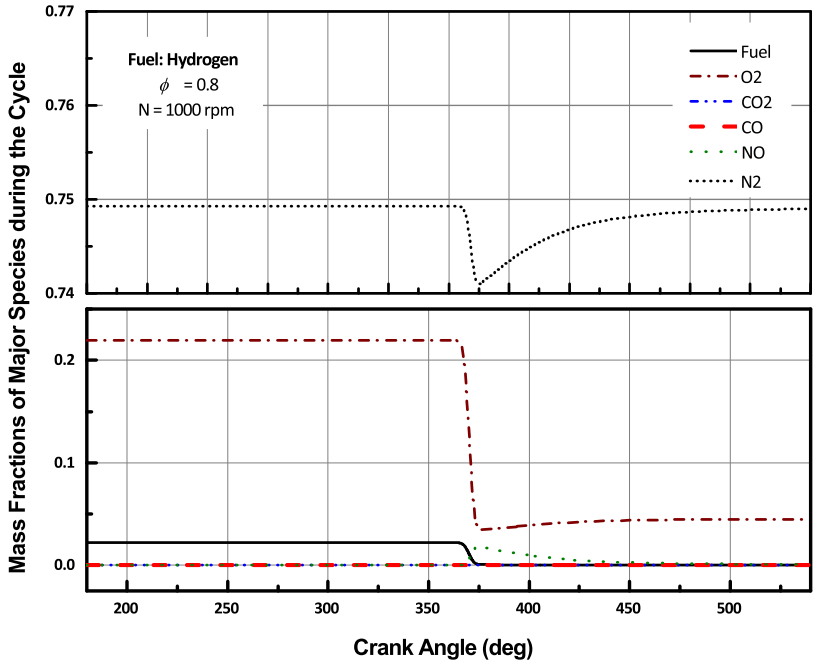


Figure 5.8: Variation of Mass Fraction in Hydrogen Combustion at $\phi = 0.8$ with Crank Angle

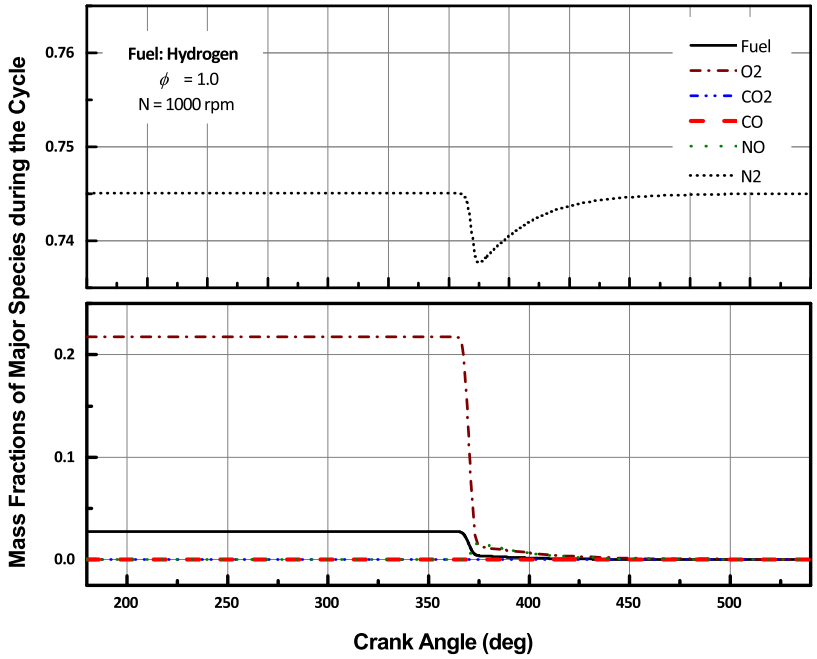


Figure 5.9: Variation of Mass Fraction in Hydrogen Combustion at $\phi = 1.0$ with Crank Angle

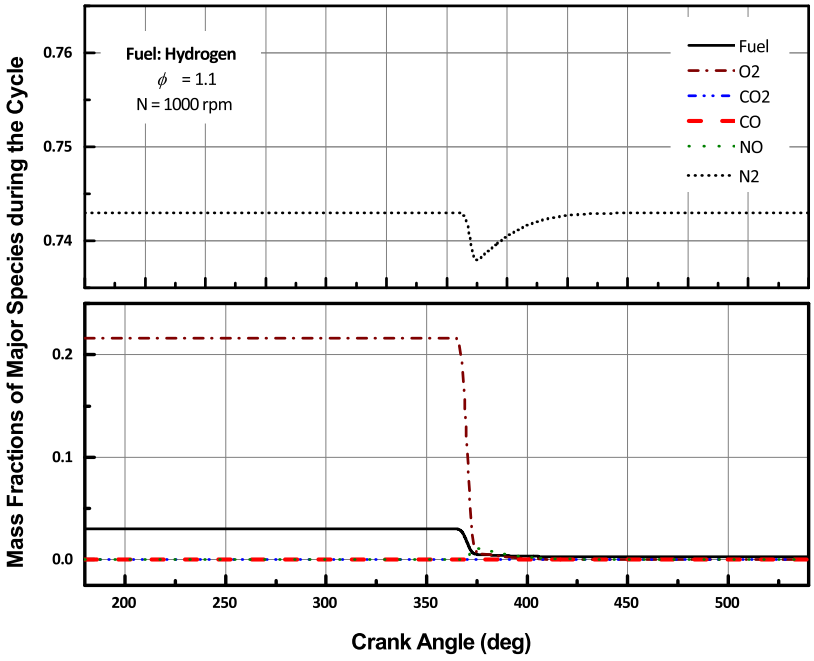


Figure 5.10: Variation of Mass Fraction in Hydrogen Combustion at $\phi = 1.1$ with Crank Angle

are small during compression and expansion processes. The value of total heat transfer for hydrogen is higher due to higher product temperature of hydrogen-air premxiture. It is evident from Fig. 5.12 that heat transfer varies little with change in equivalence ratio about stoichiometric conditions. The variation with change in speed is however, significant. As engine speed increases, it leaves less and less time per cycle for heat transfer from the combustion products. Similar trend is observed for all other fuels as in Fig. 5.12 concerning parametric variations.

The highest adiabatic flame temperature (Table 5.1) and the fastest burning velocity (Table 4.2) of hydrogen makes it very promising as an alternative fuel. However, as Fig. 5.11 suggests, heat transfer at a given speed is also highest ($\sim$ 22%) among the fuels for hydrogen. The present engine design needs more modification and improvement in terms of material and combustion parameters to harness the power from hydrogen combustion.

The variations of non-dimensional exergy values as a function of crank-angle with same engine parameters, as in Fig. 5.1 have been detailed in Fig. 5.13. The transfer of exergy with available work and cumulative exergy loss associated

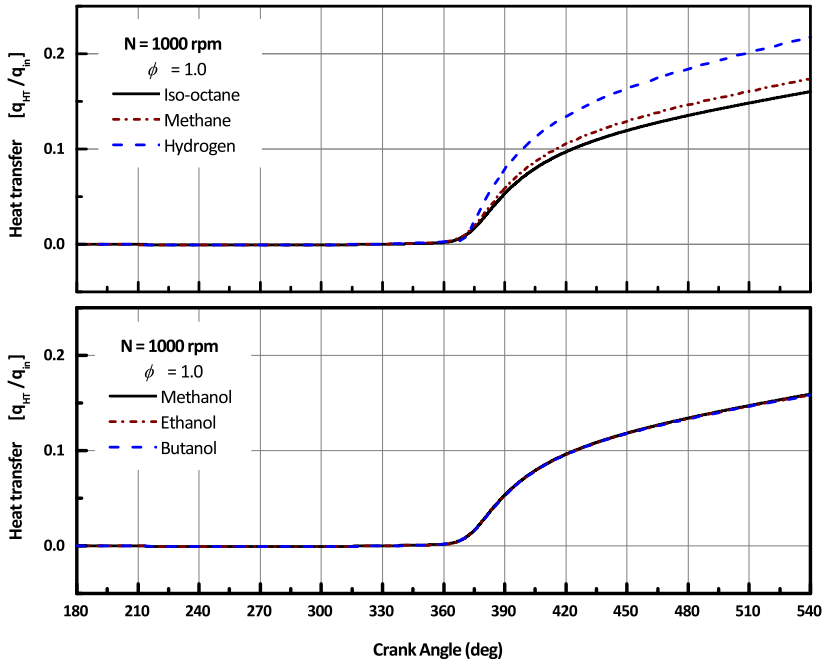


Figure 5.11: Comparison of Heat Transfer for Six Fuels at 1000 rpm and Stoichiometric Conditions

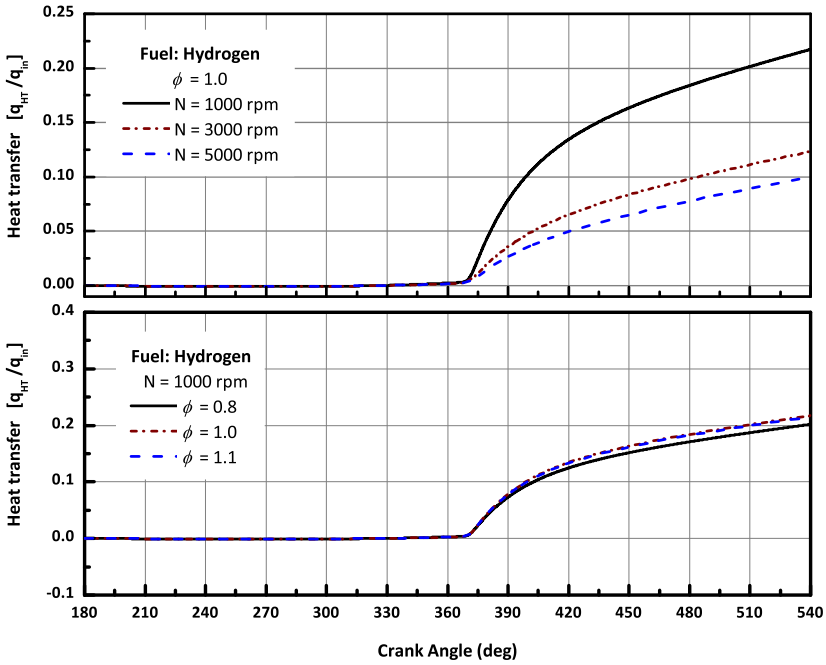


Figure 5.12: Effect of Speed and Equivalence Ratio on Heat Transfer

with heat transfer have also been plotted to visualize the conversion of total exergy from inlet valve opening (IVO) to exhaust valve closing (EVC). At IVO, total exergy equals the value of chemical exergy, $a_{ch}$, with a small contribution from high-temperature residuals as thermomechanical exergy. As the compression stroke progresses, work is supplied to the mixture and the effect is visible in the form of negative values of exergy associated with work, $a_W$. The compression process increases pressure and temperature of the charge thus increasing the thermomechanical exergy, $a_{th}$ and results in the rise in total exergy, $a_{tot}$ during the compression period. Heat transfer effects are negligible during this period and effectively this phase is overall adiabatic. However, the pressure and temperature of the pre-mixture is not sufficient enough to start the oxidation of the mixture or any significant dissociation and therefore chemical exergy value remains unchanged.

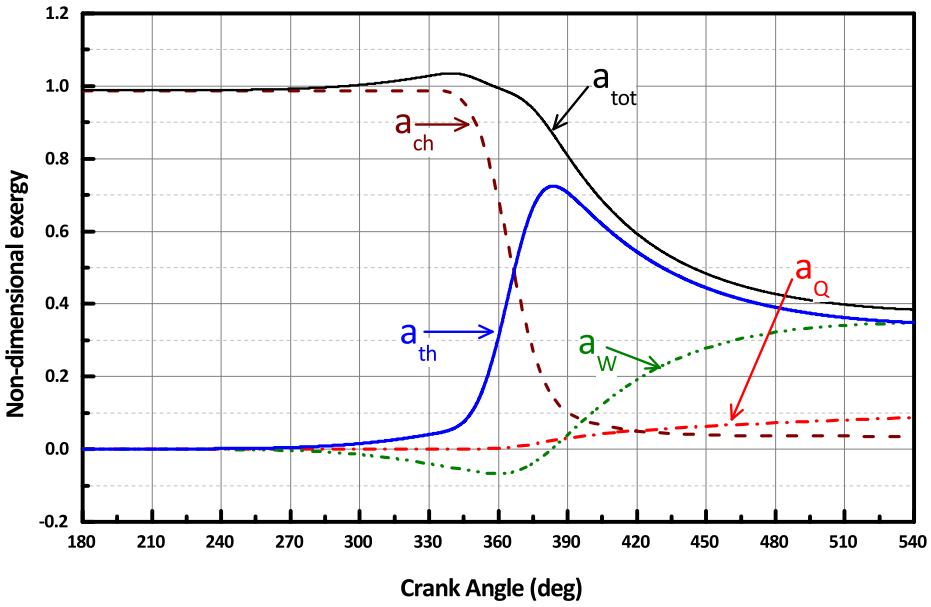


Figure 5.13: Variation of Exergy Components with Crank Angle

With the start of combustion, the chemical exergy, decreases rapidly which gives significant rise to cylinder pressure and temperature. This rise in temperature and pressure results in increase in thermomechanical exergy. As the combustion and expansion progresses, the exergy transfer with work, as well as

exergy transfer with heat loss, $a_Q$ from cylinder walls increase contributing to the decrease in total exergy. After the end of combustion, expansion stroke continues until the piston reaches the BDC. During this part of the cycle, decrease in total exergy continues due to exergy transfers (both work and heat) from the system and exergy loss associated with heat transfer is noticeable when EVO at BDC.

The remaining exergy in the cylinder at the end of expansion stroke emits with the exhaust gases, which is called the exergy transfer with the exhaust gases, $a_{ex}$. This constitutes a loss in availability as the mixture is still at pressure and temperature elevated than those of the dead state, and has been shown lumped as unaccounted exergy along with exergy destruction due to combustion and mixing in Fig. 5.16 to Fig. 5.21. As seen in Fig. 5.13, at exhaust valve opening (540 CAD), the mixture still has some chemical exergy. This is mainly the diffusive components of exergy due to the difference in concentration with the environment.

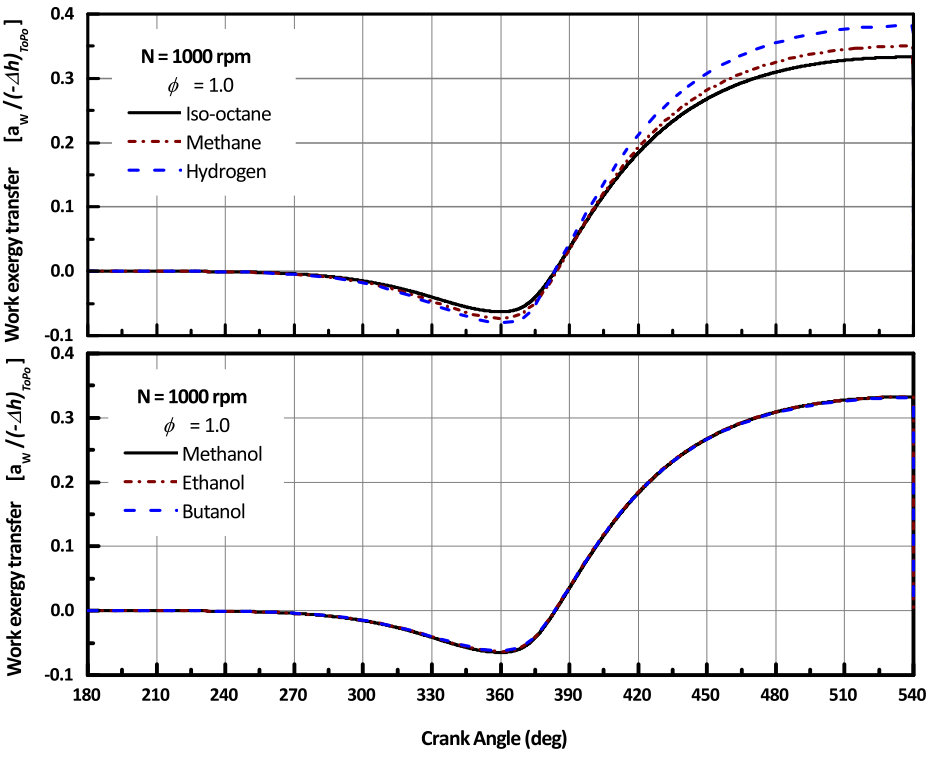


Figure 5.14: Comparison of Indicated Work Transfer for Six Fuels at 1000 rpm and Stoichiometric Conditions

Shown in Fig. 5.14 are also the variation of exergy transfer due to indicated

work interactions, $a_W$. For work interaction, the exergy is equal to the net useful work which is equal to the net work minus the work done against the surroundings [3]. All the fuels considered, except hydrogen, exhibit very close values of $a_W$ at all crank-angles. The compression of hydrogen transfers a greater amount exergy to the system compared to other fuels due to the greater degree of compressibility associated with hydrogen, the larger gas constant, and extended duration of compression stroke [16]. Also, this transfer of exergy to the system via compression work is the reason for the negative value of the curve during compression [15]. Effects of speed and equivalence ratio on work exergy transfer as shown in Fig. 5.15, are modest.

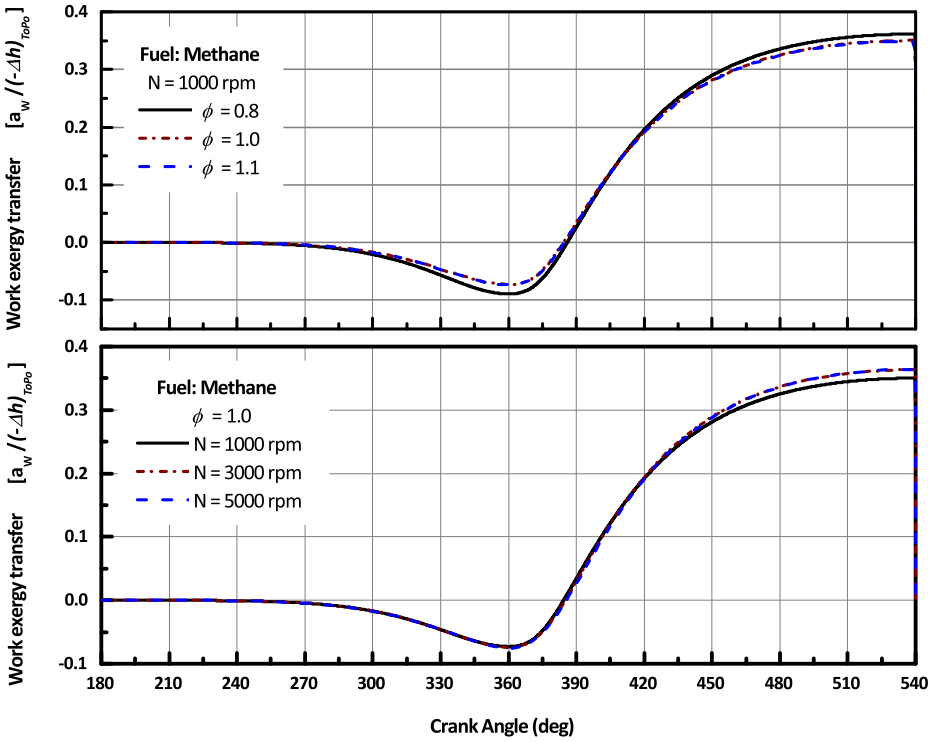


Figure 5.15: Effect of Speed and Equivalence Ratio on Indicated Work Transfer

Effect of engine speed on the division of total energy and exergy has been shown in Fig. 5.16 to Fig. 5.21 as work done, heat loss, loss with exhaust, and unaccounted losses for all six fuels. In the energy distribution, indicated values were calculated. The first general observation, as detailed in Fig. 5.12, is the reduction in percentage of heat loss as speed increases due to less time for heat

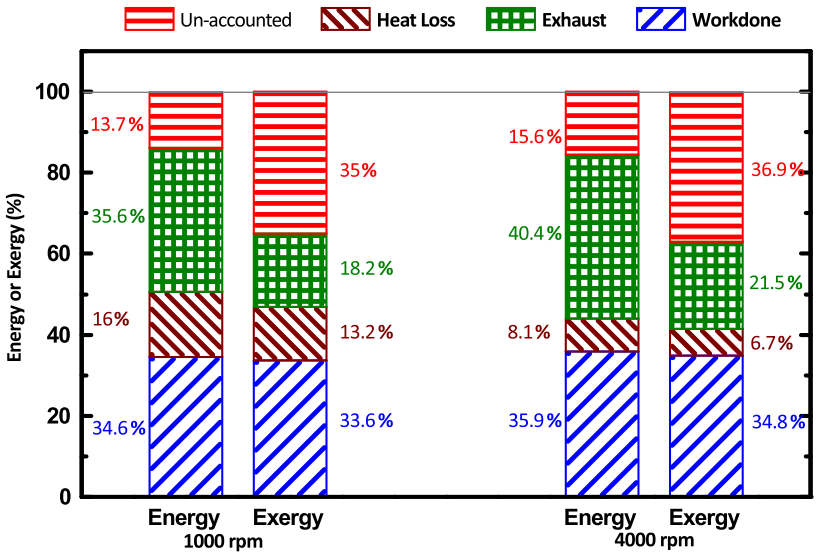


Figure 5.16: Distribution of Energy and Exergy Components at 1000 and 4000 rpm for Iso-Octane

transfer per cycle. This also implies that as speed is increased a higher fraction of the total energy and exergy is left inside the cylinder. However, from the distribution in these figures, we find that, most of it gets out with the exhaust. Therefore, it is somewhat justifiable to use energy or exergy recovery attachments like turbocharger for capturing some of this energy in the exhaust.

Secondly, with increasing speed, work done increases accordingly as the engine is being operated at full load which requires more work done per unit time as speed increases. Hydrogen combustion yielded the largest percentage of work done, 38.7% at 1000 rpm and 41.1% at 4000 rpm, with corresponding exergy values of 41.7% at 1000 rpm and 44.4% at 4000 rpm. Heat loss is also highest in its case which is a direct result of the highest adiabatic flame temperature. However, unaccounted losses are by far the least in case of hydrogen (2.3% at 1000 rpm and 8.5% at 4000 rpm, with corresponding exergy values of 3.5% at 1000 rpm and 10.6% at 4000 rpm) which can be attributed to its simplest molecular structure and fastest laminar burning velocity [14]. Considering unaccounted losses, the next best fuel to hydrogen is methane with losses of 7.4% at 1000 rpm and 9.4% at 4000 rpm, with corresponding exergy values of 27.9% at 1000 rpm and 29.9% at 4000 rpm. Methane also gives comparable work output to that of iso-octane's.

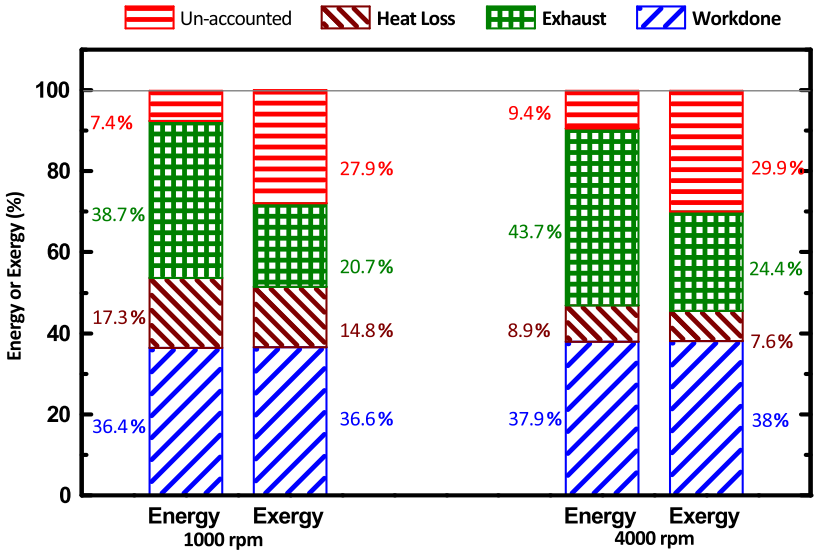


Figure 5.17: Distribution of Energy and Exergy Components at 1000 and 4000 rpm for Methane

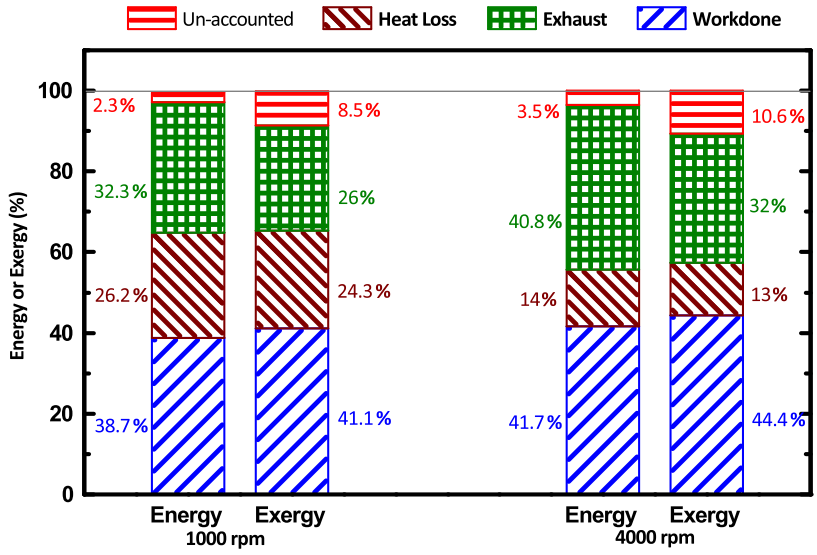


Figure 5.18: Distribution of Energy and Exergy Components at 1000 and 4000 rpm for Hydrogen

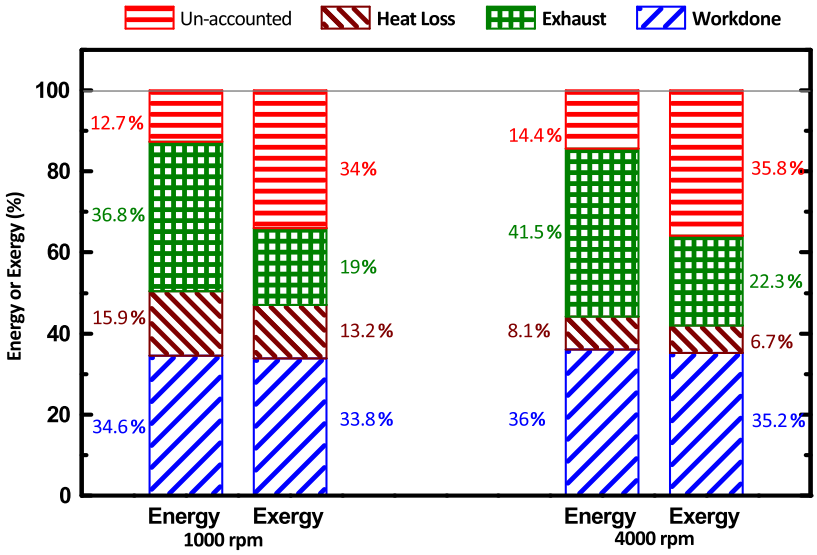


Figure 5.19: Distribution of Energy and Exergy Components at 1000 and 4000 rpm for Methanol

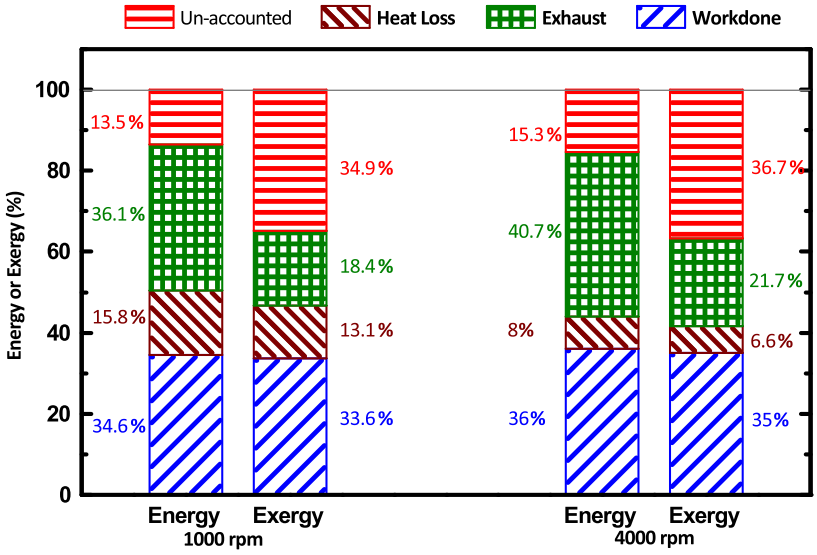


Figure 5.20: Distribution of Energy and Exergy Components at 1000 and 4000 rpm for Ethanol

Another noticeable trend in the figures is the rise in percentage of losses as speed is raised. Generally, at higher speeds, where heat transfer becomes less dominant, combustion irreversibilities other dissipative losses increase considerably [17].

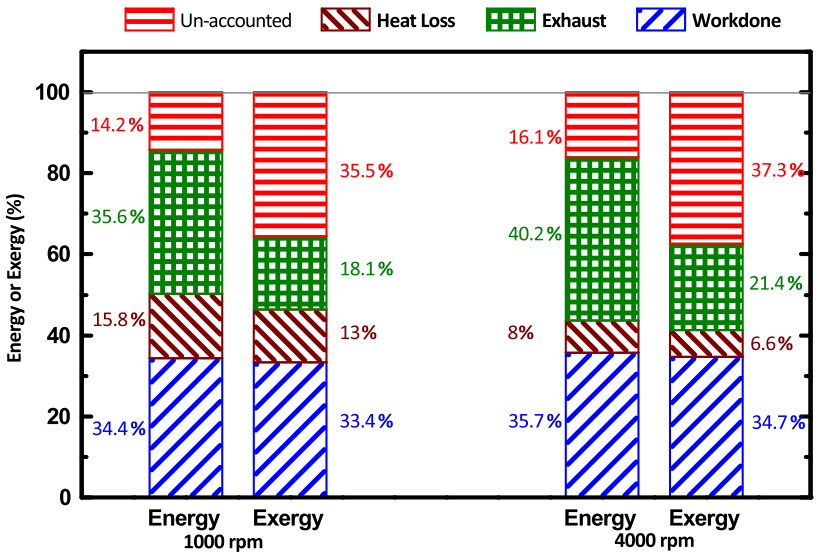


Figure 5.21: Distribution of Energy and Exergy Components at 1000 and 4000 rpm for Butanol

For all six fuels, exergy values of exhaust were much less than the corresponding energy values. This shows the necessity of exergy analysis, since the exergy of the exhaust is the maximum possible work output extractable considering it is at much less temperature and pressure than the in-cylinder conditions. Thus exergy considers the *quality* of energy, while traditional first law based analysis fails to do so, and reports a much higher energy content which can be misleading. Some other important results from Fig. 5.16 to Fig. 5.21 are,

1. At 1000 rpm, 34.4 to 38.7% of energy contained with fuel is converted to useful work, and the figure changes to 35.7 to 41.7% in case of 4000 rpm.

2. At 1000 rpm, energy loss due to heat transfer is 15.8 to 26.2% and 8.0 to 14.0% at 4000 rpm. However, associated exergy losses are 13 to 24.3% at 1000 rpm, and 6.6 to 13.0% at 4000 rpm.

3. At 1000 rpm, energy loss with exhaust is 32.3 to 38.7%, and 40.2 to 43.7% at 4000 rpm. Exergy loss with exhaust are 18.1 to 26.0% at 1000 rpm, and 21.4 to 32.0% at 4000 rpm.

4. At both the speeds, exergy destroyed due to irreversibility in hydrogen fuelled cases are found lowest. For other fuels considered, at 1000 rpm, 28.0 to 35.5% of exergy contained with fuel is destroyed due to irreversibility, and 30 to 37.3% is destroyed at 4000 rpm.

5. Engine work output and energy/exergy associated with exhaust are found to increase with engine speed, while losses due to heat transfer and irreversibilities (in case of exergy) are reduced.

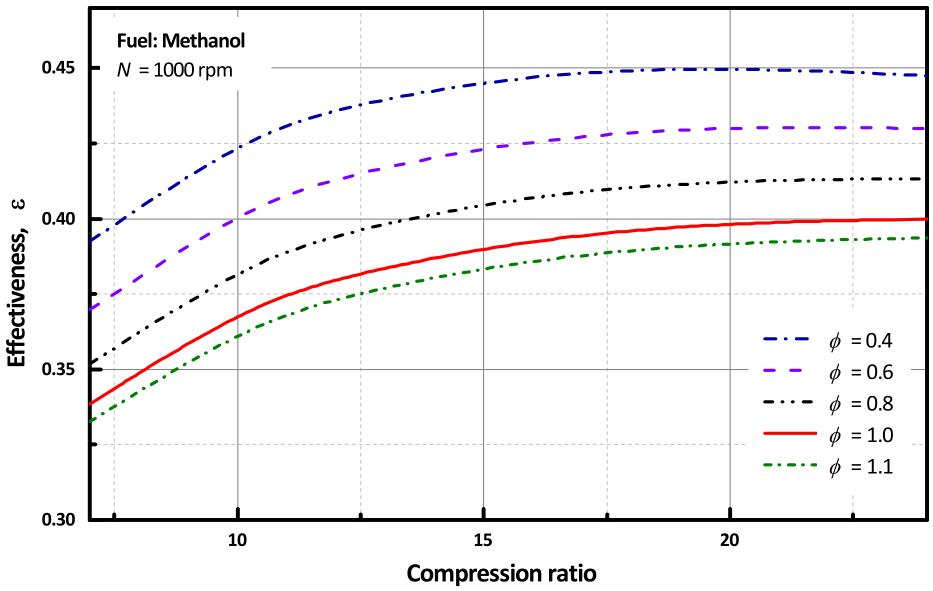


Figure 5.22: Effectiveness as a function of compression ratio and equivalence ratio

Fig. 5.22 shows the effect of variation in compression ratio and fuel-air equivalence ratio on rational exergetic efficiency or effectiveness. The general observation from this graph are:

- Increasing compression ratio at constant equivalence ratio increases effectiveness as displacement work per stroke increases.

- Increasing the equivalence ratio beyond unity decreases effectiveness due to increase in combustion irreversibilities due to lack of sufficient air
- leaning the mixture below unity raises effectiveness as for a given displacement volume, the burnt gases expand through a larger temperature ratio prior to exhaust, as in case of lean firing burned h=gas temperature after expansion decreases [17].

# Chapter 6

# Conclusion

The major conclusions of the study are:

- Less and less energy is lost as heat transfer as engine speed is increased. Clearly, less time available per cycle contributes to this cause. Heat transfer however varied little with change in equivalence ratio. Although leaner mixtures produced less heat than stoichiometric, overall energy balance was almost close in both cases, i.e. in both cases percentage of energy lost by heat transfer were similar.

- At the present engine design, hydrogen combustion is prone to more heat loss than all other fuels considered due to its considerably higher adiabatic flame temperature.

- Amount of work transfer was also relatively higher with hydrogen, since the peak pressure was higher. Percentage of work transfer increased consistently with increase in speed.

- Savings in energy loss in heat transfer at higher speeds contributed little towards any useful gain inside the cylinder, and ended up increasing percentage of energy lost with exhaust.

- In both heat loss and exhaust loss, energy accounting reports higher losses than corresponding exergy values. As exergy considers the quality of energy as well as quantity, it is a truer measure of losses incurred since in both those cases the mixture energy is of inferior quality.

- Unaccounted losses however is reported to occupy a higher percentage in exergy analysis than in energy analysis. As a definite portion of energy is unavailable for its *quality*, and losses due to entropy generation are reported in exergy accounting, it helps us to direct our efforts in the correct way in recovering energy or minimize loss.
- Unaccounted losses tend to increase with speed as losses due to combustion irreversibility and other dissipative losses increase.
- In general all three alcohols exhibit very similar performance in all aspects.

Following points can be considered in future work:

- This study considered all fuels in their pure form. There is a growing interest in some specific blends of alcohol with gasoline, and hydrogen enriched mixtures worldwide. These can be studied further.
- A reliable friction model should be able to predict the losses due to friction.
- Experimental heat transfer data can be used to improve the model since Woschni's correlation performs poorly with hydrogen.

# Appendix A

# Programming Methodology for the Thermodynamic Model

Development of the thermodynamic model is summarized in the following steps:

- The coding procedure starts with the initialization of Cantera [19] and loading of the fuel database file. This database file contains the description of the major species to be considered and dictates the thermo-kinetic behavior of the chemical system.

- Global input parameters such as, environmental temperature and pressure, equivalence ratio, compression ratio, geometric parameters of the engine, engine speed etc. are stored. These are user defined inputs, and are varied when necessary.

- Intake mixture is set up using the constants given and heating values are calculated using Cantera. Also, values of $\Delta g$ and $\Delta h$ of the mixture are computed. These values are later required in both energy and exergy based analyses.

- Using equations (4.31), (4.27) and (4.28), and employing the iteration technique described in section 4.3.1 the residual fraction is calculated, which remains inside the cylinder to get mixed with the intake charge in the next cycle.

- Wiebe parameters are calculated using equations (4.35) and (4.32), where data from Table 4.1 are used as reference parameters. These parameters vary according to engine speed, and prescribed conditions for MBT. After that, using equations (4.34) and (4.32), heat input as a function of crank angle is generated.

- In a separate sub-routine, heat loss as a function of crank angle is calculated using equations (4.36) and (4.37). Relevant details of heat loss calculations are covered in detail in section 4.3.3.

- Exergy modules are defined for calculation of exergy distribution during the main run sequence. Thermomechanical and chemical exergy formulations presented in chapter 3 are used for these calculations. These modules are later used to calculate detailed reactive and diffusive exergies of the mixture.

- During the main run discretized form of the closed system energy equation given by equation (4.42) and the ideal gas equation is solved for pressure and temperature respectively using the equilibrium properties calculated with Cantera. Value of $k$ is calculated at each step, since it is a function of cylinder pressure, temperature and composition of the mixture. All species concentrations throughout the run cycle are stored.

- Finally, in the post processing phase, exergies associated with heat and work interactions and overall exergy distributions are computed, and relative performance are put into graphical form for extensive studies.

## A.1 Flowchart

Basic progression of the code is presented in the following flowchart. Blocks with dark background indicate schemes developed in the present study, while blocks with white background represent previously developed schemes or open source codes. Appropriate referencing has been done in indicated sections.

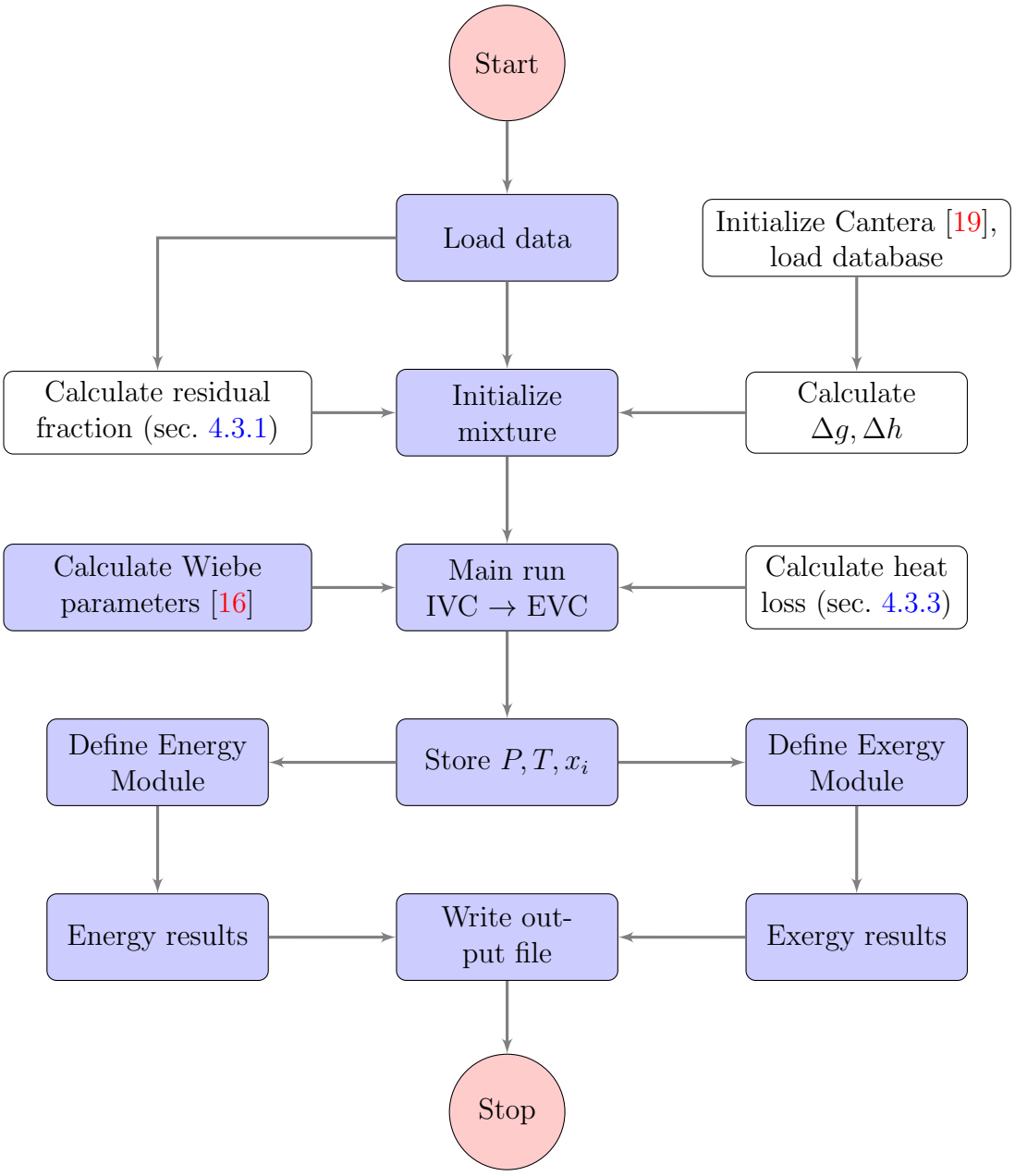
Start
Load data
Initialize Cantera [19], load database
Calculate residual fraction (sec. 4.3.1)
Initialize mixture
Calculate $\Delta g, \Delta h$
Calculate Wiebe parameters [16]
Main run IVC → EVC
Calculate heat loss (sec. 4.3.3)
Define Energy Module
Store $P, T, x_i$
Define Exergy Module
Energy results
Write output file
Exergy results
Stop

# Appendix B

# Equilibrium Calculation Procedure of CANTERA

## B.1 Solution Procedure and Algorithm

### B.1.1 The Stoichiometric Formulation

From equation (4.50), it is clear that the mole numbers $\mathbf{n}$ are function of the extents of reaction $\boldsymbol{\xi}$ of the $R$ stoichiometric equations. Hence we modify equation (4.55) as

$$G = G(T, P, \boldsymbol{\xi}) \tag{B.1}$$

Thus the problem is one of minimizing $G$, for fixed $T$ and $P$, in terms of $R$ $\xi_j$'s. The first order necessary conditions for a minimum in G are

$$\left(\frac{\partial G}{\partial \boldsymbol{\xi}}\right)_{T,P} = \mathbf{0} \tag{B.2}$$

or

$$\Delta G_j = \left(\frac{\partial G}{\partial \xi_j}\right)_{T,P,\xi_{k\neq j}} = 0; \quad j = 1, 2, \ldots, R \tag{B.3}$$

There are $R = N - C$ equations in the set (B.3). Since

$$\left(\frac{\partial G}{\partial \xi_j}\right)_{T,P,\xi_{k\neq j}} = \sum_{i=1}^{N} \left(\frac{\partial G}{\partial n_i}\right)_{T,P,n_{k\neq i}} \left(\frac{\partial n_i}{\partial \xi_j}\right)_{\xi_{k\neq j}} \quad ; \quad j = 1, 2, \ldots, R, \tag{B.4}$$

then on combining equations (B.4),(4.57), and (4.52),

$$\sum_{i=1}^{N} \nu_{ij}\, \mu_i = 0; \quad j = 1, 2, \ldots, R \tag{B.5}$$

When appropriate expressions for the $\mu_i$ are introduced into the equations in terms of free-energy data and the mole numbers, the solution of these equations provides the composition of the system at equilibrium. For an ideal gas, at a reference or standard state pressure ($P^\circ$) of unity, the chemical potential is defined as

$$\mu(T, P) = \mu^\circ(T) + RT \ln P, \tag{B.6}$$

where $P$ must be in the same unit of pressure as $P^\circ$. In the preceding equation, $\mu^\circ(T)$ is called the standard chemical potential which is a function of $T$ only. Similarly, when considering an ideal-gas solution, the equation of chemical potential for a constituent species becomes

$$\mu_i(T, P, x_i) = \mu^\circ(T) + RT \ln p_i, \tag{B.7}$$

Taking $x_i$ as the mole fraction of species $i$, $n_t$ as the total number of moles in the solution, the partial pressure $p_i$ of species $i$ is defined as

$$p_i = \left(\frac{n_i}{n_t}\right) P \equiv x_i\, P, \tag{B.8}$$

Introducing equation (B.8) into equation (B.7),

$$\mu_i(T, P, x_i) = \mu^\circ(T) + RT \ln P + RT \ln x_i \tag{B.9}$$

Solution of equation (B.2) and (B.5)using equation (B.9) then provides the equilibrium properties.

### B.1.2 Discretization and Preprocessing

Equation (4.50) is discretized for iteration as

$$\mathbf{n}^{(m+1)} = \mathbf{n}^{(m)} + \lambda^{(m)}\,\boldsymbol{\delta}\mathbf{n}^{(m)} \tag{B.10}$$

where $m$ is an iteration index. The scaler quantity $\lambda$ is called a step-size parameter, which determines the distance between successive iterations in the direction defined by $\boldsymbol{\delta}\mathbf{n}^{(m)}$. The changes in the mole numbers $\boldsymbol{\delta}\mathbf{n}^{(m)}$ from any estimate $\mathbf{n}^{(m)}$ satisfying the element-abundance constraints are related to new $\xi$ variables by

$$\delta n_i^{(m)} = \sum_{j=1}^{R} \nu_{ij}\delta\xi_j^{(m)}; \quad i = 1, 2, \ldots, N \tag{B.11}$$

Since the Gibbs function $G$ is a function of the reaction-extent variables $\boldsymbol{\xi}$, the chemical equilibrium problem is essentially one of minimizing $G(\boldsymbol{\xi})$. Hence we restate the necessary conditions for the minimization given by equations (B.2) and (B.5) in terms of $\boldsymbol{\xi}$ as

$$\boldsymbol{\Delta G} \equiv \mathbf{N}^T\boldsymbol{\mu}\,(\boldsymbol{\xi}) = \mathbf{0} \tag{B.12}$$

Expanding equation (B.5) about $\mathbf{n}^{(m)}$ in a Taylor series, neglecting the second- and higher-order terms, and setting the result to zero, we get

$$\sum_{l=1}^{R}\sum_{k=1}^{N}\sum_{i=1}^{N} \nu_{ij}\left(\frac{\partial\mu_i}{\partial n_k}\right)^{(m)}\left(\frac{\partial n_k}{\partial\xi_l}\right)^{(m)}\delta\xi_l^{(m)} = -\sum_{i=1}^{N}\nu_{ij}\,\mu_i^{(m)}; \quad j = 1, 2, \ldots, R, \tag{B.13}$$

where superscript $(m)$ denotes evaluation at $\mathbf{n}^{(m)}$. Considering the formulation of chemical potential in equation (B.9), it follows that

$$\frac{\partial\mu_i}{\partial n_k} = RT\left(\frac{\delta_{ik}}{n_i} - \frac{1}{n_t}\right), \tag{B.14}$$

where $\delta_{ik}$ is the Kronecker delta.

In equation (B.10), $\boldsymbol{\delta}\mathbf{n}^{(m)}$ is usually chosen at each iteration so that

$$\left(\frac{dG}{d\lambda^{(m)}}\right)_{\lambda^{(m)}=0} = \sum_{i=1}^{N}\left(\frac{\partial G}{\partial \xi_i}\right)_{\boldsymbol{\xi}^{(m)}} \delta\xi_i^{(m)} < 0 \tag{B.15}$$

unless $\left({}^{\partial f}/_{\partial \xi_i}\right)_{\boldsymbol{\xi}^{(m)}} = 0$. An algorithm satisfying equation (B.15) is called a descent method. The step-size parameter $\lambda^{(m)}$ is chosen so that $G(\mathbf{n}^{(m)} + \lambda^{(m)}\,\boldsymbol{\delta}\mathbf{n}^{(m)})$ is smaller than $G(\boldsymbol{\delta}\mathbf{n}^{(m)})$. Equation (B.15) ensures this is possible.

The VCS algorithm follows the following procedure [79] in choosing the step-size parameter $\lambda$. First the value of

$$\left(\frac{dG}{d\lambda}\right)_{\lambda=1} = \sum_{i=1}^{N}\left(\frac{\partial G}{\partial \xi_i}\right)_{\lambda=1} \delta\xi_i^{(m)} < 0 \tag{B.16}$$

is calculated. If the quantity is negative or zero, it is assumed that the minimizing value of $\lambda$ has not been passed yet, and the next iteration is carried out with $\lambda^{(m)} = 1$ in equation (B.10). If the quantity in equation (B.16) is positive, $\lambda^{(m)}$ is set as

$$\lambda^{(m)} = \frac{\left({}^{dG}/_{d\lambda}\right)_{\lambda=0}}{\left({}^{dG}/_{d\lambda}\right)_{\lambda=0} - \left({}^{dG}/_{d\lambda}\right)_{\lambda=1}} \tag{B.17}$$

Equation (B.17) ensures that $0 < \lambda^{(m)} < 1$ since it is assumed that a minimum in $G(\lambda)$ at $\lambda = 1$ has already been passed.

### B.1.3 Solution

The solution procedure uses a second-variation method where $G(\boldsymbol{\xi})$ is approximated near each $\boldsymbol{\xi}^{(m)}$ by a quadratic function and finds the minimum of that approximation. The quadratic function $Q(\boldsymbol{\xi})$ is the first two terms of the Taylor series expansion of $G(\boldsymbol{\xi})$ at $\boldsymbol{\xi}^{(m)}$, given by

$$\begin{aligned} Q\left(\boldsymbol{\xi}\right) = G\left(\boldsymbol{\xi}^{(m)}\right) &+ \sum_{i=1}^{N}\left(\frac{\partial G}{\partial \xi_i}\right)_{\boldsymbol{\xi}^{(m)}}\left(\xi_i - \xi_i^{(m)}\right) \\ &+ \frac{1}{2}\sum_{i=1}^{N}\sum_{j=1}^{N}\left(\frac{\partial^2 G}{\partial \xi_i\,\partial \xi_j}\right)_{\boldsymbol{\xi}^{(m)}}\left(\xi_i - \xi_i^{(m)}\right)\left(\xi_j - \xi_j^{(m)}\right) \end{aligned} \tag{B.18}$$

here $(\partial^2 G/\partial\xi_i\,\partial\xi_j)$ is known as the Hessian matrix. The necessary conditions that $Q$ be a minimum with respect with respect to $\boldsymbol{\xi}$ are

$$\frac{\partial Q}{\partial \xi_i} = 0; \quad i = 1, 2, \ldots, N \tag{B.19}$$

In equation (B.18), this yields

$$\left(\frac{\partial G}{\partial \xi_i}\right)_{\boldsymbol{\xi}^{(m)}} + \sum_{j=1}^{N} \left(\frac{\partial^2 G}{\partial \xi_i\,\partial \xi_j}\right)_{\boldsymbol{\xi}^{(m)}} \left(\xi_j - \xi_j^{(m)}\right) = 0; \quad i = 1, 2, \ldots, N \tag{B.20}$$

Equation (B.20) is a set of $N$ linear equations in the $N$ unknown elements of the vector $\boldsymbol{\delta\xi}^{(m)} = \boldsymbol{\xi} - \boldsymbol{\xi}^{(m)}$. We use $\boldsymbol{\delta\xi}^{(m)}$ in equations (B.11) and (B.10) from equation (B.20) as

$$\boldsymbol{\delta\xi}^{(m)} = -\left(\frac{\partial^2 G}{\partial \boldsymbol{\xi}^2}\right)^{-1}_{\boldsymbol{\xi}^{(m)}} \left(\frac{\partial G}{\partial \boldsymbol{\xi}}\right)_{\boldsymbol{\xi}^{(m)}} \tag{B.21}$$

where superscript $(-1)$ denotes a matrix inverse. In order to calculate inverse of the Hessian matrix, using equations (B.14), (4.52) and (B.13), we get

$$\begin{aligned}\frac{\partial^2 G}{\partial \xi_i\,\partial \xi_j} &= \frac{\partial}{\partial \xi_j}\left(\sum_{k=1}^{N} \nu_{ki}\,\mu_k\right) \\ &= RT \sum_{k=1}^{N}\sum_{l=1}^{N} \nu_{ki}\,\nu_{lj}\left(\frac{\delta_{kl}}{n_k} - \frac{1}{n_t}\right); \qquad i, j = 1, 2, \ldots, R,\end{aligned} \tag{B.22}$$

where $\delta_{kl}$ is the Kronecker delta. Equation (B.22) can be rewritten as

$$\frac{1}{RT}\frac{\partial^2 G}{\partial \xi_i\,\partial \xi_j} = \sum_{k=1}^{N} \frac{\nu_{ki}\,\nu_{kj}}{n_k} - \frac{\overline{\nu}_i\,\overline{\nu}_j}{n_t}; \quad i, j = 1, 2, \ldots, R, \tag{B.23}$$

where

$$\overline{\nu}_i = \sum_{k=1}^{N} \nu_{ki} \tag{B.24}$$

The stoichiometric matrix **N** is chosen by satisfying

$$\sum_{k=1}^{N} \frac{\nu_{ki}\,\nu_{kj}}{n_k} = \delta_{ij}, \tag{B.25}$$

which renders the Hessian matrix easy to inverse. Also, noting that the product $\nu_{ki}\nu_{kj}$ for $i \neq j$ is zero when $k$ refers to a noncomponent species ($k > M$) since each noncomponent species has a non stoichiometric coefficient only in one stoichiometric vector. When $i = j$, $\nu_{ki}\nu_{kj} = 1$ for such $k$ values [79]. The entries of the Hessian matrix are thus, numbering the component species from 1 to $M$ and the noncomponent species from $(M + 1)$ to $N$,

$$\frac{1}{RT}\frac{\partial^2 G}{\partial\xi_i\,\partial\xi_j} = \frac{\delta_{ij}}{n_{j+M}} + \sum_{k=1}^{M} \frac{\nu_{ki}\,\nu_{kj}}{n_k} - \frac{\overline{\nu}_i\,\overline{\nu}_j}{n_t}; \quad i, j = 1, 2, \ldots, R \tag{B.26}$$

With this formulation the Hessian matrix can be considered diagonal, and can be directly inverted giving

$$RT\left(\frac{\partial^2 G}{\partial\xi_i\,\partial\xi_j}\right)^{-1} \approx \left(\frac{1}{n_{i+M}} + \sum_{k=1}^{M} \frac{\nu_{ki}^2}{n_k} - \frac{\overline{\nu}_i^2}{n_t}\right)^{-1} \delta_{ij}; \quad i, j = 1, 2, \ldots, R \tag{B.27}$$

The VCS algorithm for a single ideal phase thus consists of using equation (B.21) with (B.27) and iteratively adjust each stoichiometric equation by an amount

$$\delta\xi_j^{(m)} = -\left(\frac{1}{n_{j+M}^{(m)}} + \sum_{k=1}^{M} \frac{\nu_{kj}^2}{n_k^{(m)}} - \frac{\overline{\nu}_j^2}{n_t}\right)^{-1} \frac{\Delta G_j^{(m)}}{RT}; \quad j = 1, 2, \ldots, R \tag{B.28}$$

### B.1.4 VCS Algorithm

The Villars-Cruise-Smith algorithm starts by cheking for optimum basis and makes necessary calculations. It then computes the step size parameters and carries out the minimization loop. The solution procedure can be presented by the following flowchart,

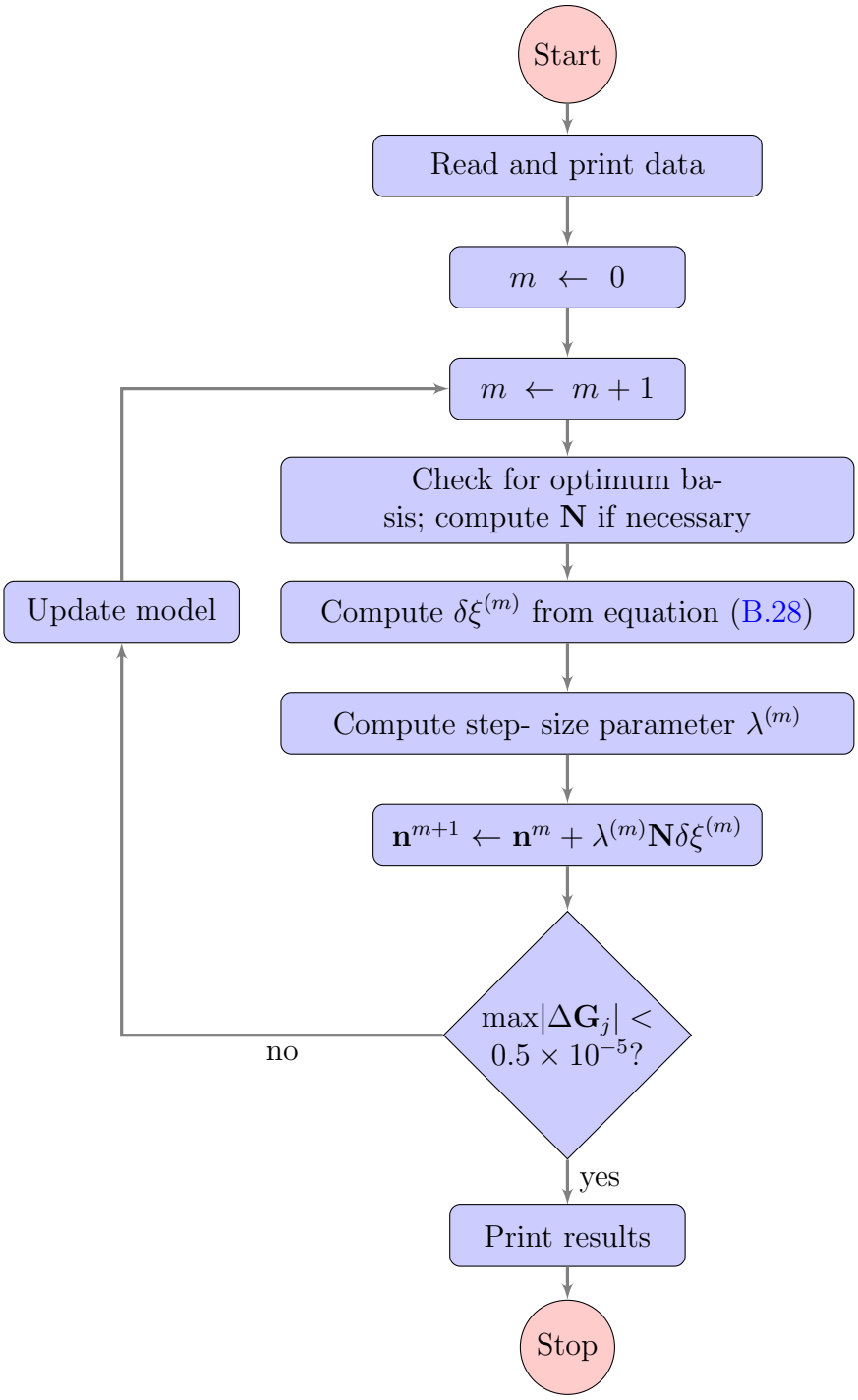
Start
Read and print data
$m \leftarrow 0$
$m \leftarrow m + 1$
Check for optimum basis; compute $\mathbf{N}$ if necessary
Compute $\delta\xi^{(m)}$ from equation (B.28)
Compute step- size parameter $\lambda^{(m)}$
$\mathbf{n}^{m+1} \leftarrow \mathbf{n}^m + \lambda^{(m)}\mathbf{N}\delta\xi^{(m)}$
$\max|\Delta\mathbf{G}_j| < 0.5 \times 10^{-5}$?
no
yes
Update model
Print results
Stop

# Appendix C

# Published Paper

**Proceedings of ASME 2013 Power Conference**
**Power2013**
**July 29-August 1, 2013, Boston, Massachusetts, USA**

**Power2013-98279**

# ENERGY AND EXERGY BASED ANALYSES OF A MULTI-FUELLED SI ENGINE

**M. Z. Haq***
Department of Mechanical Engineering
Bangladesh University of Engineering and Technology
Dhaka-1000
Bangladesh
Email: zahurul@me.buet.ac.bd

**A. Morshed**
Department of Mechanical Engineering
Bangladesh University of Engineering and Technology
Dhaka-1000
Bangladesh
Email: amorshed@me.buet.ac.bd

## ABSTRACT

*The paper presents energy and exergy based analyses of a single cylinder, four-stroke, spark ignition engine fuelled by six different fuels namely iso-octane, methane, hydrogen, methanol, ethanol and n-butanol. Wiebe function is used to predict realistic burn rates. Since the Wiebe function parameters are generally optimized for conventional fuels, the current study modifies them for different alternative fuels using available burning velocity data. Heat losses throughout the cycle have been predicted by empirical correlations. Analyses are carried out to quantify energy and exergy of the premixed fuel-air mixture inside the engine cylinder at various phases of the cycle and some results obtained from the study are validated against data available in literature. Both energy and exergy destructions are found to be dependent on the fuels and engine operating parameters. Results show that at 1000 rpm, about 34-39% of energy contained in the fuel is converted into useful work and this quantity is found to increase with engine speed. Exergies associated with exhaust are found significantly lower than the corresponding energy values for all fuels. The present study highlights the necessity of both energy and exergy analyses to probe and identify the sources of work potential losses in SI engines in various phases of the cycle.*

**Keywords:** *Energy, Exergy, SI Engine Modelling, Alternative Fuels, Engine Performance*

*Address all correspondence to this author.

## NOMENCLATURE

| | |
|---|---|
| $a_{ch}$ | Chemical exergy (kJ/kg-mix) |
| $a_Q$ | Exergy associated with heat transfer (kJ/kg-mix) |
| $a_{th}$ | Thermomechanical exergy (kJ/kg-mix) |
| $a_{tot}$ | Total exergy (kJ/kg-mix) |
| $a_W$ | Exergy associated with work interaction (kJ/kg-mix) |
| $g$ | Specific Gibbs energy (kJ/kg-mix) |
| $h$ | Specific enthalpy (kJ/kg-mix) |
| $I$ | Irreversibility (kJ/kg-mix) |
| $k$ | Specific heat capacity ratio (-) |
| $N$ | Engine speed (rpm) |
| $P$ | Gas pressure inside cylinder (kPa) |
| $R$ | Specific gas constant (kJ/kg-K) |
| $R_c$ | Compression ratio (-) |
| $s$ | Specific entropy (kJ/kg-K) |
| $T$ | Gas temperature inside cylinder (K) |
| $u_l$ | Laminar burning velocity (m/s) |
| $x_i$ | Mole fraction (-) |
| $y_i$ | Mass fraction (-) |
| $y_s$ | Fuel mass fraction in stoichiometric mixture (-) |
| $\theta$ | Crank angle (deg) |
| $\mu$ | Specific chemical potential (kJ/kg-mix) |

Subscripts:

| | |
|---|---|
| $i$ | Identifies constituent of a mixture |
| 0 | Restricted equilibrium with the environment |
| 00 | Unrestricted equilibrium with the environment |

## 1 INTRODUCTION

As available fuel reserves diminish, and exhaust regulations become more stringent, it gets ever more important to understand the operations and underlying processes in detail in order to make more efficient and economic use of fuels in internal combustion engines. By nature, all real processes suffer from irreversibility. So, identifying the sources of irreversibility, their variation with the change in engine operational parameters and ways to obviate them as much as possible have received much attention in recent years.

With increasing fuel prices and the possibility of diminishing supplies in the years ahead, the importance of developing systems which make effective use of energy is apparent [1]. The first law of thermodynamics has widely been used as a primary tool to assess the performance of such energy conversion devices. It is an expression of energy conservation which asserts that 'energy' is a thermodynamic property which can be transformed from one form to another but its total amount is conserved. The second law of thermodynamics asserts that 'energy' has quality as well as quantity. It provides an alternative and revealing means of assessing and comparing processes and systems rationally and meaningfully by introducing 'exergy'. Exergy based analysis yields a true measure of how nearly actual performance approaches the ideal, and clearly identifies the causes and the sources of thermodynamic losses and consequent impact on the environment. Exergy analysis can assist in improving and optimizing design [2].

Engine cycle modelling and simulation along with experimental validation can provide parametric and comparative performance analysis of different fuels at significantly lower expense of time and money. It can also be used to prognosticate the causes of irreversibility when employed in conjecture with a categorical exergy analysis. The present study employs a zero-dimensional, single zone combustion with Wiebe function based finite heat release model of a spark-ignition engine. Wiebe parameters have been modified according to laminar burning velocity and engine speeds to achieve MBT conditions. The model accommodates the temperature and composition dependence of the specific heats of mixture constituents. Realistic phenomena such as phased burn combustion, spark advance and heat transfer to the cylinder walls has been incorporated. Provision has been kept for residual burnt gas fraction and the cycle is simulated from inlet valve closure to exhaust valve opening at a resolution of one-tenth of an engine crank-angle degree.

The thermodynamic state points, determined from the first law analysis are used to determine the exergy leading to the revelation of the fact that a portion of a given amount of energy is 'available' to produce useful work, while the remaining portion is 'unavailable' due to the developed irreversibility. Exergy represents the upper limit on the amount of work an engine can deliver without violating thermodynamic laws, and irreversibility can be viewed as wasted work potential or the lost opportunity to do useful work [3]. This lost opportunities manifest themselves in environmental degradation and avoidable emissions. The performance of an engine can be improved by minimising irreversibility associated with it [1].

## 2 MODELLING, SIMULATION and ANALYSIS

### 2.1 Governing Equations of the SI Engine Cycle

Simulation of a single cylinder SI engine has been done based on [4]. Here, compression, combustion and expansion of gases occur inside the cylinder after the inlet valve closing (IVC) and before exhaust valve opening (EVO) in a closed system. From the first law of thermodynamics:

$$\delta Q_{fuel}(\theta) - \delta Q_{loss}(\theta) \equiv \delta Q_{net}(\theta) = dU(\theta) + \delta W(\theta) \quad (1)$$

Since, $\delta W = PdV$ and $dU = mC_v dT$, and assuming ideal gas behaviour ($PV = mRT$), the infinitesimal change in cylinder pressure, $dP$ can be expressed as a function of the crank angle, $\theta$, cylinder pressure, $P$, cylinder volume, $V$ and the net heat input, $Q_{net}$ [4] :

$$dP(\theta) = -kP(\theta)\left[\frac{dV(\theta)}{V(\theta)}\right] + (k-1)\left[\frac{\delta Q_{net}(\theta)}{V(\theta)}\right] \quad (2)$$

The specific heat ratio, $k = C_p/C_v$ influences the size and shape of the heat release profile and cylinder pressure development [5]. Therefore, realistic values of $k$ are estimated from detailed thermodynamic equilibrium composition of gases at every instant for prevailing pressure and temperature.

In order to evaluate Eq. 2, the cylinder volume, $V(\theta)$ is required that is given by [4] as:

$$V(\theta) = \frac{V_D}{R_c - 1} + \frac{V_D}{2}\left[\left(\frac{2L_c}{L_s}\right) + 1 - \cos\theta - \sqrt{\left(\frac{2L_c}{L_s}\right)^2 - \sin^2\theta}\right] \quad (3)$$

where, $V_D(=\frac{\pi}{4}B^2L_s)$ is the displacement volume, $B$ is the bore and $L_s$ is the stroke length, $R_c$ is the compression ratio and $L_c$ is the connecting rod length.

In ideal SI engine cycle, fuel is assumed to burn instantaneously to result in constant volume combustion at TDC. In actual engines, finite time is required to burn the fuel-air mixture. In the present study, mass fraction burnt as a function of crank-angle is calculated using the Wiebe function [6]:

$$y_b(\theta) = \begin{cases} 1 - \exp\left[-\xi\left(\frac{\theta-\theta_s}{\Delta\theta_b}\right)^{\psi}\right] & \text{if } \theta_s \le \theta \le \theta_s + \Delta\theta_b \\ 0 & \text{if } \theta < \theta_s,\ \theta > \theta_s + \Delta\theta_b \end{cases} \quad (4)$$

where,

| | |
|---|---|
| $y_b(\theta)$ | mass fraction burnt at a crank-angle, $\theta$ |
| $\theta_s$ | crank angle at the start of combustion |
| $\Delta\theta_b$ | total combustion duration ($y_b = 0$ to $y_b \approx 0.99$) |
| $\psi$ | 'Wiebe form factor' |
| $\xi$ | 'Wiebe efficiency factor' |

The Wiebe parameters are adjustable parameters and values of $\psi$ = 5 and $\xi$ = 3 have been reported to fit well with experimental data for conventional fuels [6]. There is a dearth of such data for alternative fuels and these fuels exhibit different burning velocities to affect the burn duration and requires consequent adjustment of spark timing. For example, hydrogen has a very high laminar burning velocity (Table 2) with consequent short burn duration, and therefore demands less spark-advance.

It has become widely accepted that turbulent flames in SI engines can be treated as an array of laminar flamelets with no turbulence structure residing within them and the actual burning parameters are usually normalized by laminar burning velocities [7, 8]. Following correlation [9] to adjust burn duration in response to change in engine speed and laminar burning velocity is used:

$$\frac{\Delta\theta_b}{\Delta\theta_{b,ref}} = \left[\frac{N}{N_{ref}}\right]^{1/3}\left[\frac{u_{l,ref}}{u_l}\right]^{2/3} \tag{5}$$

In the present study, experimental data of [10] are used as the reference, and engine specification is reported in Table 1. Evaluation of Eq. 4 also requires the estimation of spark-timing, $\theta_s$. For optimum maximum brake torque (MBT) spark-timing, half of the charge is burnt at about $10^0$ after TDC [6] , and this criteria is used to estimate $\theta_s$. Laminar burning velocities at 400 K temperature are used as some of liquid fuels may not form proper pre-mixture at 300 K. Calculated values of $\Delta\theta_b$ and $\theta_s$ for the fuels at two engine speeds are reported in Table 2.

**TABLE 1**. Reference engine specification, same as in [10].

| $B$ | $L_s$ | $L_c$ | $R_c$ | $\theta_s$ | $\Delta\theta_b$ |
|---|---|---|---|---|---|
| 0.0763 m | 0.1111 m | 0.160 m | 7 | $330^0$ | $60^0$ |

Heat release from the combustion of fuel, $\delta Q_{fuel}$ can be written as:

$$\delta Q_{fuel}(\theta) = Q_{LHV}\cdot y_s \cdot dy_b(\theta)\cdot(1-f) \tag{6}$$

, where $f$ is the residual gas fraction, and $y_s$ is the mass fraction of fuel in the stoichiometric fuel-air pre-mixture and is related to stoichiometric fuel-air ratio, $(F/A)_s$:

$$y_s = \frac{(F/A)_s}{(F/A)_s + 1} \tag{7}$$

**TABLE 2**. Spark advance and burn duration

| Fuel | $u_l$ [m/s] | speed [rpm] | $\Delta\theta_b$ [deg] | $\theta_s$ [deg] | $P_{max}$ [MPa] | $T_{max}$ [K] |
|---|---|---|---|---|---|---|
| Iso-Octane | 0.537 | 1000 | 44.2 | 15.0 | 4.50 | 2548 |
| | [11] | 4000 | 70.2 | 30.0 | 4.13 | 2503 |
| Methane | 0.572 | 1000 | 42.4 | 14.1 | 4.40 | 2609 |
| | [12, 13] | 4000 | 67.3 | 28.2 | 4.05 | 2563 |
| Hydrogen | 4.25 | 1000 | 11.1 | -3.7 | 5.36 | 3294 |
| | [14] | 4000 | 17.7 | 0.05 | 5.17 | 3291 |
| Methanol | 0.675 | 1000 | 38.0 | 11.6 | 4.56 | 2525 |
| | [15] | 4000 | 60.3 | 24.3 | 4.19 | 2485 |
| Ethanol | 0.640 | 1000 | 39.3 | 12.4 | 4.57 | 2526 |
| | [16] | 4000 | 62.4 | 25.5 | 4.18 | 2483 |
| Butanol | 0.585 | 1000 | 41.8 | 13.7 | 4.53 | 2531 |
| | [16] | 4000 | 66.3 | 27.7 | 4.16 | 2487 |

The heat loss from the gases to the cylinder walls, $\delta Q_{loss}(\theta)$, at an engine speed, $N$ can be determined with a Newtonian convection equation:

$$\delta Q_{loss}(\theta) = h_g(\theta)\cdot A_w(\theta)\cdot\left\{T(\theta) - T_w\right\}\cdot\frac{d\theta}{2\pi N} \tag{8}$$

The cylinder wall temperature, $T_w$ is the spatial-averaged mean temperature of the exposed cylinder wall, the head and the piston crown. The exposed cylinder area, $A_w(\theta)$ is the sum of the cylinder bore and head area, and the piston crown area:

$$\begin{aligned} A_w(\theta) &= A_{wall} + A_{head} + A_{piston} \\ &= 2V_D\left\{\frac{1}{L_s} + \frac{1}{B}\left[\left(\frac{2L_c}{L_s}\right) + 1 - \cos\theta - \sqrt{\left(\frac{2L_c}{L_s}\right)^2 - \sin^2\theta}\right]\right\} \end{aligned} \tag{9}$$

The heat transfer coefficient, $h_g(\theta)$ is the instantaneous area averaged heat transfer coefficient, and is related to engine parameters in Woschni correlation [4] as:

$$h_g(\theta) = 3.26\,[P(\theta)]^{0.8}\cdot[U_g(\theta)]^{0.8}\cdot B^{-0.2}\cdot[T(\theta)]^{-0.55} \tag{10}$$

where the units of $h_g$, $P$, $U_g$, $B$, and $T$ are W/m$^2$K, kPa, m/s, m and K, respectively. Here, $U_g$ is the characteristic gas velocity which is proportional to the mean piston speed during intake,

compression, and exhaust. During combustion and expansion, it is assumed that the gas velocities are increased by the pressure rise resulting from the combustion, so the characteristic gas velocity is affected by both mean piston speed, $\bar{U_p} = 2NL_s$, and cylinder pressure rise, $(P - P_m)$. Hence,

$$U(\theta) = 2.28\bar{U_P} + 0.00324T_0 \left[\frac{V(\theta)}{V_D}\right] \left[\frac{P(\theta) - P_m(\theta)}{P_0}\right] \quad (11)$$

Motoring pressure, $P_m$ is obtained by simulating the code without heat release and its value is estimated using [17]:

$$P_m(\theta) = P_0 \left[\frac{V_0}{V(\theta)}\right]^{1.3} \quad (12)$$

At the end of the exhaust stroke, when the engine exhaust valves open (at $\theta = \theta_{EVO}$), gas pressure, $P_{EVO}$ is greater than exhaust pressure, $P_e$. Hence, gas blow-down and gas displacement occur. Since, the engine cylinder have a finite clearance volume, some of the exhaust gases are left in the clearance volume. This residual gas will mix with the incoming fresh-charge giving rise to its temperature while reducing engine volumetric efficiency. Hence, residual gas fraction, $f$ is the ratio of the gas mass in the cylinder at the end of the exhaust stroke to the mass of the charge at the time of inlet valve close ($\theta = \theta_{IVC}$), and its values can be estimated using [4]:

$$f = \frac{1}{R_c} \left[\frac{P_e}{P_{EVC}}\right]^{\frac{1}{k}} \quad (13)$$

, for un-throttled engine, $P_e$ = 1 atm. Hence, temperature at the beginning of the cycle, $T_{IVC}$ is related to $f$ in [4] as:

$$T_{IVC} = (1 - f) \cdot T_i + f \cdot T_e \cdot \left[1 - \left(1 - \frac{P_i}{P_e}\right)\left(\frac{k-1}{k}\right)\right] \quad (14)$$

### 2.2 Simulation of SI Engine Model

In the present study, governing equations of the SI engine) are numerically solved for each time step, the time step used is for $0.1^o$ crank-angle and the solution 'marches' in time. All liquid fuels are considered vapour at IVC. Since fuel vaporization process is a complex combination of fluid flow, heat transfer and fuel properties, it is difficult to establish a consistent and fair technique to accommodate the effects of fuel vaporization. The calculation for a cycle stops at the end of power stroke when the exhaust valve opens (EVO) and values of $P_e$ and $T_e$ are noted to calculate the residual mass fraction, $f$ (Eq. 13) and $T_{IVC}$ (Eq. 14). The calculation cycle is repeated with estimated values of $f$ and $T_{IVC}$ until converged solution is achieved. Details of the calculation procedure is presented in [18, 19].

### 2.3 Estimation of Equilibrium Composition and Thermodynamic Properties

For practical chemical equilibrium, stoichiometric combustion of a fuel, $C_\alpha H_\beta O_\gamma N_\delta$ in dry air containing 21% Oxygen and 79% Nitrogen, by volume can be written as [4]:

$$\varepsilon \overbrace{C_\alpha H_\beta O_\gamma N_\delta}^{fuel} + \overbrace{(0.21O_2 + 0.79N_2)}^{air} \rightarrow \nu_1 N_2 + \nu_2 O_2 + \nu_3 CO + \nu_4 H_2 + \nu_5 CO_2 + \nu_6 H_2O + \nu_7 H + \nu_8 O + \nu_9 NO + \nu_{10} OH$$

$\varepsilon$ is the molar fuel-air ratio, and is related to $(F/A)_s$:

$$(F/A)_s = \frac{\varepsilon(12.01\alpha + 1.008\beta + 16.00\gamma + 14.01\delta)}{28.85} \quad (15)$$

Atom balancing of the combustion chemical reaction yields the following four equations:

$$C: \quad \varepsilon\alpha = (x_3 + x_5)N_t \quad (16)$$
$$H: \quad \varepsilon\beta = (2x_4 + 2x_6 + x_7 + x_{10})N_t \quad (17)$$
$$O: \varepsilon\gamma + 0.42 = (2x_2 + x_3 + 2x_5 + x_6 + x_8 + x_9 + x_{10})N_t \quad (18)$$
$$N: \varepsilon\delta + 1.58 = (2x_1 + x_9)N_t \quad (19)$$

where, $N_t$ is the total number of moles and $x$ is the mole fractions satisfying the condition:

$$\sum x_i = 1 \quad (20)$$

The introduction of the following six equilibrium constants for six non-redundant reactions provide the required equations to solve the ten unknown mole fractions, $x_i$, and total number of moles, $N_t$:

$$\frac{1}{2}H_2 \rightleftharpoons H \quad \Longrightarrow \quad K_{p1} = \frac{x_7 \cdot P^{1/2}}{x_4^{1/2}} \quad (21)$$

$$\frac{1}{2}O_2 \rightleftharpoons O \quad \Longrightarrow \quad K_{p2} = \frac{x_8 \cdot P^{1/2}}{x_2^{1/2}} \quad (22)$$

$$\frac{1}{2}H_2 + \frac{1}{2}O_2 \rightleftharpoons OH \quad \Longrightarrow \quad K_{p3} = \frac{x_{10}}{x_2^{1/2} \cdot x_4^{1/2}} \quad (23)$$

$$\frac{1}{2}O_2 + \frac{1}{2}N_2 \rightleftharpoons NO \quad \Longrightarrow \quad K_{p4} = \frac{x_9}{x_1^{1/2} \cdot x_2^{1/2}} \quad (24)$$

$$H_2 + \frac{1}{2}O_2 \rightleftharpoons H_2O \quad \Longrightarrow \quad K_{p5} = \frac{x_6}{x_2^{1/2} \cdot x_4 \cdot P^{1/2}} \quad (25)$$

$$CO + \frac{1}{2}O_2 \rightleftharpoons CO_2 \quad \Longrightarrow \quad K_{p6} = \frac{x_5}{x_2^{1/2} \cdot x_3 \cdot P^{1/2}} \quad (26)$$

In the above reactions, expressions of the equilibrium constants $K_p$'s are related to standard state specific Gibbs function, $\Delta g^o$:

$$\ln K_p = -\left[\frac{\Delta g^o}{RT}\right] \tag{27}$$

The chemical equilibrium is dictated by Gibbs free energy since, at constant temperature and pressure, chemical reactions are spontaneous in the direction of decreasing Gibbs energy. For complex reactive systems like the combustion system considered in the current study, evaluation of pertinent thermodynamic properties (e.g. Gibbs Function) are calculated with NASA polynomials by determining the thermodynamic properties of mixture constituent species at different temperatures and at the standard pressure. These polynomials are curve fits that express thermodynamic properties as functions of temperature [6]. If the gaseous mixture is assumed to be an ideal gas, then the effect of pressure on specific heats and enthalpy are negligible, and the value of entropy at pressures other than 1 atm is determined by using the following equation:

$$s = -R\ln(P/P_o) + \sum_{i=1}^{n} y_i(s_i^o - R_i \ln x_i) \tag{28}$$

where, $y_i$ and $x_i$ are the mass and mole fractions of species $i$, $R$ is the mixture gas constant, $R_i$ is the gas constant of species $i$, and $s_i^o$ is the temperature dependent portion of the specific entropy for species $i$.

From the estimated values of enthalpy and entropy at a given temperature, values of internal energy, $u$ and Gibbs free energy, $g$ can be determined using the following equations:

$$g = h - Ts \tag{29}$$

$$u = h - RT \tag{30}$$

Properties of the mixture are estimated using: $u = \sum y_i u_i$, $h = \sum y_i h_i$, $s = \sum y_i s_i$ and $y_i = x_i M_i / \sum x_i M_i$.

### 2.4 Estimation of Exergy

Exergy, also known as availability, of a system emerges as the sum of two contributions: thermomechanical exergy, $a_{th}$ and chemical exergy, $a_{ch}$ [2]. Hence,

$$a_{tot} = a_{th} + a_{ch} \tag{31}$$

Thermomechanical exergy, $a_{th}$ is the work which is obtained by taking the system by means of reversible physical processes, from its initial state to the state of restricted equilibrium with the environment ($P_0$ and $T_0$) while exchanging heat only with the environment. In the case of restricted equilibrium the system is kept separate from the environment by a physical boundary to prevent mixing and chemical interaction with the environment [20].

At the restricted dead-state, the control mass is only in thermomechanical equilibrium with the environment. In principle, the difference between the compositions of the system at the restricted dead-state and the environment can be used to obtain additional work. Chemical exergy, $a_{ch}$ is the work which is obtained by taking the system by means of reversible processes, from the state of restricted equilibrium with the environment to unrestricted equilibrium with the environment [20].

The maximum additional work obtained in this way is called the chemical exergy [1]. Hence, the expressions for these exergies are given by [2] as:

$$a_{th} = u + P_o v - T_o s - \sum_{i=1}^{n} y_i \mu_{i,0} \tag{32}$$

$$a_{ch} = \sum_{i=1}^{n} y_i(\mu_{i,0} - \mu_{i,00}) \tag{33}$$

The quantity $\mu_{i,0}$ is the chemical potential of species $i$ in the restricted dead state, whereas $\mu_{i,00}$ represents the value in the environmental dead state. The subscript "0" is used to identify properties of the thermomechanical or restricted dead state, and the subscript "00" is used to represent the properties at the environmental dead state. The numerical values of ($T_o$, $P_o$) for the dead state are those of dead environmental state, assumed 300 K and 101.325 kPa in the present study. For ideal gas:

$$\mu_{i,T} = g_{i,T}^o + RT\ln\left(\frac{P_i}{P_o}\right) \tag{34}$$

$$\mu_{i,0} - \mu_{i,00} = RT_o \ln\left(\frac{P_{i,0}}{P_{i,00}}\right) \tag{35}$$

The total exergy content within fuel-air premixture is consumed as the exergy transfer due to work and heat, and exergy destruction due to combustion and irreversibility. Exergy due to work transfer, $a_W$ is defined as the availability of the system to do actual work on a changing control volume against its surroundings [21]. The maximum work obtainable from fuel combustion is defined as the fuel exergy, $a_{fuel}$. Equations required to estimate various exergy values are reported in Table 3.

## 3 RESULTS and DISCUSSIONS

Because SI engines are air breathing, for a stoichiometric air-fuel pre-mixture, chemical energy entering into the engine

**TABLE 3**. Exergy equations for various processes [6].

| Mechanism | Equation |
|---|---|
| Work transfer | $a_W = \int \delta w = \int P dv$ |
| Heat transfer | $a_Q = \int (1 - T_o/T)\delta q$ |
| Fuel exergy | $a_{fuel} = -(\Delta g)_{ToPo}$ |

cylinder depends on the fuel, and its chemical energy, stoichiometric fuel-air mass ratio and the pre-mixture density. For identical conditions of pressure and temperatures, same volume of pre-mixture is drawn into engine cylinder and energy density (energy content per unit volume) is directly related to the engine output power. Reported in Table 4 are some of the heat release parameters estimated for six fuels. Lower heating values (LHV) of fuels are found to vary significantly for different fuels. However, different fuel requires different amount of air to complete its combustion which results in variation in the values fuel mass-fraction, $y_s$. Specific energy of fuel-air pre-mixture ($(-\Delta h)_{ToPo}$) is important, and when the values for different fuels are observed, it is seen that their values converge to a narrow band. In SI engines, fixed volume of pre-mixture is inducted into engine cylinder and therefore the both the values of energy and exergy densities are important and their values are presented in Table 4 .

Shown in Fig. 1 are the variations of estimated gas pressure inside engine cylinder plotted as a function of crank-angle for ideal Otto cycle and a modelled result for a compression ratio of 7. Experimental results of [10] and modelled results of [22] have also been reported for the purpose of validation. The compression process being almost isentropic gives matching variations between ideal and actual cycle upto ignition. However, after the start of combustion, actual pressure change is much less than that of the ideal cycle since the actual combustion process is not instantaneous resulting in slower rate of heat release. As can be seen, the agreement between the predicted values and the experimental [10] and modelled [22] results are good.

Figures 2 and 3 show respectively cylinder pressure and temperature variation at 1000 rpm for the fuels from intake valve closing to exhaust valve opening. The peak pressure and temperatures for 1000 and 4000 rpm have been reported in Table 2. Although burning velocity and fuel properties are varied, the spark timing adjustment yielded peak pressure for all fuels except hydrogen at the same crank angle as expected for MBT conditions. This is a good indication that, little modification is needed in SI engines in terms of comparable performance in alternative fuels if combustion parameters are correctly adjusted. It is to be noted that the slight rise in temperature of the intake charge in Fig. 3 is due to the mixing with high temperature residuals.

Shown in Fig. 4 are the variations of non-dimensional exergy values as a function of crank-angle with same engine parameters,

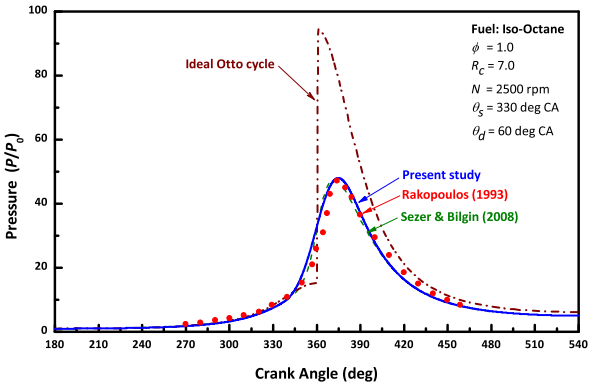


**FIGURE 1**. Pressure vs. crank-angle diagrams.

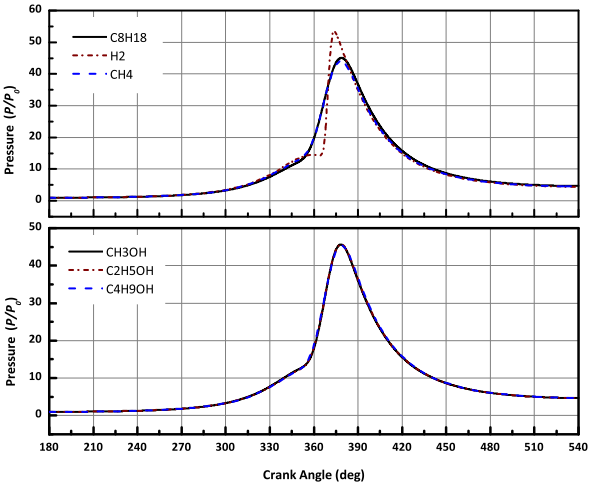


**FIGURE 2**. Pressure vs. crank-angle diagrams at 1000 rpm.

as in Fig. 1. Available work and cumulative exergy loss associated with heat transfer has also been plotted to visualize the conversion of total exergy from IVO to EVC. At IVO, total exergy equals the value of chemical exergy, $a_{ch}$. As the compression stroke progresses, work is supplied to the mixture and the effect is visible in the form of negative values of exergy associated with work, $a_W$. However, compression increases pressure and temperature of the charge thus increasing the thermomechanical exergy, $a_{th}$ and results in the rise in total exergy, $a_{tot}$ during the compression period. During this phase the heat transfer effects are negligible and effectively this phase is overall adiabatic. However, the pressure and temperature of the pre-mixture is not sufficient enough to start the oxidation of the mixture and therefore chemical exergy value remains unchanged.

**TABLE 4**. Estimated thermodynamic properties of the fuels.

| Fuel | $y_s$ | LHV | $T_{ad}$ | $(-\Delta h)_{P_oT_o}$ | $(-\Delta g)_{P_oT_o}$ | $\rho(-\Delta g)_{P_oT_o}$ | $(\Delta g/\Delta h)_{P_oT_o}$ |
|---|---|---|---|---|---|---|---|
| | (-) | (MJ/kg-fuel) | (K) | (kJ/kg-mix) | (kJ/kg-mix) | (kJ/m$^3$-mix) | (-) |
| Iso-Octane | 0.0624 | 44.7 | 2270 | 2786 | 2873 | 3507 | 1.031 |
| Methane | 0.0552 | 50.0 | 2224 | 2760 | 2755 | 3052 | 0.998 |
| Hydrogen | 0.0285 | 120.0 | 2379 | 3422 | 3183 | 2668 | 0.930 |
| Methanol | 0.1346 | 21.1 | 2219 | 2841 | 2903 | 3424 | 1.022 |
| Ethanol | 0.1006 | 27.7 | 2235 | 2789 | 2866 | 3466 | 1.028 |
| Butanol | 0.0825 | 33.8 | 2257 | 2793 | 2878 | 3528 | 1.031 |

$y_s \equiv$ Stoichiometric fuel-air mass ratio

$(-\Delta h)_{P_oT_o} \equiv$ Specific energy (energy per unit mass of mixture)

$(-\Delta g)_{P_oT_o} \equiv$ Specific exergy (exergy per unit mass of mixture)

$\rho(-\Delta g)_{P_oT_o} \equiv$ Exergy density (exergy per unit volume of mixture)

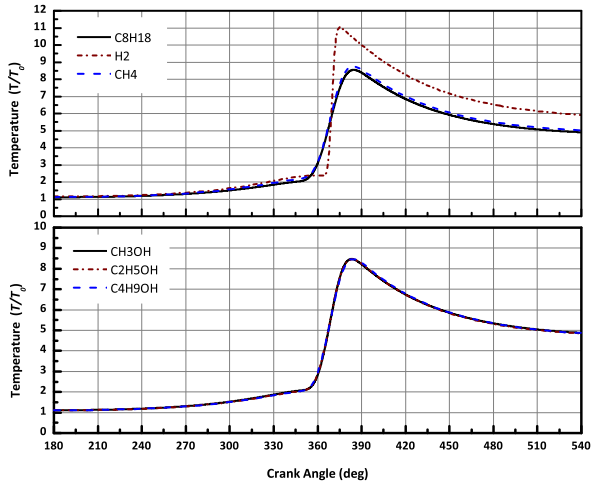


**FIGURE 3**. Temperature vs. crank-angle diagrams at 1000 rpm.

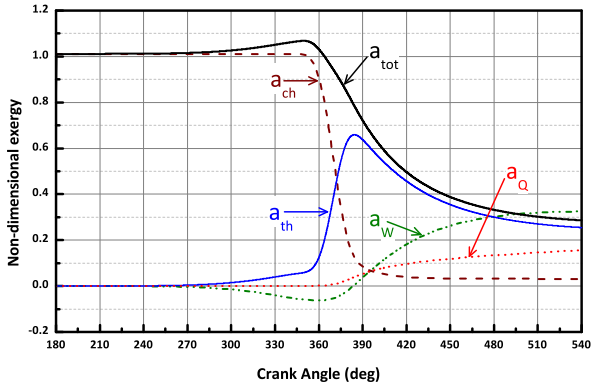


**FIGURE 4**. Variations of the non-dimensional exergy and its components with crank angle at 1000 rpm.

With the start of combustion, the chemical exergy, $a_{ch}$ decreases rapidly which gives significant rise to cylinder pressure and temperature. This rise in temperature and pressure results in increase in thermomechanical exergy, $a_{th}$. As the combustion and expansion progresses, the exergy transfer with work, $a_W$ as well as exergy transfer with heat loss, $a_Q$ from cylinder walls increase contributing to the decrease in total exergy, $a_{tot}$. After the end of combustion, expansion stroke continues until the piston reaches the BDC. During this part of the cycle, decrease in total exergy continues due to exergy transfers (both work and heat) from the system and exergy loss associated with heat transfer, $a_Q$ is noticeable when EVO at BDC. The remaining exergy in the cylinder at the end of expansion stroke emits with the exhaust gases, which is called the exergy transfer with the exhaust gases, $a_{ex}$. This constitutes a loss in availability as the mixture is still at pressure and temperature elevated than those of the dead state.

Variation of total exergy with crank-angle is shown in Fig. 5. Hydrogen premxiture starts with lower values of $a_{tot}$ and its value rises faster and maintains higher values during exhaust. Alcohols exhibit very close values of $a_{tot}$ in all the crank-angles.

Shown in Fig. 6 are the variation of exergy transfer due to work interactions, $a_W$. For work interaction, the exergy is equal to the net useful work which is equal to the net work minus the

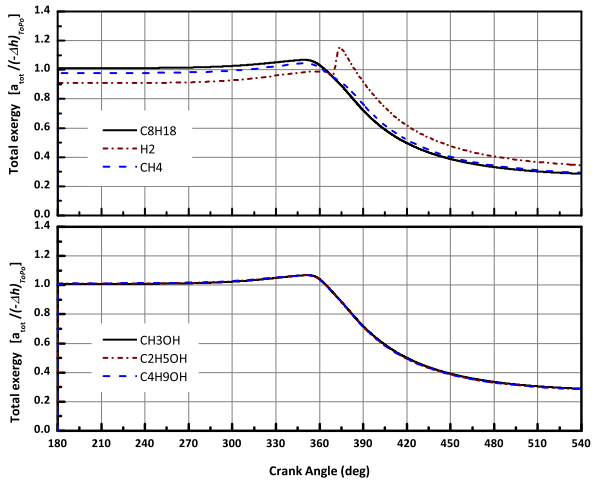


**FIGURE 5**. Variations of $a_{tot}$ with crank angle for six fuels at 1000 rpm.

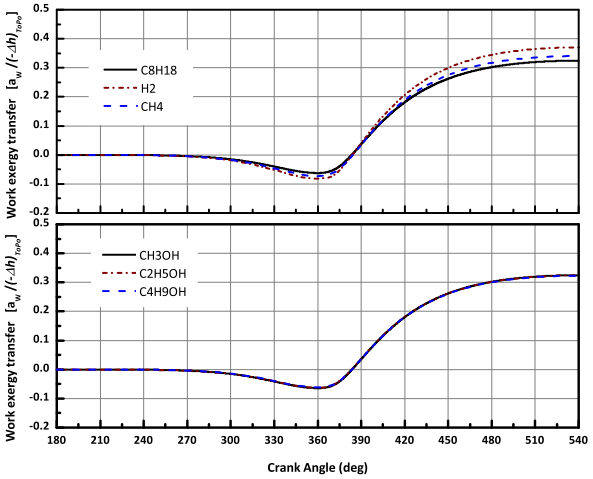


**FIGURE 6**. Variations of $a_W$ with crank angle for six fuels at 1000 rpm.

work done against the surroundings [2]. All the fuels considered, except hydrogen, exhibit very close values of $a_W$ at all crank-angles. The compression of hydrogen transfers a greater amount exergy to the system compared to other fuels due to the greater degree of compressibility associated with hydrogen, the larger gas constant, and extended duration of compression stroke. Also, this transfer of exergy to the system via compression work is the reason for the negative value of the curve during compression [21] . Exergy transfer associated with heat transfer, $a_Q$ is plotted in Fig. 7. All the fuels considered, except hydrogen, exhibit very close values of $a_Q$ at all crank-angles. Compared to the combustion process, the rate of heat transfer exergy exchanges are small during compression and expansion processes. The values of $a_Q$ for hydrogen are higher due to higher product temperature of hydrogen-air pre-mixture.

Distribution of energy and exergy usage in the key processes of the SI engine at two different speeds for stoichiometric octane-fuelling has been shown in Fig. 8. Total in-cylinder energy is consumed as work output, transferred heat, unaccounted energy loses e.g. blow-down and pumping processes (grouped as $Q_{misc}$) and energy carried out by exhaust gases. However, exergy based analysis provides a deeper insight by identifying the fact that chemical and thermal interactions between reactants and products during combustion cause exergy destruction at a considerable level. Moreover, mixing and blow-down of gases contribute to the generation of irreversibility, $I$. As a result, a portion of the exergy is lost due to combustion and other irreversibility and the rest is exhausted. Energy balance does not take into account of the irreversibility and consequent degradation of its quality during conversion. Addressing these irreversibility can play a key

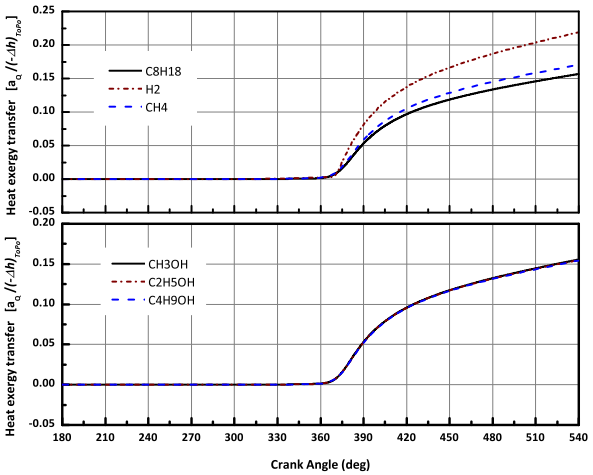


**FIGURE 7**. Variations of $a_Q$ with crank angle for six fuels at 1000 rpm.

role in future design and performance improvement.

Several important features can also be observed with engine speed variations. Increasing engine speed leaves less time for heat transfer from the cylinder, and reduces associated energy and exergy losses. The remaining energy ends up increasing the exhaust temperature and constitutes a higher loss with exhaust at higher engine speeds. Therefore, higher engine speed also results in lower exergy losses associated with heat transfer and higher exergy losses associated with exhaust. However, net work

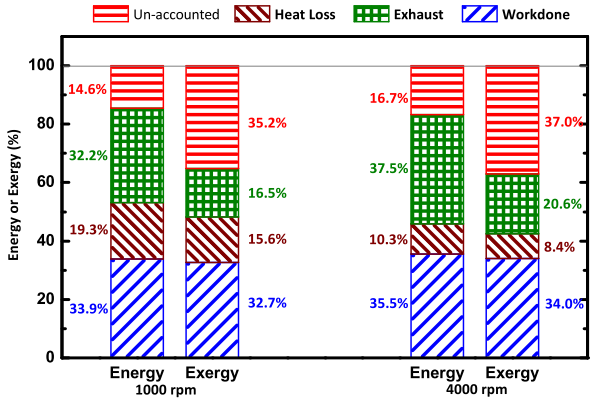


**FIGURE 8**. Energy and exergy distribution for stoichiometric iso-octane fuelling.

done and work potential values are comparable in both speeds. Similar analyses have been carried out for all the fuels and the corresponding values are reported in Table 5.

**TABLE 5**. Summary of results.

| Fuel | Speed | $W_{net}$ | $Q_{HT}$ | $Q_{ex}$ | $Q_{misc}$ | $a_W$ | $a_Q$ | $a_{Ex}$ | $I$ |
|---|---|---|---|---|---|---|---|---|---|
| | [rpm] | [%] | [%] | [%] | [%] | [%] | [%] | [%] | [%] |
| Iso-Octane | 1000 | 33.9 | 19.3 | 32.2 | 14.6 | 32.7 | 15.6 | 16.5 | 35.2 |
| | 4000 | 35.5 | 10.3 | 37.5 | 16.7 | 34.0 | 8.4 | 20.6 | 37.0 |
| Methane | 1000 | 35.6 | 21.0 | 35.0 | 8.4 | 35.4 | 17.6 | 19.0 | 28.0 |
| | 4000 | 37.4 | 11.3 | 40.8 | 10.5 | 37.2 | 9.4 | 23.4 | 30.0 |
| Hydrogen | 1000 | 38.7 | 26.2 | 32.3 | 2.3 | 41.1 | 24.3 | 26.0 | 8.5 |
| | 4000 | 41.7 | 14.0 | 40.8 | 3.5 | 44.4 | 13.0 | 32.0 | 10.6 |
| Methanol | 1000 | 33.9 | 19.2 | 33.3 | 13.6 | 33.0 | 16.0 | 17.0 | 34.0 |
| | 4000 | 35.6 | 10.2 | 38.6 | 15.6 | 34.5 | 8.2 | 21.3 | 36.0 |
| Ethanol | 1000 | 33.9 | 19.1 | 32.5 | 14.5 | 33.0 | 15.4 | 16.6 | 35.0 |
| | 4000 | 35.5 | 10.2 | 37.8 | 16.5 | 34.4 | 8.2 | 20.1 | 37.3 |
| Butanol | 1000 | 33.7 | 19.0 | 32.1 | 15.2 | 32.7 | 15.2 | 16.3 | 35.8 |
| | 4000 | 35.5 | 10.1 | 37.4 | 17.2 | 34.3 | 8.0 | 20.0 | 37.7 |

Exergy distribution for hydrogen is noticeably different than other fuels. The best outcome of hydrogen combustion is the lowest generation of irreversibility which is due to the simple molecular structure and fastest combustion. However at the present engine design, a lot of exergy is lost in heat transfer and exhaust due to high combustion temperatures. Compared to iso-octane and alcohols, methane showed better results in terms of lower exergy loss with irreversibility and higher work availability. All three alcohols showed similar variation in exergy distribution with irreversibility increasing with higher alcohols. However, work availability and heat transfer for the alcohols were very similar to those of iso-octanes.

From the analysis of six different fuels considered in the present study, some of the key results obtained are:

1. At 1000 rpm, 33.9 to 38.7% of energy contained with fuel is converted to useful work, and the figure changes to 35.5 to 41.7% in case of 4000 rpm.
2. At 1000 rpm, energy loss due to heat transfer is 19.0 to 26.2% and 10.1 to 14.0% at 4000 rpm. However, associated exergy losses are 15.2 to 24.3% at 1000 rpm, and 8.0 to 13.0% at 4000 rpm.
3. At 1000 rpm, energy loss with exhaust is 32.1 to 35.0%, and 37.4 to 40.8% at 4000 rpm. Exergy loss with exhaust are 16.3 to 19.0% at 1000 rpm, and 20.0 to 32.0% at 4000 rpm.
4. At both the speeds, exergy destroyed due to irreversibility in hydrogen fuelled cases are found lowest. For other fuels considered, at 1000 rpm, 28.0 to 35.2% of energy contained with fuel is destroyed due to irreversibility, and 30 to 37.7% is destroyed at 4000 rpm.
5. Engine work output and energy/exergy associated with exhaust are found to increase with engine speed, while losses due to heat transfer and irreversibility (in case of exergy) are reduced.

## 4 CONCLUSIONS

Comprehensive first- and second-law of thermodynamics based analyses are carried out for a single cylinder SI engine fuelled by six different fuels, namely iso-octane, hydrogen, methane, methanol, ethanol and n-butanol. The results highlight the importance of exergy based analyses to probe and identify the sources of work potential losses in different phases of the SI engine cycle.

## REFERENCES

[1] Moran, M. J., 1982. *Availability Analysis: A Guide to Efficient Energy Use*. Prentice-Hall.

[2] Wark, Jr., K., 1995. *Advanced Thermodynamics For Engineers*. McGraw-Hill.

[3] Li, K. W., 1996. *Applied Thermodynamics: Availability Methods and Energy Conversion*. Taylor & Francis.

[4] Ferguson, C. R., and Kirkpatrick, A. T., 2001. *Internal Combustion Engines: Applied Thermosciences*. John Wiley & Sons.

[5] Shehata, M., 2010. "Cylinder pressure, performance parameters, heat release, specific heats ratio and duration of combustion for spark ignition engine". *Energy*, ***35***(12), pp. 4710 – 4725.

[6] Heywood, J. B., 1988. *Internal Combustion Engine Fundamentals*. McGraw-Hill.

[7] Bradley, D., 1992. "How fast can we burn?". In Symposium (International) on Combustion, Vol. 24, Elsevier, pp. 247–262.

[8] Haq, M. Z., 2006. "Effect of developing turbulence and markstein number on the propagation of flames in methane-air premixture". *Journal of Engineering for Gas Turbines and Power-Transactions of The ASME,* ***128 (2)***, pp. 455–462.

[9] Sher, E., and Bar-Kohany, T., 2002. "Optimization of variable valve timing for maximizing performance of an unthrottled si engine–a theoretical study". *Energy,* ***27***(8), pp. 757 – 775.

[10] Rakopoulos, C. D., 1993. "Evaluation of a spark ignition engine cycle using first and second law analysis techniques". *Energy Conversion and Management,* ***34***(12), pp. 1299 – 1314.

[11] Bradley, D., Hicks, R., Lawes, M., Sheppard, C., and Woolley, R., 1998. "The measurement of laminar burning velocities and markstein numbers for iso-octane-air and iso-octane-heptane-air mixtures at elevated temperatures and pressures in an explosion bomb". *Combustion and Flame,* ***115***(12), pp. 126 – 144.

[12] Gu, X. J., Haq, M. Z., Lawes, M., and Woolley, R., 2000. "Laminar burning velocity and markstein lengths of methane-air mixtures". *Combustion and Flame,* ***121***(1-2), pp. 41 – 58.

[13] Haq, M., 1998. "Fundamental studies of premixed combustion". PhD thesis, University of Leeds.

[14] Milton, B., and Keck, J., 1984. "Laminar burning velocities in stoichiometric hydrogen and hydrogen-hydrocarbon gas mixtures". *Combustion and Flame,* ***58***(1), pp. 13 – 22.

[15] Liao, S., Jiang, D., Huang, Z., Shen, W., Yuan, C., and Cheng, Q., 2007. "Laminar burning velocities for mixtures of methanol and air at elevated temperatures". *Energy Conversion and Management,* ***48***(3), pp. 857 – 863.

[16] Broustail, G., Seers, P., Halter, F., Morac, G., and Mounaim-Rousselle, C., 2011. "Experimental determination of laminar burning velocity for butanol and ethanol iso-octane blends". *Fuel,* ***90***(1), pp. 1 – 6.

[17] Stone, R., 1999. *Introduction to Internal Combustion Engines*. Macmillan Press Ltd.

[18] Morshed, A., 2013. "Energy and exergy based analyses of a multi-fuelled si engine". Master's thesis, Department of Mechanical Engineering, Bangladesh university of Engineering & Technology. in progress.

[19] Haq, M. Z., and Mohiuddin, M. R., 2011. "Thermodynamic analysis of a multi-fueled single cylinder si engine". *ASME Conference Proceedings,* ***2011***(54907), pp. 1541–1550.

[20] Kotas, T. J., 2012. *The Exergy Method of Thermal Plant Analysis*. Exergon Publishing Co.

[21] Nieminen, J., and Dincer, I., 2010. "Comparative exergy analyses of gasoline and hydrogen fuelled ICEs". *International Journal of Hydrogen Energy,* ***35***(10), pp. 5124 – 5132.

[22] Sezer, I., Altin, I., and Bilgin, A., 2009. "Exergetic analysis of using oxygenated fuels in spark-ignition (si) engines". *Energy & Fuels,* ***23***(4), pp. 1801–1807.

# References


[1] J. L. Lumley. *Engines: An Introduction*. Cambridge University Press, 1999. 1

[2] R. N. Colvile, E. J. Hutchinson, R. F. Warren, and J. S. Mindell. *Air Pollution Science for the 21st Century*, chapter The transport sector as a source of air pollution, pages 187–239. Elsevier, 2002. 1

[3] T. J. Kotas. *The Exergy Method of Thermal Plant Analysis*. Paragon Publishing, 2012. 2, 3, 15, 18, 22, 25, 61

[4] M. J. Moran. *Availability analysis: a guide to efficient energy use*. ASME Press, 1989. 2

[5] K. Wark. *Advanced thermodynamics for engineers*. McGraw-Hill series in mechanical engineering. McGraw-Hill Higher Education, 1995. 3

[6] OECD/IEA. World energy outlook 2009. Technical report, International Energy Agency, 2009. 3

[7] R. Daniel, G. Tian, H. Xu, and S. Shuai. Ignition timing sensitivities of oxygenated biofuels compared to gasoline in a direct-injection si engine. *Fuel*, 99:72–82, 2012. 3, 14

[8] S. Szwaja and J. D. Naber. Combustion of n-butanol in a spark-ignition ic engine. *Fuel*, 89(7):1573–1582, 2010. 3, 13

[9] Y. Ra and R. D. Reitz. A combustion model for ic engine combustion simulations with multi-component fuels. *Combustion and Flame*, 158(1):69–90, 2011. 3, 8

[10] Y. Yacoub, R. Bata, and M. Gautam. The performance and emission characteristics of c1-c5 alcohol-gasoline blends with matched oxygen content in a single-cylinder spark ignition engine. *Proceedings of the Institution of Mechanical Engineers*, 212:363–379, 1998. 3, 13

[11] S. Verhelst and T. Wallner. Hydrogen-fueled internal combustion engines. *Progress in Energy and Combustion Science*, 35:490–527, 2009. 3, 11, 14, 50

[12] H. Bayraktar and O. Durgun. Investigating the effects of lpg on spark ignition engine combustion and performance. *Energy Conversion and Management*, 46:2317–2333, 2005. 3, 14

[13] S. Rousseau, B. Lemoult, and M. Tazerout. Combustion characterization of natural gas in a lean burn spark-ignition engine. *Proceedings of the Institution of Mechanical Engineers*, 213:481–489, 1999. 3, 12

[14] J. A. Caton. Implications of fuel selection for an si engine: Results from the first and second laws of thermodynamics. *Fuel*, 89:3157–3166, 2010. 3, 11, 16, 62

[15] J. Nieminen and I Dincer. Comparative exergy analyses of gasoline and hydrogen fuelled ices. *International Journal of Hydrogen Energy*, 35(10):5124–5132, 2010. 3, 9, 16, 61

[16] M. Z. Haq and A. Morshed. Energy and exergy based analyses of a multi-fuelled si engine. In *Proceedings of ASME 2013 Power Conference (Power2013)*. ASME, 2013. 3, 16, 27, 39, 61, 72

[17] J. B. Heywood. *Internal combustion engine fundamentals*. McGraw-Hill series in mechanical engineering. McGraw-Hill, 1988. 3, 6, 10, 12, 29, 30, 32, 34, 36, 38, 39, 41, 42, 65, 67

[18] C. D. Rakopoulos and E. G. Giakoumis. Second-law analyses applied to internal combustion engines operation. *Progress in Energy and Combustion Science*, 32:2–47, 2006. 3, 9, 15

[19] D. Goodwin. *Cantera 2.0: Documentation*. Cantera, 2012. 5, 43, 70, 72

[20] J. B. Heywood. *Engine Combustion Modeling - An Overview*, chapter 1, pages 1–38. Plenum Press, 1980. 7

[21] R. S. Benson and P. C. Baruah. Performance and emission predictions for a multi-cylinder spark ignition engine. *Proceedings of the Institution of Mechanical Engineers*, 191:339–354, 1977. 7

[22] G. P. Beretta, M. Rashidi, and J. C. Keck. Turbulent flame propagation and combustion in spark ignition engines. *Combustion and Flame*, 52:217–245, 1983. 7

[23] M. Metghalchi and J. C. Keck. Burning velocities of mixtures of air with methanol, isooctane and indolene at high pressure and temperature. *Combustion and Flame*, 48:191–210, 1982. 7, 12, 13

[24] B. E. Milton and J. C. Keck. Laminar burning velocities in stoichiometric hydrogen and hydrogen-hydrocarbon gas mixtures. *Combustion and Flame*, 58(1):13–22, 1984. 7, 40

[25] D. Bradley, R. A. Hicks, M. Lawes, C. G. W. Sheppard, and R. Woolley. The measurement of laminar burning velocities and markstein numbers for iso-octane–air and iso-octane–n-heptane–air mixtures at elevated temperatures and pressures in an explosion bomb. *Combustion and Flame*, 115:126–144, 1998. 7, 13, 40

[26] X. J. Gu, M. Z. Haq, M. Lawes, and R. Woolley. Laminar burning velocity and markstein lengths of methane–air mixtures. *Combustion and Flame*, 121:41–58, 2000. 7, 13, 40

[27] F. Bonatesta and P. J. Shayler. Factors influencing the burn rate characteristics of a spark ignition engine with variable valve timing. *Proceedings of the Institution of Mechanical Engineers*, 222:2147–2158, 2008. 8, 12

[28] P. Giansetti, G. Colin, P. Higelin, and Y. Chamaillard. Residual gas fraction measurement and computation. *International Journal of Engine Research*, 8:347–364, 2007. 8

[29] F. Morey and P. Seers. Comparison of cycle-by-cycle variation of measured exhaust-gas temperature and in-cylinder pressure measurements. *Applied Thermal Engineering*, 30:487–491, 2010. 8, 11

[30] K. Nakata, N. Sasaki, A. Ota, and K. Kawatake. The effect of fuel properties on thermal efficiency of advanced spark-ignition engines. *International Journal of Engine Research*, 12:274–281, 2011. 8

[31] Y. Shi, H. W. Ge, and R. D. Reitz. *Computational Optimization of Internal Combustion Engines*. SpringerLink : Bücher. Springer, 2011. 8

[32] C. J. Rutland. Large-eddy simulations for internal combustion engines – a review. *International Journal of Engine Research*, 12:421–451, 2011. 8

[33] C. D. Rakopoulos. Evaluation of a spark ignition engine cycle using first and second law analysis techniques. *Energy Conversion and Management*, 34(12):1299–1314, 1993. 9, 16, 39, 51

[34] C. D. Rakopoulos and C. N. Michos. Generation of combustion irreversibilities in a spark ignition engine under biogas-hydrogen mixtures fueling. *International Journal of Hydrogen Energy*, 34(10):4422–4437, 2009. 9, 16

[35] C. D. Rakopoulos, M. A. Scott, D. C. Kyritsis, and E. G. Giakoumis. Availability analysis of hydrogen/natural gas blends combustion in internal combustion engines. *Energy*, 33(2):248–255, 2008. 9, 16

[36] C. A. Finol and K. Robinson. Thermal modelling of modern diesel engines: proposal of a new heat transfer coefficient correlation. *Proceedings of the Institution of Mechanical Engineers*, 225:1544–1560, 2011. 9, 11

[37] J. B. Heywood and J. A. Caton. An experimental and analytical study of heat transfer in an engine exhaust port. *International Journal of Heat and Mass Transfer*, 24(4):581–595, 1981. 9, 11

[38] D. Sandoval and J. B. Heywood. An improved friction model for spark-ignition engines. In *Society of Automotive Engineers, Inc. Paper No. 2003-01-0725*, SAE 2003 World Congress & Exhibition, 2003. 9

[39] G. Fontana and E. Galloni. Experimental analysis of a spark-ignition engine using exhaust gas recycle at wot operation. *Applied Energy*, 87(7):2187–2193, 2010. 9

[40] M. S. Shehata. Cylinder pressure, performance parameters, heat release, specific heats ratio and duration of combustion for spark ignition engine. *Energy*, 35(12):4710–4725, 2010. 9

[41] G. Borman and K. Nishiwaki. Internal-combustion engine heat transfer. *Progress in Energy and Combustion Science*, 13:1–46, 1987. 9, 10, 11, 41

[42] W. J. D. Annand. Heat transfer in the cylinders of reciprocating internal combustion engines. *Proceedings of the Institution of Mechanical Engineers*, 177(36):973–990, 1963. 10

[43] G. Woschni. A universally applicable equation for the instantaneous heat transfer coefficient in the internal combustion engine. In *Society of Automotive Engineers, Inc. Paper No. 670931*, 1967. 10, 41

[44] C. A. Finol and K. Robinson. Thermal modelling of modern engines: a review of empirical correlations to estimate the in-cylinder heat transfer coefficient. *Proceedings of the Institution of Mechanical Engineers*, 220:1765–1781, 2006. 10

[45] S. H. Chan and J. Zhu. Modelling of engine in-cylinder thermodynamics under high values of ignition retard. *International Journal of Thermal Sciences*, 40:94–103, 2001. 11

[46] A. K. Oppenheim and A. L Kuhl. Life of fuel in engine cylinder. In *Society of Automotive Engineers, Inc. Paper No. 980780*, 1998. 11

[47] J. I. Ghojel. Review of the development and applications of the wiebe function: a tribute to the contribution of ivan wiebe to engine research. *International Journal of Engine Research*, 11:297–312, 2010. 11, 39

[48] E. Sher and Y. Hacohen. On the modeling of a si 4-stroke cycle engine fueled with hydrogen-enriched gasoline. *International Journal of Hydrogen Energy*, 12(11):773–781, 1987. 11, 14

[49] H. Bayraktar and O. Durgun. Development of an empirical correlation for combustion durations in spark ignition engines. *Energy Conversion & Management*, 45:1419–1431, 2003. 12

[50] F. Lindström, Ångström. H. E., G. Kalghati, and C. E. Möller. An empirical si combustion model using laminar burning velocity correlations. In *Society of Automotive Engineers, Inc. Paper No. 2005-01-2106*, 2005. 12

[51] F. Bonatesta, B. Waters, and P. J. Shayler. Burn angles and form factors for wiebe function fits to mass fraction burned curves of a spark ignition engine with variable valve timing. *International Journal of Engine Research*, 11:177–186, 2010. 12

[52] C. R. Ferguson and A. T. Kirkpatrick. *Internal combustion engines: applied thermosciences*. John Wiley & Sons, 2001. 13, 32, 38

[53] D. Bradley. Combustion and the design of future engine fuels. *Proceedings of the Institution of Mechanical Engineers*, 223:2751–2765, 2009. 13

[54] Ö. L. Gülder. Burning velocities of ethanol-isooctane blends. *Combustion and Flame*, 56(3):261–268, 1984. 13

[55] G. Broustail, P. Seers, F. Halter, G. Moréac, and C. Mounaim-Rousselle. Experimental determination of laminar burning velocity for butanol and ethanol iso-octane blends. *Fuel*, 90(1):1–6, 2011. 13, 40

[56] M. B. Çelik, B. Özdalyan, and F. Alkan. The use of pure methanol as fuel at high compression ratio in a single cylinder gasoline engine. *Fuel*, 90:1591–1598, 2011. 14

[57] F. Salimi, A. H. Shamekhi, and A. M. Pourkhesalian. Role of mixture richness, spark and valve timing in hydrogen-fuelled engine performance and emission. *International Journal of Hydrogen Energy*, 34(9):3922–3929, 2009. 14

[58] R. Ebrahimi. Effect of specific heat ratio on heat release analysis in a spark ignition engine. *Scientia Iranica*, 18(6):1231–1236, 2011. 14

[59] J. W. Gibbs, H. A. Bumstead, and R. G. Van Name. *Scientific Papers of J. Willard Gibbs ...: Thermodynamics*. Scientific Papers of J. Willard Gibbs. Longmans, Green and Company, 1906. 15

[60] D. S. Scott. Exergy. *International Journal of Hydrogen Energy*, 28:369–375, 2003. 15, 17

[61] J. Szargut. International progress in second law analysis. *Energy*, 5:709–718, 1980. 15

[62] T. J. Kotas. Exergy concepts for thermal plant. *International Journal of Heat and Fluid Flow*, 2(3):105–114, 1980. 15

[63] T. J. Kotas. Exergy criteria of performance for thermal plant: Second of two papers on exergy techniques in thermal plant analysis. *International Journal of Heat and Fluid Flow*, 2(4):147–163, 1980. 15

[64] D. R. Morris and J. Szargut. Standard chemical exergy of some elements and compounds on the planet earth. *Energy*, 11(8):733–755, 1986. 15

[65] R. W. Haywood. A critical review of the theorems of thermodynamic availability, with concise formulations. *Journal of Mechanical Engineering Science*, 16(3):160–173, 1974. 15

[66] M. V. Sussman. Mechanochemical availability. *Nature*, 256(5514):195–198, 1975. 15

[67] M. V. Sussman. Steady-flow availability and the standard chemical availability. *Energy*, 5:793–802, 1980. 15

[68] G. P. Beretta and J. C. Keck. Energy and entropy balances in a combustion chamber: Analytical solution. *Combustion Science and Technology*, 30:19–29, 1983. 15

[69] J. H. Van Gerpen and H. N. Shapiro. Second-law analysis of diesel engine combustion. *Journal of Engineering for Gas Turbines and Power*, 112:129–137, 1990. 16

[70] K-Y. Teh, S. L. Miller, and C. F. Edwards. Thermodynamic requirements for maximum internal combustion engine cycle efficiency. part 1: optimal combustion strategy. *International Journal of Engine Research*, 9:449–465, 2008. 16

[71] K-Y. Teh, S. L. Miller, and C. F. Edwards. Thermodynamic requirements for maximum internal combustion engine cycle efficiency. part 2: work extraction and reactant preparation strategies. *International Journal of Engine Research*, 9:467–481, 2008. 16

[72] J. Dewulf, H. Van Langenhove, B. Muys, S. Bruers, B. R. Bakshi, G. F. Grubb, D. M. Paulus, and E. Sciubba. Exergy: Its potential and limitations in environmental science and technology. *Environmental Science & Technology*, 42(7):2221–2232, 2008. 17

[73] S. Soylu and J. H. Van Gerpen. Development of empirically based burning rate sub-models for a natural gas engine. *Energy Conversion & Management*, 45:467–481, 2004. 37

[74] D. Bradley. How fast can we burn? In *Twenty-Fourth Symposium (International) on Combustion*, pages 247–262. The Combustion Institute, 1992. 39

[75] M. Z. Haq. Effect of developing turbulence and markstein number on the propagation of flames in methane-air premixture. *Journal of Engineering for Gas Turbines and Power*, 128(2):455–462, 2006. 39

[76] E. Sher and T. Bar-Kohany. Optimization of variable valve timing for maximizing performance of an unthrottled si engine–a theoretical study. *Energy*, 27:757–775, 2002. 39

[77] S. Liao, D. Jiang, Z. Huang, W. Shen, C. Yuan, and Q. Cheng. Laminar burning velocities for mixtures of methanol and air at elevated temperatures. *Energy Conversion and Management*, 48(3):857–863, 2007. 40

[78] R. Stone. *Introduction to Internal Combustion Engines*. Society of Automotive Engineers, 1999. 42

[79] W. R. Smith and R. W. Missen. *Chemical reaction equilibrium analysis: theory and algorithms*. Wiley series in chemical engineering. Wiley, 1982. 43, 76, 78

[80] W. R. Smith and R. W. Missen. What is chemical stoichiometry? *Chemical Engineering Education*, 13:26–32, 1979. 44

[81] I. Sezer and A. Bilgin. Mathematical analysis of spark ignition engine operation via the combination of the first and second laws of thermodynamics. *Proceedings of the Royal Society A: Mathematical, Physical and Engineering Science*, 464:3107–3128, 2008. 51